ЖУРНАЛ ОРГАНІЧНОЇ ТА ФАРМАЦЕВТИЧНОЇ ХІМІЇ

JOURNAL OF ORGANIC AND PHARMACEUTICAL CHEMISTRY

У журналі розглянуто проблеми синтезу й аналізу органічних та елементо-органічних сполук, аналогів природних сполук і лікарських субстанцій, наведено результати фізико-хімічних досліджень у вищезазначених напрямах. Також з погляду (біо)органічної, фармацевтичної, аналітичної та фізичної хімії проаналізовано питання з різних аспектів рослинництва, ґрунтознавства й дослідження навколишнього середовища.

Для працівників науково-дослідних установ, вищих навчальних закладів та фахівців хімічного, фармацевтичного, біологічного, медичного і сільськогосподарського профілів.

V. V. Burianov[1,2], D. A. Lega[1,3], V. G. Makhankova[1,2], Yu. M. Volovenko[2], S. V. Kolotilov[4],
D. M. Volochnyuk[1,2,5], S. V. Ryabukhin[1,2,5]

[1] Enamine Ltd., 78, Chervonotkatska str., Kyiv, 02094, Ukraine
[2] Taras Shevchenko National University of Kyiv, 60, Volodymyrska str., Kyiv, 01033, Ukraine
[3] National University of Pharmacy of the Ministry of Health of Ukraine,
  53, Pushkinska str., Kharkiv, 61002, Ukraine
[4] L. V. Pisarzhevskii Institute of Physical Chemistry of the National Academy of Sciences of Ukraine,
  31, Nauki ave., Kyiv, 03028, Ukraine
[5] Institute of Organic Chemistry of the National Academy of Sciences of Ukraine,
  5, Murmanska str., Kyiv, 02660, Ukraine

Multi-faceted Commercially Sourced Pd-Supported Reduction: A View from Practical Experience

Abstract

Aim. To share our experience when working with the Pd-catalyzed hydrogenation and discuss reactions occurred contrary to our expectations, as well as express our vision of the causes for such an unusual reactivity.

Results and discussion. Catalysis is a key technology and among the central themes of both petrochemical and fine chemical industries. Although extremely useful and reliable, it can sometimes astonish researchers. The paper discusses 17 intriguing cases of the catalytic hydrogenation and hydrogenolysis reactions from our practice in the High-pressure Synthesis Laboratory (Enamine Ltd.). All examples presented are characterized by peculiar performance of commercially sourced heterogeneous palladium-containing catalysts (Pd/C or Pd(OH)$_2$). Thus, some cases were characterized by reduced activity of the catalyst (or even its complete loss), meaning that reaction conditions found before to be suitable for reduction appeared to be "broken", and we had to search for a new, often harsher reaction setup. Curiously, it is a matter of classical Pd-catalyzed hydrogenations of N$^+$–O$^-$ and C=C fragments. Apparently, these results indicate the heterogeneity of commercially available catalysts and are related to their fine internal structure, in particular the surface morphology. Another interesting issue the article deals with is chemoselectivity of the catalytic hydrogenation. Sometimes some reactions led to astonishing results going across theoretical views and expectations. Saturation of benzene rings instead of (or accompanying) debenzylation, breaking of the common order of hydrogenation for compounds containing several aromatic parts with different resonance energies, irreproducible experiment, obtaining of different products under the same conditions, uncommon results of Pd-catalyzed reactions is the list of interesting results, which we observed and discussed in the article. Analyzing the information available in the literature and considering all the results gathered we tend to believe that the presence of impurities of noble metals (Rh, Ru, Pt) in the catalysts used to be a possible reason for these strange findings. The study supports the general idea that commercial palladium catalysts differ in efficiency, resulting in significant differences in selectivity, reaction time, and yields. Elucidating the regularities behind such empirical results is undoubtedly an interesting area of research in the field of catalysis.

Experimental part. All starting compounds exposed to hydrogenation were synthesized in Enamine Ltd. and had purity of not less than 95 %. The palladium-containing catalysts used in the experiment were purchased from 6 commercial sources within 2011 – 2022. The structure and purity of the compounds synthesized were characterized by ^{1}H NMR spectroscopy, liquid chromatography coupled with the mass spectrometry method, elemental analysis. Chromatographic experiments revealed the purity of all compounds obtained being not less than 95 %.

Conclusions. In the paper we have summarized our experience with the Pd-catalyzed hydrogenation and presented cases of unusual reactivity or unexpected outcomes of the reactions encountered in our practice. In general, complications we faced were of three types: (1) irreproducibility of the procedures most likely as the result of a changeable activity of the catalysts; (2) chemoselectivity issues when two or multireducible functional groups were present in the substrate; (3) undesirable Pd-catalyzed defunctionalization reactions. In turn, these complications led to increase in production costs, loss of time and resources. Therefore, because of this variability in the efficiency of Pd catalysts, far more efforts are required to find out the key differences between commercial sources of Pd catalysts, as well as to create protocols clearly defining the catalytic activity of each batch of the catalyst allowing to identify high-quality catalysts immediately prior to the use without wasting precious time and synthetic materials.

Keywords: catalysis; hydrogenation; heterocyclic compounds; palladium; selectivity; competing reactions

В. В. Бур'янов[1,2]**, Д. О. Лега**[1,3]**, В. Г. Маханькова**[1,2]**, Ю. М. Воловенко**[2]**, С. В. Колотілов**[4]**, Д. М. Волочнюк**[1,2,5]**, С. В. Рябухін**[1,2,5]

[1] *НВП «Єнамін», вул. Червоноткацька, 78, м. Київ, 02094, Україна*

[2] *Київський національний університет імені Тараса Шевченка,*
 вул. Володимирська, 60, м. Київ, 01033, Україна

[3] *Національний фармацевтичний університет Міністерства охорони здоров'я України,*
 вул. Пушкінська, 53, м. Харків, 61002, Україна

[4] *Інститут фізичної хімії імені Л. В. Писаржевського Національної академії наук України,*
 просп. Науки, 31, м. Київ, 03028, Україна

[5] *Інститут органічної хімії Національної академії наук України,*
 вул. Мурманська, 5, м. Київ, 02660, Україна

Багатогранне відновлення, каталізоване комерційно доступним паладієм: погляд на реакцію із практичного досвіду

Анотація

Мета. Метою статті було поділитися нашим досвідом роботи з Pd-каталізованим гідруванням і обговорити реакції, що відбувалися всупереч нашим очікуванням, а також висловити своє бачення причин такої незвичайної реакційної здатності.

Результати та їх обговорення. Каталіз є ключовою технологією та однією з центральних тем як нафтохімічної, так і тонкої хімічної промисловості. Хоча він є надзвичайно корисним і надійним підходом, іноді він може дивувати дослідників. У пропонованій статті розглянуто 17 цікавих випадків реакції каталітичного гідрування з нашої практики в Лабораторії синтезів під високим тиском (НВП «Єнамін»). Усі наведені приклади характеризуються своєрідною поведінкою комерційно доступних гетерогенних паладієвмісних каталізаторів (Pd/C або Pd(OH)$_2$). Так, деякі випадки характеризувалися зниженою активністю каталізатора (або навіть повною її втратою). Іншими словами, умови реакції, які ми раніше вважали придатними для відновлення, виявилися «зламаними», і нам довелося шукати нові, часто жорсткіші умови для проведення реакції. Цікаво, що мова йде про класичне Pd-каталізоване гідрування N$^+$–O$^-$ і C=C фрагментів. Певно, ці результати свідчать про різнорідність комерційно доступних каталізаторів і пов'язані з їхньою тонкою внутрішньою структурою, зокрема морфологією поверхні. Іншим цікавим питанням, висвітленим у статті, є хемоселективність каталітичного гідрування. Так, іноді реакція призводила до вражаючих результатів, що суперечили теоретичним поглядам і очікуванням. Насичення бензольних кілець замість дебензилювання (або разом із ним), порушення загального порядку гідрування для сполук, які містять кілька ароматичних частин з різною енергією резонансу, невідтворюваний експеримент, отримання різних продуктів за використання однакових умов, нетипові результати реакцій, каталізованих Pd, – це список тих результатів, які ми спостерігали та обговорюємо в статті. Аналізуючи наявну в літературі інформацію та враховуючи всі зібрані результати, ми схильні вважати причиною цих дивних знахідок наявність у використаних каталізаторах домішок благородних металів (Rh, Ru, Pt). Дослідження несе загальну ідею про те, що комерційні паладієві каталізатори відрізняються за ефективністю, що призводить до значних відмінностей у селективності, часі реакції та виході. З'ясування закономірностей, що стоять за такими емпіричними результатами, безсумнівно, є важливим напрямом досліджень у царині каталізу.

Експериментальна частина. Усі вихідні сполуки, піддавані гідруванню, було синтезовано в ТОВ «Єнамін». Вони мали чистоту не менше 95 %. Використовувані в експерименті каталізатори з паладієм було закуплено у 6 комерційних джерел упродовж 2011−2022 років. Структуру та чистоту синтезованих сполук схарактеризовано методами ^{1}H ЯМР-спектроскопії, рідинної хроматографії в поєднанні з мас-спектрометричним методом, елементного аналізу. Хроматографічні досліди засвідчили, що чистота всіх одержаних сполук становить не менше 95 %.

Висновки. У статті узагальнено досвід роботи з Pd-каталізованим гідруванням і розглянуто випадки незвичайної реактивності або неочікуваних результатів реакцій, які зустрічалися в нашій практиці. Загалом ускладнення, з якими ми зіткнулися, були трьох типів: (1) невідтворюваність процедур, найпевніше, у результаті варіативної активності каталізаторів; (2) проблеми хемоселективності, у випадку присутності в субстраті кількох функціональних груп, здатних до відновлення; (3) небажані реакції дефункціоналізації, каталізовані Pd. Своєю чергою ці ускладнення призвели до збільшення витрат на виробництво, втрати часу та ресурсів. Саме через таку варіабельність ефективності паладієвих каталізаторів потрібно значно більше зусиль, щоб з'ясувати ключові відмінності між комерційними джерелами Pd-каталізаторів, а також створити протоколи, які чітко визначають каталітичну активність кожної партії каталізатора, що дозволяє ідентифікувати високоактивні Pd-каталізатори безпосередньо перед використанням і не втрачати дорогоцінний час та синтетичні матеріали.

Ключові слова: каталіз; гідрування; гетероциклічні сполуки; паладій; селективність; конкурентні процеси

■ Introduction

Catalysis is the most powerful method of controlling and directing chemical reactions, and it is widely used as a viable avenue for preparing compounds, which are hard to access by common catalyst-less approaches. Thus, as of 2002, more than 70% of industrial processes were catalytic, and, indeed, the value has only increased over the years [1]. Moreover, it was estimated that production of more than 90% of all chemical products requires at least one catalytic step [2].

Undoubtedly, the catalytic hydrogenation (and hydrogenolysis as well) has an enormous impact on and constitutes a key technology in petrochemical, fine chemical, pharmaceutical and environmental industries. The statement is eloquently supported by two Nobel prizes awarded to *Paul Sabatier* (1912, "for his method of hydrogenating organic compounds in the presence of finely disintegrated metals…"), and *William S. Knowles* and *Ryoji Noyori* (2001, "for their work on chirally catalyzed hydrogenation reactions") [3–5]. A large-scale conversion of benzene to cyclohexane and the production of *L*-DOPA, a drug used to treat Alzheimer's disease, are instructive examples of the reaction. Over more than 100 years numerous catalysts, both homogeneous and heterogeneous, have been adjusted to the hydrogenation though usually most of them contain a noble-metal core (Au [6], Pt [7], Rh [8], Ru [9], Ir [10], or Pd [11]) as an active site for the reaction. As indicated by a patent landscape analysis, the process of developing new catalysts has accelerated over the last 25 years [12]. Thus, starting from the middle of 1990s more than 1000 patents have appeared in the scientific field as compared to only about 500 for the previous 70 years (from 1925 to 1995). It is noteworthy, that the amount of patents protecting heterogeneous catalysts increases twice as fast as homogeneous ones. The fact accounts for advantages of the heterogeneous nature of former ones as they are recoverable and reusable, hence showing excellent economy properties, as well as suitable for flow chemistry processes. Therefore, it is no wonder that the catalytic hydrogenation occupies about 10–20% of the reactions used to produce chemicals [13].

In this regard, palladium is probably the most widely used metal component in the heterogeneous catalytic hydrogenation with carbon-supported palladium being a well-established heterogeneous catalyst. Thus, the largest number of patent families (1753 for the period of 2011–2015) was identified for palladium. Moreover, this amount is unceasingly growing [14]. About 75% of modern industrial hydrogenation processes are carried out in the presence of a Pd/C catalyst [15] and, no wonder, it is widely applied to the synthesis of various chemicals of industrial and academic interest [16, 17].

Despite the undoubted progress in developing catalytic systems in general and Pd-containing ones in particular, their preparation still involves complex procedures that make it difficult to obtain a reproducible catalytic body [18]. Thus, the way a heterogeneous catalyst is manufactured crucially determines its characteristics, e.g. fine structure, surface characteristics, catalytic activity, selectivity and lifetime. All of the above results in significant variability in the efficiency of commercial sources of palladium on carbon. Such a situation becomes a striking problem as the determination of catalysts' features needed for their effective application is a tedious, time- and resource-consuming task and obviously cannot be accomplished for each batch of the catalyst [1, 19]. For this reason, a few attempts have been made to standardize and determine the qualities of carbon-supported palladium aiming to provide an effective tool for the prediction of the catalyst's efficiency prior to its use and to save valuable synthetic material and time [20–22]. In spite of valuable findings, these studies did not completely eliminate the problem as they inherently contained limitations. Among others, they include awkward procedures and difficult-to-obtain standard substrates. Moreover, the methods developed cannot detect the selectivity of Pd catalysts with respect to structural variations of the substrate. As the result, palladium/carbon catalysts remain a "black box" for synthetic chemists. Nowadays, familiarizing such catalysts is essentially a trial-and-error process requiring extensive testing in order to identify efficient catalysts, and find out suitable reaction parameters of short reaction times and high isolated yields.

Hydrogenation and hydrogenolysis are principal processes in the production cycle of fine chemicals existing in our company (High-pressure Synthesis Laboratory of Enamine Ltd.). Every day we deal with the hydrogenation of numerous substrates, bur not always successfully. From time to time we obtain unexpected results varying from '*conditions found previously do not work*' to '*how is it possible for the compound to be obtained here?*'.

Often, we get in such a tight spot when switching from one catalysts' supplier to another though we could not deny a contribution of the substrate peculiarities to the unwanted outcome.

In this article we would like to share our enormous experience of working with the Pd-catalyzed hydrogenation, as well as in some cases express our vision of the reasons of such an odd reactivity. Nevertheless, this work is not intended to find out and discuss the fundamentals of hydrogenation reactions.

■ Results and discussion

The palladium-catalyzed hydrogenation can be performed with nearly all types of unsaturated bonds. In addition, even single C-O and C-N bonds can be broken under the Pd catalysis. The common range of substrates suitable for the Pd catalysis covers the following 3 groups of organic compounds: (1) unsaturated hydrocarbons and (hetero)arenes; (2) carbonyl-containing compounds; (3) classes with nitrogen-containing multiple bonds. In most of the cases, Pd is either the most satisfactory or one of the most satisfactory catalysts. However, one should emphasize here again that it is a matter of relative rates, the structure of a Pd catalyst, reaction conditions, and so on. In this regard, conditions that we found before to be suitable for reduction (referred to as '*initial conditions*' throughout the paper) sometimes appeared to be "broken" so that we had to search for new, often harsher conditions ('*modified conditions*').

The first example of conditions no longer working is given in Scheme 1. It illustrates the complete reduction of a furan moiety to obtain tetrahydrofuran derivative **2**. Usually, similar reactions proceed readily with a Pd/C catalyst under mild conditions [23, 24]. As there is no data on reducing compound **1** we have found out appropriate conditions enabling such a transformation and including 48-hour protocol. Repeating the reaction later we were stunned by the time required for 100% conversion of the starting furan

(monitoring by ^{1}H NMR) being 7 times more than it was determined before. The change is definitely caused by the activity of the catalyst, which, in turn, is related to its fine internal structure, most likely another surface morphology. The observation brings us back to the question of the reliability and reproducibility of the published procedures. One should note that compound **2** was unknown before. Considering the fact that tetrahydrofuran-3-carboxylates have been found to possess valuable biological properties [25, 26] the approach may provide access to new potent agents.

Nitrogen-containing multiple bonds are another well-established substrate for the Pd-catalyzed reduction [27]. Thus, the hydrogenation of compound **3** was already known [28] (Raney Ni, MeOH, 40°C, 40 atm, 3 h) and was formerly used as a step in the synthesis of potential inotropic agents [29, 30]. Both N-functionalities underwent reduction simultaneously resulting in 4-amino-3-methoxypyridine (**5**). Performing the reaction in the presence of 10% Pd/C we obtained the same result (Scheme 2). However, this interaction was able to surprise us the next time when intermediate N-oxide **4** was observed under the same conditions. In open sources, we were unable to find a similar transformation occurring with loss of nitro and retaining N-oxide moiety, apparently due to their close tendency to reduction. To overcome the problem of the undefined catalyst activity, we tested various conditions and found that Pd(OH)$_2$ gave the desired derivative **5**, and, importantly, the reaction was reproducible. Elucidating the regularities underlying the partial recovery is undoubtedly an interesting area of research in the field of catalysis.

Scheme 3 depicts another unexpected case representing the absence of the catalytic activity of a Pd/C catalyst. Application of the 'initial conditions' led to recovering the starting material. This may sound weird as palladium displays an excellent catalytic performance in the hydrogenation of alkene compounds, even conjugated and partially aromatic, and serves as a classical

336 h
modified conditions

Pd/C 10 %, MeOH
80°C, 100 atm

48 h
initial condtions
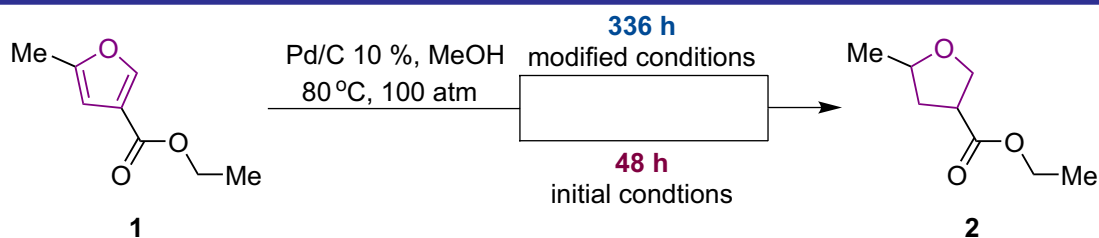
Scheme 1. The furan ring reduction – the reduced catalyst activity
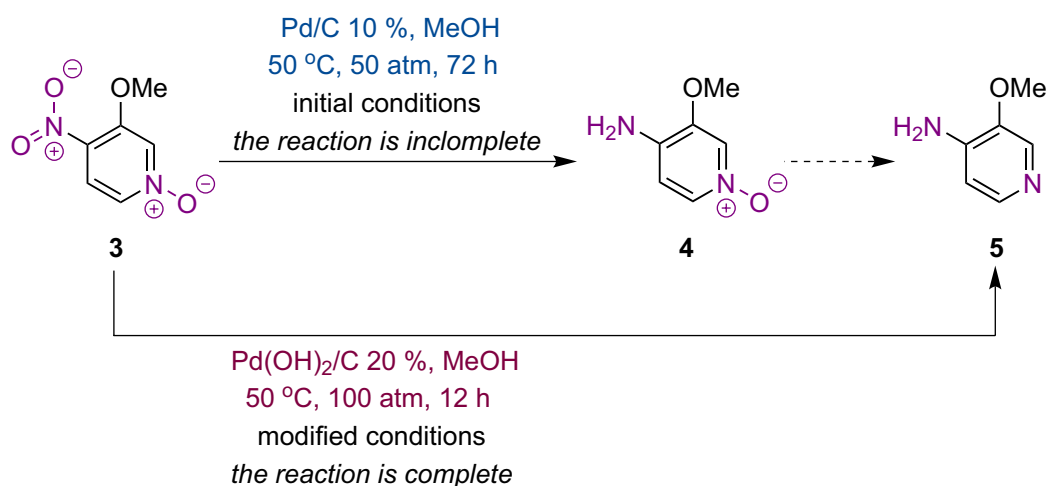
Scheme 2. A partial reduction of the nitropyridine N-oxide

catalyst in such interactions [22, 31]. Moreover, the hydrogenation of the methyl ester required 4 hours to be accomplished under similar conditions [32]. Apparently, the problem was the heterogeneity of the catalyst and the presence of microparticles instead of nanoparticles. We managed to fix the problem and obtained acid **7** applying harsher conditions in an amount of up to 20 g in a run. It is interesting to note that the reaction may have an additional value as the N-methyl derivative of isoquinolone **7** showed high efficacy in inhibiting *E. coli* DNA gyrase [33].

The reductive deoxygenation of ketones allowing the substitution of the C=O group with a CH$_2$ fragment has attracted great attention given its numerous applications in the synthesis of fine chemicals and biofuel production [34]. Since classical methods for the deoxygenation of carbonyl compounds (Barton–McCombie, Clemmensen, Wolff–Kishner methodologies) are generally associated with harsh reaction conditions, the use of stoichiometric amounts of toxic reagents, and the poor functional-group tolerance [35], a number of advanced catalytic protocols for the deoxygenation of carbonyls employing 'green' molecular hydrogen [36–39] have been reported. Some papers describe practical and mild methods for the deoxygenation utilizing supported

palladium catalysts [40–42]. We also contributed to the field as we developed a method for the reductive deoxygenation of ketoacid **8** into tolylbutyric acid **9** promoted by 10% Pd/C catalyst (Scheme 4). As with the previous reactions this protocol turned out to be unreliable. Thus, we worked out a more credible and efficient large-scale procedure employing the Pd(OH)$_2$/C catalytic system. The transformation discussed is described in only one work and based on the 'unfriendly' Huang-Minlon-Wolff-Kishner procedure, which provides compound **9** with lower yields [43]. The fact is important as acid **9** has shown to be a useful agent in treating conditions associated with ER-stress, including diabetes, hypercholesterolemia, atherosclerosis, etc. [44].

The next reaction appeared to be a tough nut to crack for the heterogeneous palladium-catalyzed reduction is the hydrogenation of metanilic acid (**10**), which succumbed to our efforts only once giving cyclohexanesulfonic acid **11** in a low yield. Our multiple later attempts resulted in nothing as the only isolated material was the starting metanilic acid with no signs of its conversion into the target compound according to the LC-MS analysis. Presumably, an answer to the riddle is hidden in the fact that Pd is less active in the saturation of aromatics than other
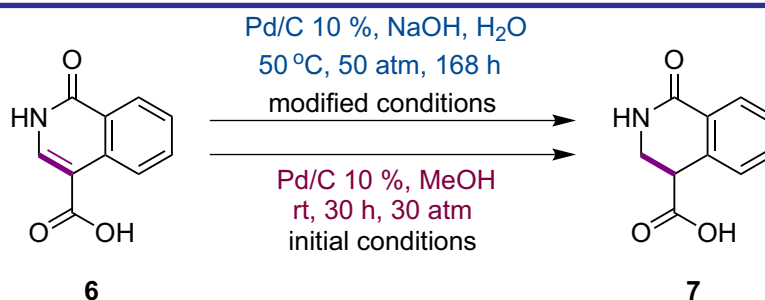
Scheme 3. The search for suitable conditions – conversion of 'alkene' into 'alkane'
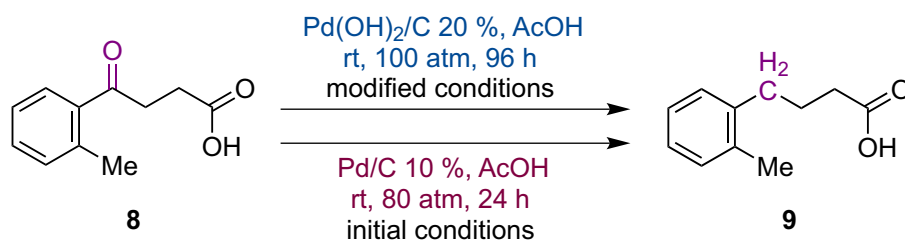
Scheme 4. The search for suitable conditions – reductive deoxygenation
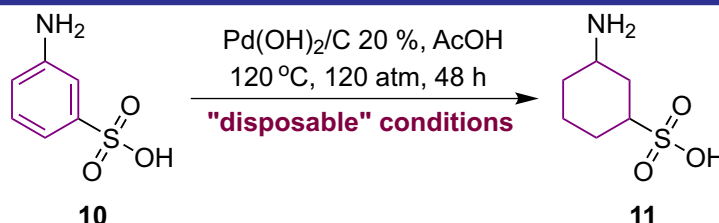
Scheme 5. A single reduction of benzene into cyclohexane

precious metals (Pt, Ru, Rh). Reduction of compound **10** was reported to be successful in good yields under the hydrogenation catalyzed by Rh supported by Al_2O_3 in acidic conditions [45]. Owing to this fact one can suspect that our 'lucky' catalyst contained an impurity of rhodium, which was a real catalyst of the reaction. Thereby, one should keep in mind that catalysts can vary in both a fine structure and purity. If the former mainly affects the activity of the catalyst, the other may turn the reaction in an unexpected direction.

Protecting groups constitute an essential instrument in the synthesis of both natural and artificial chemicals [46]. Synthetic avenues towards complex, often natural, compounds are tricky, requiring multistep protecting group manipulations [47, 48]. Additionally, only a small amount of the starting material can be available, which creates the problem of high yields and selectivity of the deprotection step [49, 50]. In this regard, the palladium-catalyzed hydrogenolysis is one of the most common problems we face. In general, it involves the removal of benzyl ether and N-benzyl protecting groups in order to release OH- and NH-functionalities. Usually everything goes smoothly, and such a deprotection sometimes becomes a serious obstacle on the way to the product, as also reported earlier [51].

Schemes 6 and 7 represent our struggle for O- (azetidinecarboxylic acid **12**) and N-debenzylation (oxazepan **14** and pyrrolidine **16**), respectively. Once deprotected easily under relatively mild ordinary conditions (10% Pd/C, MeOH, 50ºC), the reactions refused to repeat and form the target compounds **13**, **15** and **17** in the presence of the abovementioned catalytic system though some papers described the use of Pd/C in similar

preparation of heterocycles **15** and **17** [52, 53]. As in the previous cases, this is associated with a decrease in the activity of catalysts due to an increase in the particle size and changes in the surface morphology.

However, we have found that the use of palladium hydroxide is a more reliable and reproducible approach, as we noted earlier. The results obtained are somewhat consistent with those reported by *Yong Li et al.* [54]. The paper indicates the absence of the catalytic activity in some cases for Pd/C and Pd(OH)$_2$/C used separately, while their combination serves as an excellent catalyst for the removal of *O*- and *N*-benzyl fragments. Although there is currently no mechanistic basis for this observation, we believe that the formation of a Pd/Pd(OH)$_2$/C mixture during the hydrogenation may contribute to the successful outcome of reactions. Finally, we would like to note that neither the hydrogenolysis of the azetidine derivative **12** nor product **13** is covered in the literature although similar azetidine carboxylic acids have been considered as conformationally constrained GABA or β-alanine analogs and, therefore, have been evaluated for their potency as GABA-uptake inhibitors [55]. Our results expand possibilities for the research, as well as provide a new interesting experimental material for studies in the field of medical chemistry.

While foregoing results mainly concerned issues of the catalyst activity loss and searching for new suitable conditions, the next part of the work is going to highlight various selectivity aspects of the Pd-catalyzed hydrogenation and hydrogenolysis.

Sometimes reactions lead to astonishing results going across theoretical views and expectations.
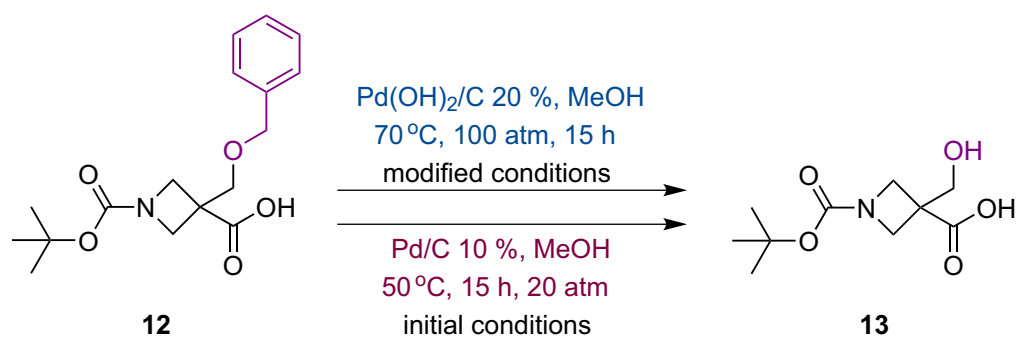
Scheme 6. The search for suitable conditions – *O*-debenzylation
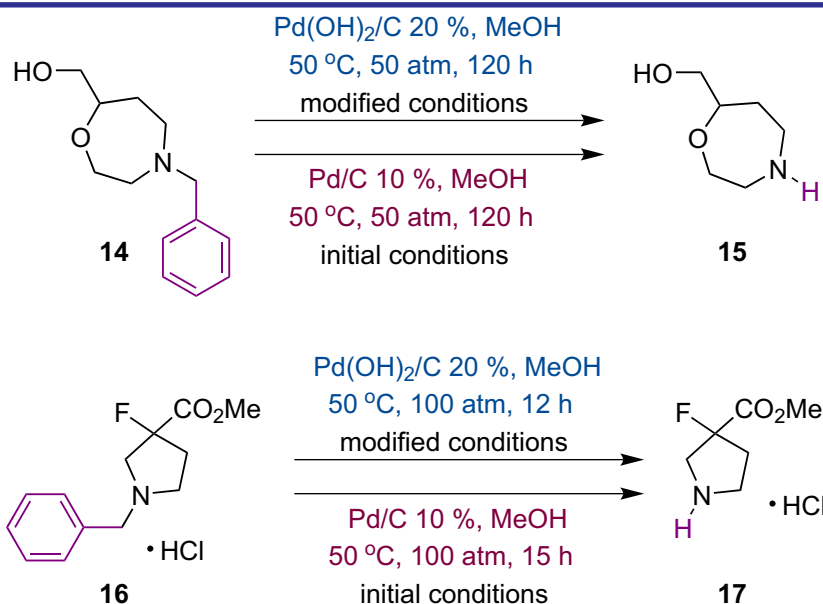
Scheme 7. The search for suitable conditions – *N*-debenzylation

In continuation of the deprotection question Schemes 8 and 9 show a kind of shocking outcomes, which we observed during the *N*- and *O*-debenzylation of derivatives of morpholine **18** and indole **21**, respectively. In the first case, we failed to obtain the target product **20**. Instead, the only recovered compound was cyclohexyl derivative **19**. The latter is obviously formed by the saturation of the benzene ring being the dominant direction of the reaction since we could not detect any traces of the desired morpholinone. The subsequent variations of the reaction conditions did not give compound **19** as well. The situation seems to be strange as palladium is often preferred over other noble-metal catalysts due to its lower propensity to cause the saturation of aromatics [56]. This unexpected dearomatization of the benzyl moiety was previously observed and reported on examples of benzyl and naphthylmethyl ethers [57, 58]. The authors suggested that the process may be attributed to the self-inhibition of the Pd/C catalyst by intramolecular nitrogen-containing basic centers. Although the structural features of substrate **18** may affect the direction of the

interaction, we think that another reasonable explanation would be the presence of other noble metal (Rh, Pt) impurities in the catalyst used.

As indicated by Scheme 9, our initial experiments on the deprotection of benzyloxy derivative **21** resulted in the isolation of ketone **22** as a single product. In this case, the hydrogenolysis was not a terminated step as it was followed by the partial hydrogenation of the benzene moiety. Curiously, despite the lower resonance energy of the separated pyrrole compared to benzene, the former was not hydrogenated during the reaction. Although the data for the debenzylation of exactly compound **21** is not available, there are plenty of other examples of the hydrogenolysis reaction employing 4-benzyloxyindoles (about 340 according to the Reaxys® database). Interestingly, all the reactions give exclusively 4-hydroxyindoles with no any allusion to ketones similar to **22**. Thus, being surprised but interested in getting additional portions of compound **22**, we increased the reaction scale to 50 g. Another surprise awaited us. The recovered material was a 3 to 1 mixture of phenol **23** and ketone **22**
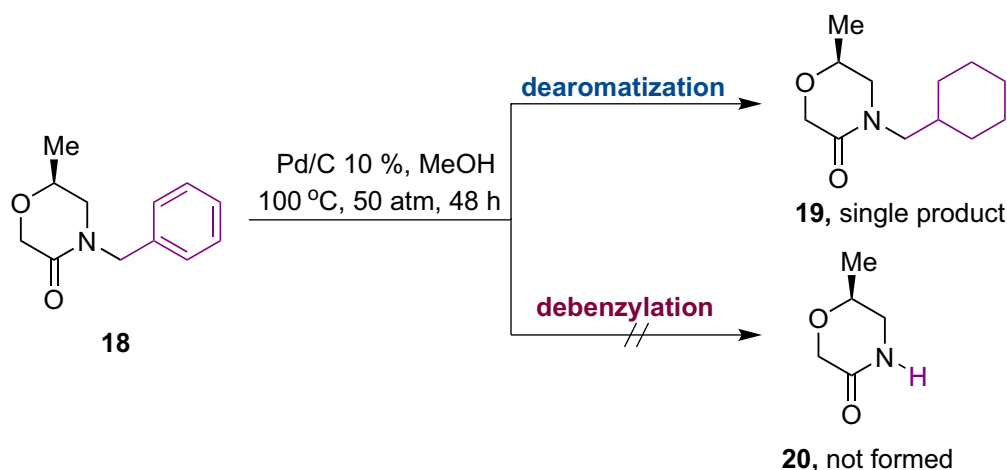
Scheme 8. An unexpected dearomatization of benzene
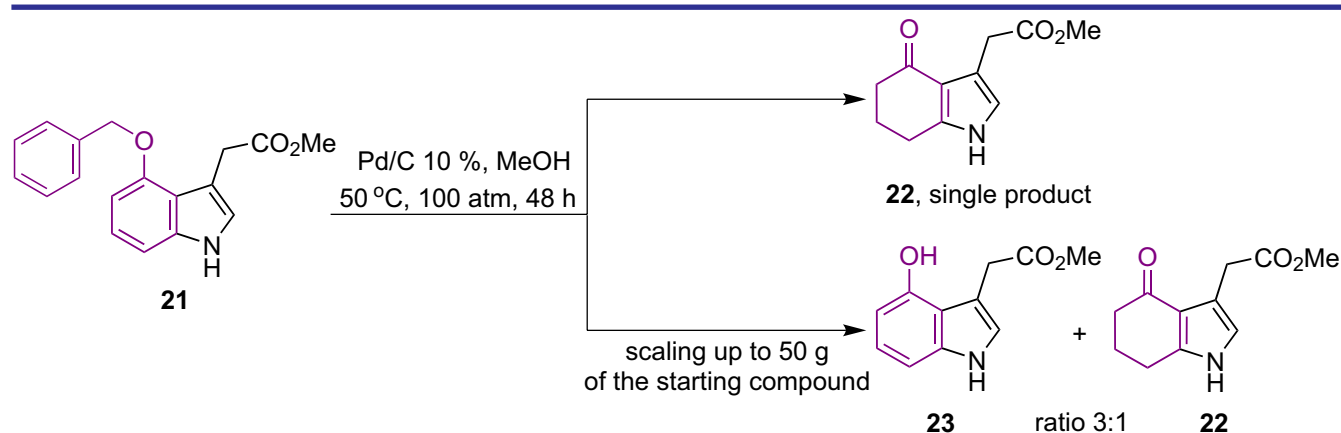
Scheme 9. An unexpected hydrogenation of the benzene moiety of indole

according to LC-MS data. The result allows us to suggest that a stepwise format of the reaction includes a primary debenzylation step followed by the benzene moiety reduction. We also tend to believe that the presence of precious metal (Rh, Pt) impurities is the cause for this behavior. Inspired by the latest experiment, we are currently making constant attempts to solve the problem and find suitable as well as reproducible reaction conditions that provide exclusively any of products **22** and **23**.

In contrast to Scheme 9, the hydrogenation of benzofuran **24** proceeded the way it was expected with the reduction of the 'less aromatic' furan moiety of the molecule and gave dihydro derivative **25** (Scheme 10). The only difficulty that we encountered was the irreproducibility of conditions previously found to be suitable. Subsequently, we managed to find satisfactory ones giving compound **25** with any batch of the catalyst.

Minor structural variations of benzofuran **24**, namely the substitution of benzene moiety with the pyridine core, drastically changed the direction of the hydrogenation reaction promoted by

10% Pd/C (Scheme 11). Thus, the reduction of furo[3,2-*c*]pyridine-2-carboxylic acid (**26**) did not give the expected 2,3-dihydro product **30**. Moreover, the selectivity observed for benzofuran **24** was lost. As evidenced results of LC-MS and ^{1}H NMR investigations of the isolated mixture, the reduction occurred stepwise with the pyridine ring reduced first (compound **27**) followed by the formation of perhydro derivative **28**. Even more interesting, numerous studies report a reduction exclusively for the furan moiety for variously substituted furo[3,2-*c*]pyridines. The information about the complete reduction of furo[3,2-*c*]pyridines is not available as well. We did not succeed in elaborating more selective conditions using Pd-containing catalysts. So far, selective reduction of compound **26** remains an open question definitely deserving attention as some 4,5,6,7-tetrahydrofuro[3,2-*c*]pyridines and octahydrofuro[3,2-*c*]pyridines have proven to be valuable pharmaceutical components [59, 60].

Another interesting example for discussing the chemoselectivity of the catalytic hydrogenation is given in Scheme 12. Compound **31** comprises 2 aromatic fragments of benzene and pyridine
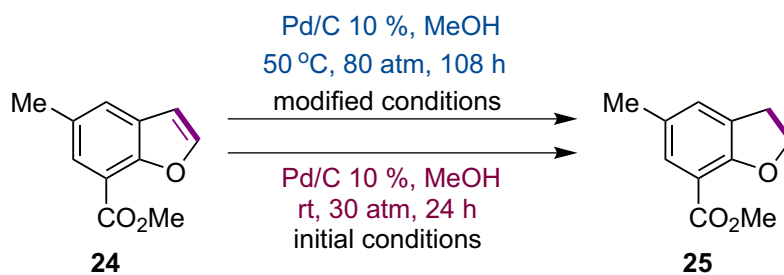
Scheme 10. The search for suitable conditions – benzofuran reduction
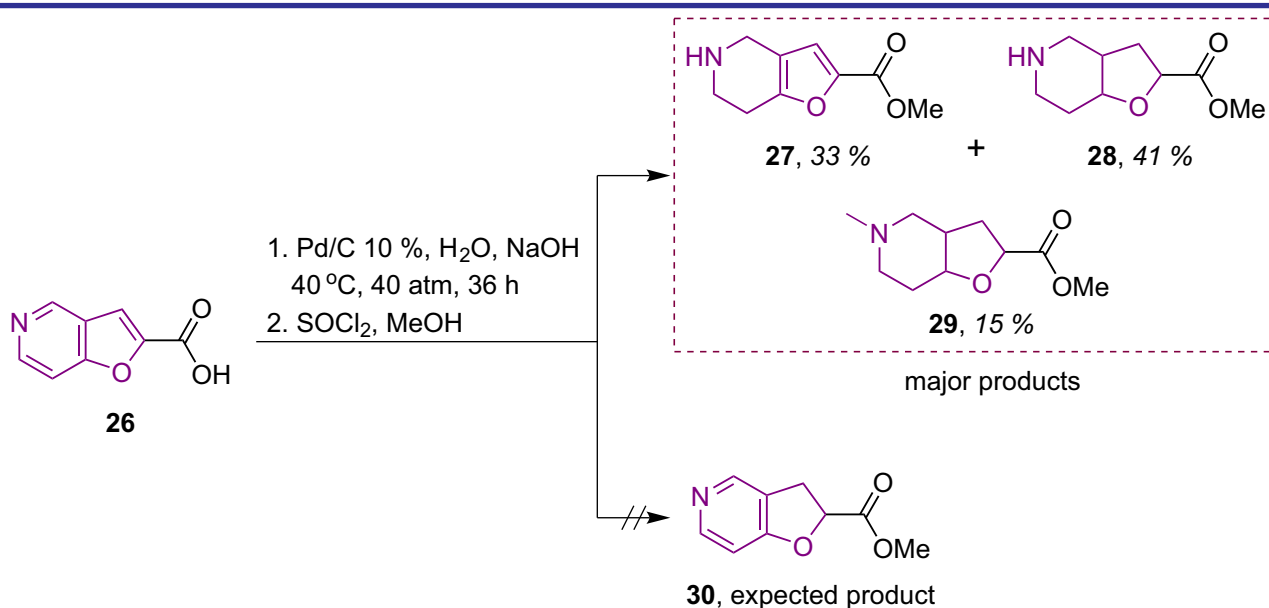
Scheme 11. Competing pathways in reduction of furo[3,2-*c*]pyridine
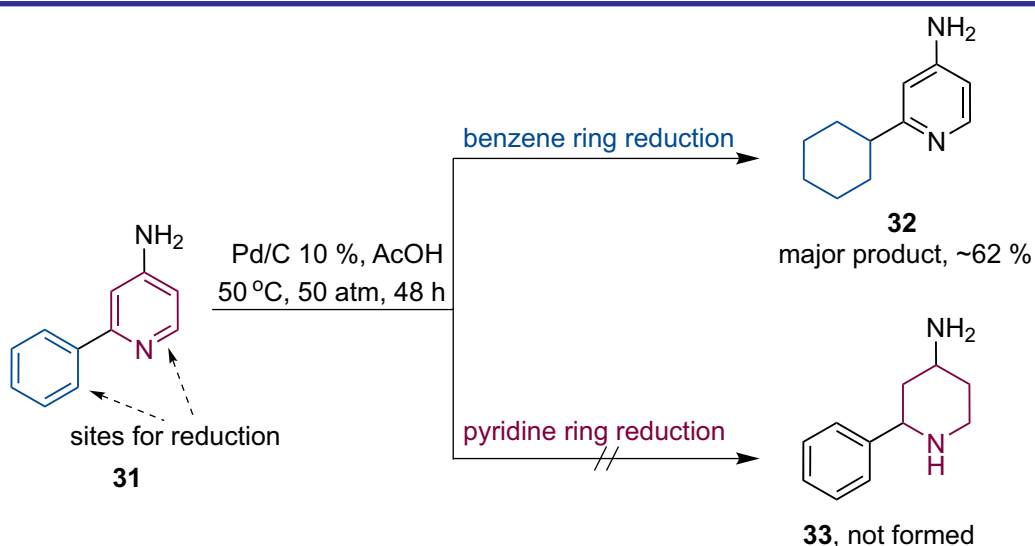
Scheme 12. Competing pathways in reduction of 2-phenylpyridine

joined by a σ-bond and both are potential sites for the catalytic reduction. Numerous studies examining the Pd-catalyzed reduction of 2-phenylpyridines have shown that the hydrogenation of the pyridine ring is best performed under acidic conditions, and phenyl rings are usually not reduced in significant amounts during the process [14, 61, 62]. We were able to find only three examples reporting the non-selective reduction of both pyridine and benzene fragments of the 2-phenylpyridine platform. Interestingly, all of these studies work with other precious metals – Ru(0) [63], Rh(II) [64], Pt(0) [65]. Moreover, the application of Ru(0) allowed the neutral benzene
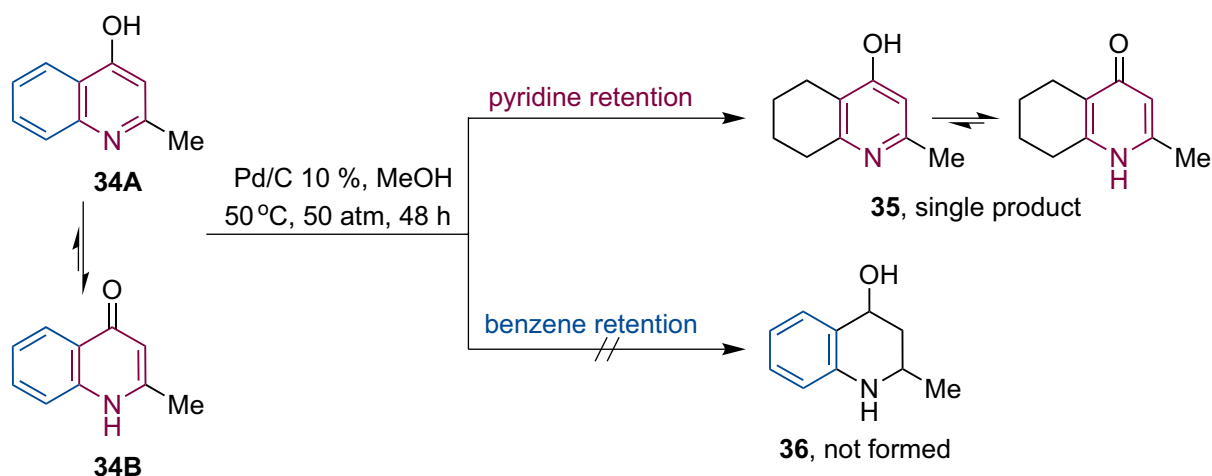
Scheme 13. Competing pathways in reduction of quinoline
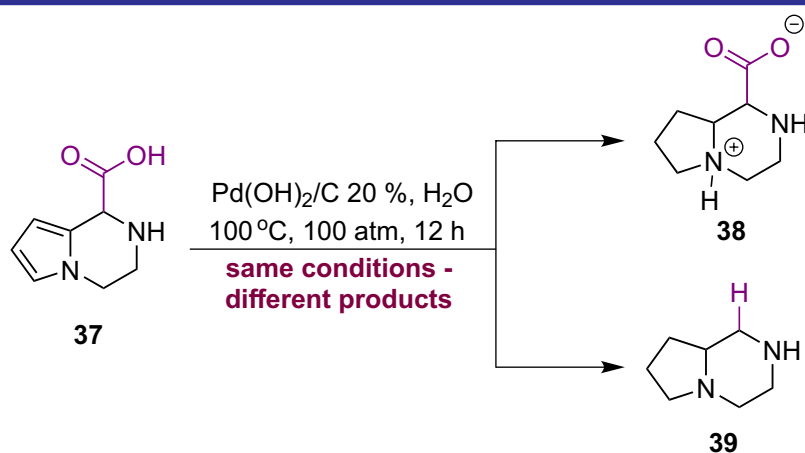
Scheme 14. An unexpected reductive decarboxylation

ring to be selectively reduced instead of the more electron-deficient pyridine ring, implying a possible directed hydrogenation by a Ru(0) catalyst. Interestingly, in our experiments on the Pd/C promoted hydrogenation of compound **31**, a dominant compound in the isolated mixture was also 2-cyclohexylpyridine **32** and not the product of the reverse chemoselectivity – piperidine **33** (according to ¹H NMR and LC-MS data). Again, we have the ground to suspect contamination of the Pd-catalyst with more active noble metals leading to controversial results.

The last substrate, we want to discuss, with two alternative centers for hydrogen attack is 4-hydroxy-2-methylquinoline (**34**). Its structure implies the formation of products **35** and **36** retaining pyridine and benzene moieties, respectively. Taking into account theoretical views of the aromaticity of benzene and pyridine one may predict that the pyridine moiety is more likely reduced as a less thermodynamically stable one. Moreover, compound **34** exists as two tautomers. In tautomer **B**, the pyridine ring loses aromaticity and becomes more susceptible to reduction as

usual (though conjugated) alkene. Nevertheless, despite our conclusions, the reaction turned out to be chemoselective giving compound **35** as the only product. Our observations are fully supported by other works reporting the same results for various 4-hydroxyquinolines in the presence of different catalytic systems [66, 67]. So far, a reasonable explanation of the experimental results is not available.

The last part of the paper discloses three amusing instances of the hydrogenation where other functionalities were involved.

The first reaction is the hydrogenation of 1,2,3,4-tetrahydropyrrolo[1,2-*a*]pyrazine-1-carboxylic acid (**37**) (Scheme 14). It was quite curious to obtain different products **38** and **39** while utilizing identical reaction conditions. If compound **38** was much expectable and desirable in the reaction, the isolation of decarboxylated derivative **39** made us feel confused. Even though reductive decarboxylation is a modern technique experiencing intensive investigations [68, 69], its proceeding is unwanted as other synthetic approaches towards compound **38** are complicated
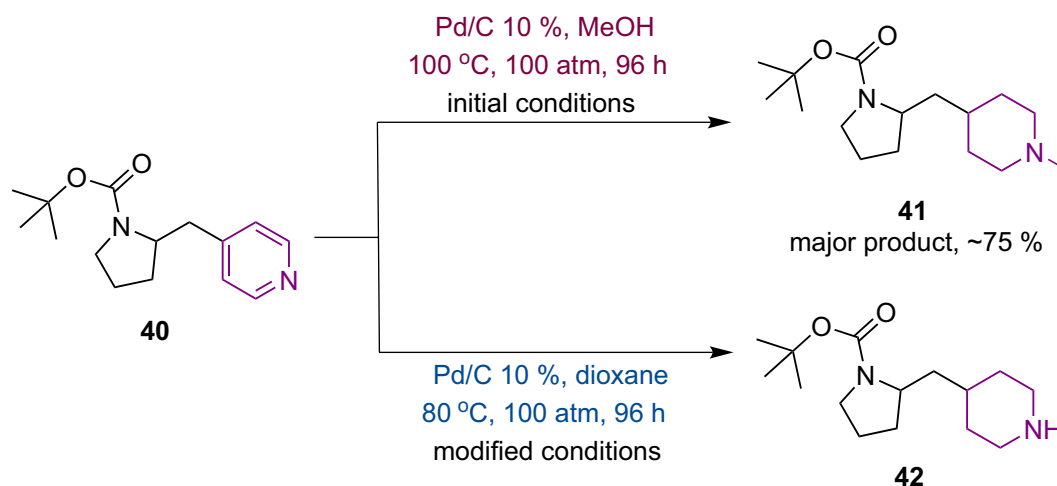
Scheme 15. An unexpected reductive *N*-methylation with methanol
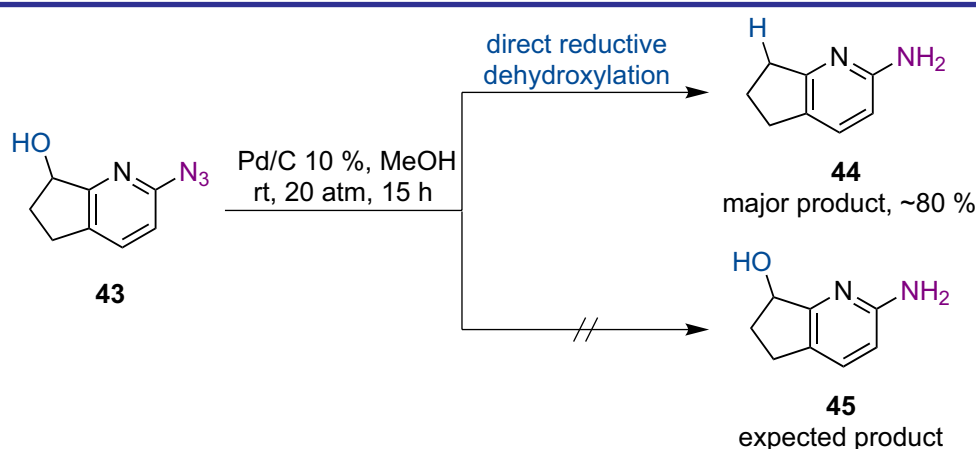
Scheme 16. An unexpected reductive dihydroxylation

and time-consuming [70]. The main question caused by the experiment is "*What is the reason for the decarboxylation and how to ensure that the same Pd-catalyzed reduction conditions give the same result?*". Unfortunately, there is no answer at the moment. We can only assume that the presence of free metal impurities can cause primary decarboxylation of the starting acid **37** followed by reduction.

We observed an undesired *N*-methylation while reducing compound **40** in the methanol solution and producing derivative **41** as a major component in the mixture. The Pd-catalyzed *N*-methylation is already known; it is sometimes used intentionally in order to obtain and simultaneously modify primary or secondary amino groups [71, 72]. To avoid the continuation of this process, we replaced methanol with indifferent 1,4-dioxane, having managed to isolate the target piperidine **42**, which is of interest for medical chemistry and is used in the synthesis of substances having a remarkable activity that inhibits the hepatocyte growth factor receptor, and thus exhibit the antitumor activity, the activity

that inhibits angiogenesis, and the activity that inhibits cancer metastasis [73].

The alcohol dehydroxylation is probably one of the fundamental transformations in organic chemistry as it plays a great role in the total synthesis of complex natural products [74]. Recently, several protocols for the reductive dihydroxylation have been published utilizing Ir and Fe catalysts [75, 76]. Palladium is not a common catalyst for the reaction [14]. In this regard, the isolation of dehydroxylated derivative **44** as a main product in the Pd/C catalyzed hydrogenation of azidoalcohol **43** was quite surprising. The formation of such a product shows that the formal debenzylation of **43** is more advantageous than the reduction of the pyridine ring. We are currently working on finding suitable reaction conditions that allow us to purposefully obtain any of the products.

■ Conclusions

Although catalytic hydrogenation reactions are vital transformations for all branches of chemical industry, commercial palladium catalysts are

variable in their fine structure (size of Pd particles, surface morphology, other metals impurities, etc.) and, consequently, in the efficiency, resulting in significant differences in selectivity, reaction times, and yields. In the paper, we have summarized our experience with Pd/C-catalysts from different commercial sources for the hydrogenation reaction and presented cases of unusual reactivity or unexpected outcomes of the reactions encountered in our practice. In general, complications we faced were of three types: (1) irreproducibility of the procedures most likely as the result of a changeable activity of the catalysts; (2) chemoselectivity issues when two or multireducible functional groups were present in the substrate; (3) undesirable Pd-catalyzed defunctionalization reactions. In turn, these complications led to increase in production costs, loss of time and resources. Therefore, because of this variability in the efficiency of Pd catalysts, far more efforts are required to find out the key differences between commercial sources of Pd catalysts, as well as to create protocols clearly defining the catalytic activity of each batch of the catalyst. Moreover, modern chemists need to have clear criteria and regulations of catalysts' quality without wasting precious time and synthetic materials.

■ Experimental part

All starting compounds exposed to hydrogenation were synthesized in Enamine Ltd. and had purity of not less than 95%. Different batches of palladium-containing catalysts used in the experiment were purchased from commercial sources (Daming Ruiheng Chemical Co., Ltd; Hangzhou J & H Chemical Co., Ltd.; Junda Pharm Chem Plant Co., Ltd.; Leap Labchem Co., Ltd; Shanghai Linsai Trade Co., Ltd.; SLN Pharmachem) within a period of 2011–2022. The solvents were distilled prior to the use. If needed, the reactions progress was monitored by ^{1}H NMR spectroscopy. The melting points were measured in open capillary tubes and given uncorrected. ^{1}H NMR spectra were recorded on a Bruker 170 Avance 500 spectrometer (500 MHz), or a Varian Unity Plus 400 spectrometer (400 MHz) in a DMSO-d_6, CDCl$_3$ or D$_2$O solution using tetramethylsilane as an internal standard. Chemical shifts were expressed in δ (ppm) units with the following description: *s* was for a singlet, *d* – a doublet, *t* – a triplet, *q* – a quartet, *p* – a pentet, *m* – a multiplet, *br*. – broadened. Mass spectra were recorded on an Agilent 1100 LCMSD SL instrument (an atmospheric pressure electrospray ionization (ES-API)) and an Agilent 5890 Series II 5972 GCMS instrument (an electron impact ionization (EI)). Chromatographic experiments revealed the purity of all tested compounds being not less than 95%. The elemental analysis was carried out in the Analytical Chemistry Laboratory of the Institute of Organic Chemistry, National Academy of Sciences of Ukraine.

Ethyl 5-methyltetrahydrofuran-3-carboxylate (2)

The solution of ethyl 5-methylfuran-3-carboxylate (**1**) (100 g, 0.649 mol) in methanol (800 mL) was charged with 10% palladium on carbon (10 g). The mixture was placed in an autoclave and hydrogenated at 80°C and 100 atm of hydrogen for 336 h. The autoclave was vented, after that the catalyst was filtered off. The solvent was removed under reduced pressure to give the title compound.

A colorless oil. Yield – 95.2 g (92.8%). Anal. Calcd for C$_8$H$_{14}$O$_3$, %: C 60.74; H 8.92. Found, %: C 60.54; H 8.98. ^{1}H NMR (400 MHz, CDCl$_3$), δ, ppm: 1.21–1.35 (6H, m, 2×CH$_3$); 1.77 (1H, dt, *J* = 12.5, 8.6 Hz, H-4^{fur}); 2.27 (1H, ddd, *J* = 12.0, 8.7, 5.6 Hz, H-4^{fur}); 3.11 (1H, qd, *J* = 8.3, 5.7 Hz, H-3^{fur}); 3.86–4.03 (2H, m, H-2^{fur}+H-5^{fur}); 4.09 (1H, dd, *J* = 8.8, 5.7 Hz, H-2^{fur}); 4.16 (2H, q, *J* = 7.1 Hz, OC<u>H</u>$_2$CH$_3$). LC-MS (ES-API), *m/z*: 159.1 [M+H]$^+$.

4-Amino-3-methoxypyridine 1-oxide (4)

To the solution of 3-methoxy-4-nitropyridine 1-oxide (**3**) (87 g, 0.512 mol) in methanol (1500 mL) 10% strength palladium on carbon (8.7 g) was added. The mixture was hydrogenated in an autoclave at 50°C and 50 atm of hydrogen for 72 h. The catalyst was then filtered off, and the solvent was removed under reduced pressure to give the title compound.

A red solid. Yield – 68.13 g (95.1%). Anal. Calcd for C$_6$H$_8$N$_2$O$_2$, %: C 51.42; H 5.75; N 19.99. Found, %: C 51.20; H 5.81; N 20.13. ^{1}H NMR (400 MHz, DMSO-d_6), δ, ppm: 3.79 (3H, s, OCH$_3$); 5.83 (2H, s, NH$_2$); 6.49 (1H, d, *J* = 6.8 Hz, H-5^{pyr}); 7.56 (1H, dd, *J* = 6.8, 1.9 Hz, H-6^{pyr}); 7.75 (1H, d, *J* = 2.0 Hz, H-2^{pyr}). LC-MS (ES-API), *m/z*: 141.0 [M+H]$^+$.

3-Methoxypyridin-4-amine (5)

To the solution of 3-methoxy-4-nitropyridine 1-oxide (**3**) (84.8 g, 0.499 mol) in methanol (1500 mL) 20% strength palladium hydroxide on carbon (8.5 g) was added. The mixture was hydrogenated in an autoclave at 50°C and 100 atm of hydrogen for 120 h. After full conversion of the starting compound the autoclave was vented, and the

catalyst was filtered off. The solvent was then removed under reduced pressure to give the target compound.

A brown powder. Yield – 60.18 g (97.3%). M. p. 88–90°C. Anal. Calcd for $C_6H_8N_2O$, %: C 58.05; H 6.50; N 22.57. Found, %: C 58.23; H 6.36; N 22.72. ^1H NMR (400 MHz, DMSO-d_6), δ, ppm: 3.80 (3H, s, OCH_3); 5.64 (2H, s, NH_2); 6.53 (1H, d, J = 5.2 Hz, H-5^{pyr}); 7.73 (1H, d, J = 5.2 Hz, H-6^{pyr}); 7.87 (1H, s, H-2^{pyr}). LC-MS (ES-API), m/z: 125.0 [M+H]$^+$.

1-Oxo-1,2,3,4-tetrahydroisoquinoline-4-carboxylic acid (7)

1-Oxo-1,2-dihydroisoquinoline-4-carboxylic acid (**6**) (70 g, 0.367 mol) was dissolved in 3500 mL of a water solution of NaOH (14.69 g, 0.367 mol) and 10% strength palladium on carbon (7 g) was then added. The mixture was placed in an autoclave and hydrogenated at 50°C and 50 atm of hydrogen for 168 h. The autoclave was vented, after that the catalyst was filtered off, and the filtrate was acidified with sodium bisulfate. The precipitate formed was filtered off, and the crude product was recrystallized from isopropyl alcohol.

A white solid. Yield – 21.61 g (30.5%). M. p. 218–220°C. Anal. Calcd for $C_{10}H_9NO_3$, %: C 62.82; H 4.75; N 7.33. Found, %: C 62.97; H 4.83; N 7.17. ^1H NMR (500 MHz, DMSO-d_6), δ, ppm: 3.54–3.68 (2H, m, CH_2); 3.83–3.95 (1H, m, CH); 7.35–7.41 (2H, m, ArH); 7.51 (1H, t, J = 7.7 Hz, ArH); 7.83 (1H, d, J = 7.9 Hz, ArH); 7.94 (1H, d, J = 5.5 Hz, NH); 12.85 (1H, br. s, COOH). LC-MS (ES-API), m/z: 192.1 [M+H]$^+$.

4-(*o*-Tolyl)butanoic acid (9)

4-Oxo-4-(*o*-tolyl)butanoic acid (**8**) (85 g, 0.443 mol) was dissolved in acetic acid (800 mL) followed by adding 10% palladium on carbon (8.5 g), and the mixture was hydrogenated at room temperature and 80 atm of hydrogen for 24 h. After completion of the reaction the solid was filtered off, the solvent was removed under reduced pressure, and the residue was recrystallized from hexane.

A white fluffy solid. Yield – 75.1 g (95.3%). M. p. 55–57°C. Anal. Calcd for $C_{11}H_{14}O_2$, %: C 74.13; H 7.92. Found, %: C 74.01; H 8.05. ^1H NMR (400 MHz, DMSO-d_6), δ, ppm: 1.74 (2H, p, J = 7.5 Hz, $CH_2C\underline{H}_2CH_2$); 2.17–2.31 (5H, m, CH_3Ar+CH_2Ar); 2.53–2.60 (2H, m, $C\underline{H}_2COOH$); 7.00–7.16 (4H, m, ArH); COOH proton is in exchange. LC-MS (ES-API), m/z: 177.2 [M-H]$^-$.

3-Aminocyclohexane-1-sulfonic acid (11)

To the solution of 3-aminobenzenesulfonic acid (**10**) (20 g, 0.116 mol) in acetic acid (400 mL)

20% palladium hydroxide on carbon (2.0 g) was added. The mixture was then hydrogenated at 120°C and 120 atm of hydrogen for 48 h. After the reaction was completed, the solid was filtered off, and the solvent was removed under reduced pressure. The residue was treated with methanol to give the title product.

A white powder. Yield – 7.8 g (37.7%). M. p. 232–234°C. Anal. Calcd for $C_6H_{13}NO_3S$, %: C 40.21; H 7.31; N 7.81. Found, %: C 40.39; H 7.16; N 7.72. ^1H NMR (400 MHz, D_2O), δ, ppm: 1.23–2.63 (8H, m); 2.80–3.95 (2H, m). LC-MS (ES-API), m/z: 180.2 [M+H]$^+$.

1-(*tert*-Butoxycarbonyl)-3-(hydroxymethyl)azetidine-3-carboxylic acid (13)

3-((Benzyloxy)methyl)-1-(*tert*-butoxycarbonyl)-azetidine-3-carboxylic acid (**12**) (130 g, 0.405 mol) was dissolved in methanol (1500 mL) and 20% palladium hydroxide on carbon (13 g) was added to the solution. The mixture was placed in an autoclave and hydrogenated at 70°C and 100 atm of hydrogen for 15 h. After cooling the autoclave was vented, the catalyst was filtered off, and the solvent was removed under reduced pressure. The residue was treated with isopropyl alcohol to give the title product.

A white solid. Yield – 87.27 g (93%). M. p. 175–177°C. Anal. Calcd for $C_{10}H_{17}NO_5$, %: C 51.94; H 7.41; N 6.06. Found, %: C 52.08; H 7.32; N 6.14. ^1H NMR (400 MHz, DMSO-d_6), δ, ppm: 1.35 (9H, s, 3×CH_3); 3.65 (2H, s, CH_2O); 3.73–4.00 (4H, m, 2×CH_2N); COOH and OH protons are in exchange. LC-MS (ES-API), m/z: 230.2 [M-H]$^-$.

(1,4-Oxazepan-7-yl)methanol (15)

The solution of (4-benzyl-1,4-oxazepan-7-yl)-methanol (**14**) (75 g, 0.339 mol) in methanol (1500 mL) containing 20% palladium hydroxide on carbon (7.5 g) was hydrogenated in an autoclave at 50°C and 50 atm of hydrogen for 120 h. After the reaction was completed, the catalyst was filtered off, and the solvent was removed under reduced pressure to give the title compound as an oil.

A pink yellow oil. Yield – 43.43 g (97.7%). Anal. Calcd for $C_6H_{13}NO_2$, %: C 54.94; H 9.99; N 10.68. Found, %: C 55.11; H 10.09; N 10.48. ^1H NMR (400 MHz, CDCl$_3$), δ, ppm: 1.49–1.65 (1H, m); 1.73–1.90 (1H, m); 1.95–2.08 (2H, m); 2.75–3.10 (4H, m); 3.32–3.50 (2H, m); 3.51–3.68 (1H, m); 3.69–3.85 (1H, m); 3.88–4.05 (1H, m). LC-MS (ES-API), m/z: 132.2 [M+H]$^+$.

Methyl 3-fluoropyrrolidine-3-carboxylate hydrochloride (17)

To the solution of methyl 1-benzyl-3-fluoropyrrolidine-3-carboxylate hydrochloride (**16**)

(175 g, 0.641 mol) in methanol (1500 mL) 20% palladium on carbon (13 g) was added. The mixture was hydrogenated at 50°C and 100 atm of hydrogen for 12 h. The autoclave was vented, and the catalyst was filtered off. The solvent was removed under reduced pressure to give the title compound.

A yellow powder. Yield – 110.5 g (94.2%). M. p. 153–155°C. Anal. Calcd for $C_6H_{11}ClFNO_2$, %: C 39.25; H 6.04; N 7.63. Found, %: C 39.41; H 6.10; N 7.82. ^{1}H NMR (400 MHz, DMSO-d_6), δ, ppm: 2.28–2.47 (2H, m); 3.24–3.34 (1H, m); 3.42–3.68 (3H, m); 3.77 (3H, s, OCH_3); 10.25 (2H, s, NH_2);. LC-MS (ES-API), m/z: 148.1 [M-Cl]$^+$.

(S)-4-(Cyclohexylmethyl)-6-methylmorpholin-3-one (19)

The title compound was prepared according to the procedure given below. Although the structure of the reaction product, as well as its purity, was confirmed while analyzing an aliquot by ^{1}H NMR and LC-MS methods, it was not isolated by the reason of low prospects for further modification.

(*S*)-4-Benzyl-6-methylmorpholin-3-one (**18**) (74 g, 0.361 mol) was dissolved in methanol (800 mL) and 10% palladium on carbon (7.4 g) was then added. The mixture was exposed to hydrogenation at 100°C and 50 atm of hydrogen for 48 h. When the time was over, a 20 mL aliquot of the solution was taken, the solvent was evaporated, and the residue was analyzed by ^{1}H NMR and LC-MS methods.

^{1}H NMR (400 MHz, DMSO-d_6), δ, ppm: 0.78–0.96 (2H, m, CH^{chex}); 1.06–1.25 (6H, m, CH_3+CH^{chex}); 1.51–1.75 (6H, m, CH^{chex}); 3.00–3.26 (4H, m, 2×CH_2N); 3.85 (1H, dqd, J = 9.1, 6.1, 3.1 Hz, $CH_3C\underline{H}$); 4.02 (2H, s, CH_2O). LC-MS (ES-API), m/z: 212.1 [M+H]$^+$.

Methyl 2-(4-oxo-4,5,6,7-tetrahydro-1*H*-indol-3-yl)acetate (22)

To the solution of methyl 2-(4-(benzyloxy)-1*H*-indol-3-yl)acetate (**21**) (5 g, 0.017 mol) in methanol (100 mL) 10% palladium on carbon (0.5 g) was added. The mixture was hydrogenated at 50°C and 100 atm of hydrogen for 48 h. Then the catalyst was filtered off, and the solvent was removed under reduced pressure. The residue was treated with isopropyl alcohol to give the title compound.

A brown powder. Yield – 1.65 g (47%). Anal. Calcd for $C_{11}H_{13}NO_3$, %: C 63.76; H 6.32; N 6.76. Found, %: C 63.54; H 6.43; N 6.87. ^{1}H NMR (400 MHz, DMSO-d_6), δ, ppm: 1.97 (2H, p, J = 6.1 Hz, H-6); 2.21 – 2.30 (2H, m, H-7); 2.71 (2H,

t, J = 6.1 Hz, H-5); 3.55 (3H, s, CH_3); 3.62 (2H, s, CH_2CO); 6.58 (1H, d, J = 2.0 Hz, H-2); 11.14 (1H, s, NH). LC-MS (ES-API), m/z: 208.1 [M+H]$^+$.

Methyl 5-methyl-2,3-dihydrobenzofuran-7-carboxylate (25)

Methyl 5-methylbenzofuran-7-carboxylate (**24**) (52 g, 0.274 mol) was dissolved in methanol (1000 mL), and the solution was charged with 10% palladium on charcoal (5.2 g). The mixture was hydrogenated in an autoclave at 50°C and 80 atm of hydrogen for 108 h. The resulting mixture was filtered, and the filtrate was evaporated *in vacuo* to give the target compound.

A white powder. Yield – 49.2 g (93.6%). Anal. Calcd for $C_{11}H_{12}O_3$, %: C 68.74; H 6.29. Found, %: C 68.52; H 6.38. ^{1}H NMR (400 MHz, DMSO-d_6), δ, ppm: 2.23 (3H, s, CH_3Ar); 3.14 (2H, t, J = 8.8 Hz, CH_2Ar); 3.77 (3H, s, OCH_3); 4.57 (2H, t, J = 8.8 Hz, OCH_2); 7.24 (1H, s, ArH); 7.37 (1H, s, ArH). LC-MS (ES-API), m/z: 193.1 [M+H]$^+$.

2-Methyl-5,6,7,8-tetrahydroquinolin-4(1*H*)-one (35)

The solution of 2-methylquinolin-4-ol (**34**) (150 g, 0.943 mol) in methanol (1500 mL) was charged with 10% strength palladium on carbon (15 g). The resulting mixture was hydrogenated at 50°C and 50 atm of hydrogen for 48 h. After the time was over, the solid was filtered off, and the filtrate was evaporated to dryness in a vacuum evaporator to give the title compound.

A beige powder. Yield – 149 g (96.9%). M. p. 239–241°C. Anal. Calcd for $C_{10}H_{13}NO$, %: C 73.59; H 8.03; N 8.58. Found, %: C 73.71; H 7.92; N 8.54. ^{1}H NMR (500 MHz, DMSO-d_6), δ, ppm: 1.53–1.71 (5H, m); 2.11 (3H, s, CH_3); 2.18–2.26 (3H, m); 5.75 (1H, s, H-3); 10.88 (1H, s, NH). LC-MS (ES-API), m/z: 164.2 [M+H]$^+$.

Octahydropyrrolo[1,2-*a*]pyrazine-1-carboxylic acid (38) and octahydropyrrolo[1,2-*a*]pyrazine (39)

The title compounds turned out to be the products of the hydrogenation reaction utilizing the same starting compound and the same conditions (given below), but using different batches of 20% Pd(OH)$_2$/C catalyst. The loadings of the initial pyrrole were 0.5 g to have octahydropyrrolo[1,2-*a*]pyrazine and 3.2 g for octahydropyrrolo[1,2-*a*]pyrazine-1-carboxylic acid. The procedure below is given for an occasion of the decarboxylated derivative; for another product, the quantities are proportional.

The solution of 1,2,3,4-tetrahydropyrrolo[1,2-*a*]pyrazine-1-carboxylic acid (**37**) (0.5 g, 0.003 mol) in water (10 mL) was loaded with 20% palladium

hydroxide on carbon (0.05 g), and the mixture was hydrogenated at 100°C and 100 atm of hydrogen for 12 h. After completion of the reaction the catalyst was filtered off, and the solvent was evaporated under reduced pressure providing the title compound.

Octahydropyrrolo[1,2-a]pyrazine-1-carboxylic acid (**38**)

A white powder. Yield – 3.11 g (95%). Anal. Calcd for $C_8H_{14}N_2O_2$, %: C 56.45; H 8.29; N 16.46. Found, %: C 56.28; H 8.41; N 16.68. ^{1}H NMR (500 MHz, DMSO-d_6), δ, ppm: 1.26 (1H, s); 1.53–1.81 (4H, m); 2.06 (2H, q, $J = 8.8$ Hz); 2.22 (1H, t, $J = 12.0$ Hz); 2.76 (1H, t, $J = 12.2$ Hz); 2.90–3.11 (3H, m); 3.21 (1H, d, $J = 11.8$ Hz); 8.36 (1H, s, NH^+). LC-MS (ES-API), m/z: 171.1 [M+H]$^+$.

Octahydropyrrolo[1,2-a]pyrazine (**39**)

A colorless oil. Yield – 0.35 g (92%). B. p. 85–88°C (0.03 atm). Anal. Calcd for $C_7H_{14}N_2$, %: C 66.62; H 11.18; N 22.20. Found, %: C 66.73; H 11.05; N 22.38. ^{1}H NMR (400 MHz, DMSO-d_6), δ, ppm: 1.07–1.28 (1H, m); 1.45–1.77 (4H, m); 1.80–2.11 (3H, m); 2.17–2.27 (1H, m); 2.53–2.61 (1H, m); 2.70–2.77 (1H, m); 2.78–2.97 (3H, m). GC-MS (EI), m/z: 126.0 [M]$^+$.

***tert*-Butyl 2-(piperidin-4-ylmethyl)pyrrolidine-1-carboxylate (42)**

tert-Butyl 2-(pyridin-4-ylmethyl)pyrrolidine-1-carboxylate (**40**) (15.15 g, 0.058 mol) was dissolved in 1,4-dioxane (300 mL) followed by adding 10% palladium on carbon (1.5 g) and the mixture was hydrogenated at 80°C and 100 atm of hydrogen for 96 h. After completion of the reaction the solid was filtered off, and the solvent was removed under reduced pressure to give the title compound.

A white powder. Yield – 13.4 g (86.5%). M. p. 73–75°C. Anal. Calcd for $C_{15}H_{28}N_2O_2$, %: C 67.13; H 10.52; N 10.44. Found, %: C 67.32; H 10.44; N 10.58. ^{1}H NMR (500 MHz, CDCl$_3$), δ, ppm: 0.95–1.40 (4H, m); 1.46 (9H, s, 3×CH$_3$); 1.56–2.11 (8H, m); 2.52–2.67 (2H, m); 2.95–3.11 (2H, m); 3.25–3.43 (2H, m); 3.78–3.98 (1H, m). LC-MS (ES-API), m/z: 269.2 [M+H]$^+$.

■ References

1. Petrov, L. Problems and Challenges About Accelerated Testing of the Catalytic Activity of Catalysts. In *Principles and Methods for Accelerated Catalyst Design and Testing*; Derouane, E. G., Parmon, V., Lemos, F., Ribeiro, F. R., Eds. Springer Netherlands: Dordrecht, 2002; pp 13–69. https://doi.org/10.1007/978-94-010-0554-8_2.

2. Röper, M. Homogene Katalyse in der Chemischen Industrie. Selektivität, Aktivität und Standzeit. *Chem. unserer Zeit* **2006,** *40* (2), 126–135. https://doi.org/10.1002/ciuz.200600373.

3. Zhang, L.; Zhou, M.; Wang, A.; Zhang, T. Selective Hydrogenation over Supported Metal Catalysts: From Nanoparticles to Single Atoms. *Chem. Rev.* **2020,** *120* (2), 683–733. https://doi.org/10.1021/acs.chemrev.9b00230.

4. Meemken, F.; Baiker, A. Recent Progress in Heterogeneous Asymmetric Hydrogenation of C=O and C=C Bonds on Supported Noble Metal Catalysts. *Chem. Rev.* **2017,** *117* (17), 11522–11569. https://doi.org/10.1021/acs.chemrev.7b00272.

5. Wang, D.; Astruc, D. The Golden Age of Transfer Hydrogenation. *Chem. Rev.* **2015,** *115* (13), 6621–6686. https://doi.org/10.1021/acs.chemrev.5b00203.

6. Cai, R.; Ellis, P. R.; Yin, J.; Liu, J.; Brown, C. M.; Griffin, R.; Chang, G.; Yang, D.; Ren, J.; Cooke, K.; Bishop, P. T.; Theis, W.; Palmer, R. E. Performance of Preformed Au/Cu Nanoclusters Deposited on MgO Powders in the Catalytic Reduction of 4-Nitrophenol in Solution. *Small* **2018,** *14* (13), 1703734. https://doi.org/10.1002/smll.201703734.

7. Zhang, S.; Xia, Z.; Ni, T.; Zhang, Z.; Ma, Y.; Qu, Y. Strong electronic metal-support interaction of Pt/CeO2 enables efficient and selective hydrogenation of quinolines at room temperature. *J. Catal.* **2018,** *359*, 101–111. https://doi.org/10.1016/j.jcat.2018.01.004.

8. Deraedt, C.; Ye, R.; Ralston, W. T.; Toste, F. D.; Somorjai, G. A. Dendrimer-Stabilized Metal Nanoparticles as Efficient Catalysts for Reversible Dehydrogenation/Hydrogenation of N-Heterocycles. *J. Am. Chem. Soc.* **2017,** *139* (49), 18084–18092. https://doi.org/10.1021/jacs.7b10768.

9. Prechtl, M. H. G.; Scariot, M.; Scholten, J. D.; Machado, G.; Teixeira, S. R.; Dupont, J. Nanoscale Ru(0) Particles: Arene Hydrogenation Catalysts in Imidazolium Ionic Liquids. *Inorg. Chem.* **2008,** *47* (19), 8995–9001. https://doi.org/10.1021/ic801014f.

10. Tamura, M.; Yonezawa, D.; Oshino, T.; Nakagawa, Y.; Tomishige, K. In Situ Formed Fe Cation Modified Ir/MgO Catalyst for Selective Hydrogenation of Unsaturated Carbonyl Compounds. *ACS Catalysis* **2017,** *7* (8), 5103–5111. https://doi.org/10.1021/acscatal.7b01055.

11. Ayass, W. W.; Miñambres, J. F.; Yang, P.; Ma, T.; Lin, Z.; Meyer, R.; Jaensch, H.; Bons, A.-J.; Kortz, U. Discrete Polyoxopalladates as Molecular Precursors for Supported Palladium Metal Nanoparticles as Hydrogenation Catalysts. *Inorg. Chem.* **2019,** *58* (9), 5576–5582. https://doi.org/10.1021/acs.inorgchem.8b03513.

12. Stoffels, M. A.; Klauck, F. J. R.; Hamadi, T.; Glorius, F.; Leker, J. Technology Trends of Catalysts in Hydrogenation Reactions: A Patent Landscape Analysis. *Adv. Synth. Catal.* **2020,** *362* (6), 1258–1274. https://doi.org/10.1002/adsc.201901292.

13. Nerozzi, F. Heterogeneous Catalytic Hydrogenation. *Platinum Met. Rev.* **2012,** *56* (4), 236–241. https://doi.org/10.1595/147106712X654187.

14. King, A. O.; Larsen, R. D.; Negishi, E.-I. Palladium-Catalyzed Heterogeneous Hydrogenation. In *Handbook of Organopalladium Chemistry for Organic Synthesis*, 2002; pp 2719–2752. https://doi.org/10.1002/0471212466.ch124.

15. Baimuratova, R. K.; Andreeva, A. V.; Uflyand, I. E.; Shilov, G. V.; Bukharbayeva, F. U.; Zharmagambetova, A. K.; Dzhardimalieva, G. I. Synthesis and Catalytic Activity in the Hydrogenation Reaction of Palladium-Doped Metal-Organic Frameworks Based on Oxo-Centered Zirconium Complexes. *Journal of Composites Science* **2022,** *6* (10), 299. https://doi.org/10.3390/jcs6100299.

16. Rao, R. G.; Blume, R.; Hansen, T. W.; Fuentes, E.; Dreyer, K.; Moldovan, S.; Ersen, O.; Hibbitts, D. D.; Chabal, Y. J.; Schlögl, R.; Tessonnier, J.-P. Interfacial charge distributions in carbon-supported palladium catalysts. *Nature Communications* **2017,** *8* (1), 340. https://doi.org/10.1038/s41467-017-00421-x.

17. Iost, K. N.; Borisov, V. A.; Temerev, V. L.; Surovikin, Y. V.; Pavluchenko, P. E.; Trenikhin, M. V.; Arbuzov, A. B.; Shlyapin, D. A.; Tsyrulnikov, P. G.; Vedyagin, A. A. Carbon support hydrogenation in Pd/C catalysts during reductive thermal treatment. *Int. J. Hydrogen Energy* **2018**, *43* (37), 17656–17663. https://doi.org/10.1016/j.ijhydene.2018.07.182.

18. Campanati, M.; Fornasari, G.; Vaccari, A. Fundamentals in the preparation of heterogeneous catalysts. *Catal. Today* **2003**, *77* (4), 299–314. https://doi.org/10.1016/S0920-5861(02)00375-9.

19. Albers, P. W.; Möbus, K.; Wieland, S. D.; Parker, S. F. The fine structure of Pearlman's catalyst. *Phys. Chem. Chem. Phys.* **2015**, *17* (7), 5274–5278. https://doi.org/10.1039/C4CP05681G.

20. Crawford, C. J.; Qiao, Y.; Liu, Y.; Huang, D.; Yan, W.; Seeberger, P. H.; Oscarson, S.; Chen, S. Defining the Qualities of High-Quality Palladium on Carbon Catalysts for Hydrogenolysis. *Org. Process Res. Dev.* **2021**, *25* (7), 1573–1578. https://doi.org/10.1021/acs.oprd.0c00536.

21. Ivanytsia, M. O.; Lytvynenko, A. S.; Tverdyi, D. O.; Burianov, V. V.; Sotnik, S. O.; Kolotilov, S. V.; Riabukhin, S. V.; Volochniuk, D. M. Sposib otsinky aktyvnosti katalizatoriv reaktsii hidruvannia orhanichnykh spoluk [A method of evaluating the activity of catalysts for reactions of hydrogenation of organic compounds, *in Ukrainian*]. UA Patent 124641, Oct 20, 2021.

22. Mousavi, S.; Nazari, B.; Keshavarz, M. H.; Bordbar, A.-K. A Simple Method for Safe Determination of the Activity of Palladium on Activated Carbon Catalysts in the Hydrogenation of Cinnamic Acid to Hydrocinnamic Acid. *Ind. Eng. Chem. Res.* **2020**, *59* (5), 1862–1874. https://doi.org/10.1021/acs.iecr.9b06087.

23. Stamm, S.; Linden, A.; Heimgartner, H. Chiral Heterospirocyclic 2*H*-Azirin-3-amines as Synthons for 3-Amino-2,3,4,5-tetrahydrofuran-3-carboxylic Acid and Their Use in Peptide Synthesis. *Helv. Chim. Acta* **2003**, *86* (5), 1371–1396. https://doi.org/10.1002/hlca.200390124.

24. Soldermann, C. P.; Quancard, J.; Schlapbach, A.; Simic, O.; Tintelnot-Blomley, M.; Zoller, Th. Novel pyrazolo pyrimidine derivatives and their use as malt1 inhibitors. WO2015181747A1, Dec 3, 2015.

25. Peters, O.; Haaf, K. B.; Lindell, S. D.; Bojack, G.; Law, K. R.; Machettira, A. B.; Dietrich, H.; Gatzweiler, E.; Rosinger, Ch. H. Herbicidally active 3-phenylisoxazoline-5-carboxamides of tetrahydro and dihydrofuran carboxylic acids and esters. US2021292312A1, Sep 23, 2021.

26. Zhou, W.; Peng, Y.; Li, S.-S. Semi-synthesis and anti-tumor activity of 5,8-O-dimethyl acylshikonin derivatives. *Eur. J. Med. Chem.* **2010**, *45* (12), 6005–6011. https://doi.org/10.1016/j.ejmech.2010.09.068.

27. Mao, Z.; Gu, H.; Lin, X. Recent Advances of Pd/C-Catalyzed Reactions. *Catalysts* **2021**, *11*, 1078. https://doi.org/10.3390/catal11091078.

28. Wu, Z.-Q.; Jiang, X.-K.; Li, Z.-T. Hydrogen bonding-mediated self-assembly of square and triangular metallocyclophanes. *Tetrahedron Lett.* **2005**, *46* (46), 8067–8070. https://doi.org/10.1016/j.tetlet.2005.06.173.

29. Barraclough, P.; Black, J. W.; Cambridge, D.; Collard, D.; Firmin, D.; Gerskowitch, V. P.; Glen, R. C.; Giles, H.; Hill, A. P. Inotropic 'A' ring substituted sulmazole and isomazole analogs. *J. Med. Chem.* **1990**, *33* (8), 2231–2239. 10.1021/jm00170a030.

30. Plaquevent, J.-C.; Chichaoui, I. Réduction régiospécifique des bipyridines. *Tetrahedron Lett.* **1993**, *34* (33), 5287–5288. https://doi.org/10.1016/S0040-4039(00)73975-X.

31. Mondal, J.; Trinh, Q. T.; Jana, A.; Ng, W. K. H.; Borah, P.; Hirao, H.; Zhao, Y. Size-Dependent Catalytic Activity of Palladium Nanoparticles Fabricated in Porous Organic Polymers for Alkene Hydrogenation at Room Temperature. *ACS Applied Materials & Interfaces* **2016**, *8* (24), 15307–15319. https://doi.org/10.1021/acsami.6b03127.

32. Frackenpohl, J.; Zeiss, H.-J.; Heinemann, I.; Willms, L.; Müller, Th.; Busch, M.; Von Koskull-Döering, P.; Rosinger, Ch. H.; Dittgen, J.; Hills, M. J. Use of substituted isoquinolinones, isoquinolindiones, isoquinolintriones and dihydroisoquinolinones or in each case salts thereof as active agents against abiotic stress in plants. US2014302987A1, Oct 9, 2014.

33. Yu, Y.; Guo, J.; Cai, Z.; Ju, Y.; Xu, J.; Gu, Q.; Zhou, H. Identification of new building blocks by fragment screening for discovering GyrB inhibitors. *Bioorg. Chem.* **2021**, *114*, 105040. https://doi.org/10.1016/j.bioorg.2021.105040.

34. Baumann, K.; Knapp, H.; Strnadt, G.; Schulz, G.; Grassberger, M. A. Carbonyl to methylene conversions at the tricarbonyl-portion of ascomycin derivatives. *Tetrahedron Lett.* **1999**, *40* (44), 7761–7764. https://doi.org/10.1016/S0040-4039(99)01622-6.

35. Clive, D. L. J.; Wang, J. A Tin Hydride Designed To Facilitate Removal of Tin Species from Products of Stannane-Mediated Radical Reactions. *J. Org. Chem.* **2002**, *67* (4), 1192–1198. https://doi.org/10.1021/jo010885c.

36. Vannice, M. A.; Poondi, D. The Effect of Metal-Support Interactions on the Hydrogenation of Benzaldehyde and Benzyl Alcohol. *J. Catal.* **1997**, *169* (1), 166–175. https://doi.org/10.1006/jcat.1997.1696.

37. Wang, W.; Yang, Y.; Luo, H.; Hu, T.; Liu, W. Amorphous Co–Mo–B catalyst with high activity for the hydrodeoxygenation of bio-oil. *Catal. Commun.* **2011**, *12* (6), 436–440. https://doi.org/10.1016/j.catcom.2010.11.001.

38. Zaccheria, F.; Ravasio, N.; Ercoli, M.; Allegrini, P. Heterogeneous Cu-catalysts for the reductive deoxygenation of aromatic ketones without additives. *Tetrahedron Lett.* **2005**, *46* (45), 7743–7745. https://doi.org/10.1016/j.tetlet.2005.09.041.

39. Argouarch, G. Mild and efficient rhodium-catalyzed deoxygenation of ketones to alkanes. *New J. Chem.* **2019**, *43* (28), 11041–11044. https://doi.org/10.1039/C9NJ02954K.

40. Volkov, A.; Gustafson, K. P. J.; Tai, C.-W.; Verho, O.; Bäckvall, J.-E.; Adolfsson, H. Mild Deoxygenation of Aromatic Ketones and Aldehydes over Pd/C Using Polymethylhydrosiloxane as the Reducing Agent. *Angew. Chem. Int. Ed.* **2015**, *54* (17), 5122–5126. https://doi.org/10.1002/anie.201411059.

41. Bejblová, M.; Zámostný, P.; Červený, L.; Čejka, J. Hydrodeoxygenation of benzophenone on Pd catalysts. *Applied Catalysis A: General* **2005**, *296* (2), 169–175. https://doi.org/10.1016/j.apcata.2005.07.061.

42. Gong, S. W.; He, H. F.; Zhao, C. Q.; Liu, L. J.; Cui, Q. X. Convenient Deoxygenation of Aromatic Ketones by Silica-Supported Chitosan Schiff Base Palladium Catalyst. *Synth. Commun.* **2012**, *42* (4), 574–581. https://doi.org/10.1080/00397911.2010.527423.

43. Newman, M. S.; Cline, W. K. A new synthesis of 2,9-dimethylpicene. *J. Org. Chem.* **1951**, *16* (6), 934–940. https://doi.org/10.1021/jo01146a017.

44. Uysal, T.; Cosford, N. D. P. Compounds and methods for treatment of disorders associated with er stress. WO2007111994A2, Oct 4, 2007.

45. Egli, R.; Eugster, C. H. Über die selektive katalytische Reduktion von substituierten Anilinen zu substituierten Cyclohexylaminen und von Benzol- bzw. Phenyl-alkan-sulfonsäuren zu Cyclohexan- bzw. Cyclohexylalkan-sulfonsäuren. *Helv. Chim. Acta* **1975**, *58* (8), 2321–2346. https://doi.org/10.1002/hlca.19750580814.

46. Wuts, P. G. M.; Greene, T. W. *Greene's Protective Groups in Organic Synthesis*; John Wiley & Sons, 2006. https://doi.org/10.1002/0470053488.

47. Guazzelli, L.; Crawford, C. J.; Ulc, R.; Bowen, A.; McCabe, O.; Jedlicka, A. J.; Wear, M. P.; Casadevall, A.; Oscarson, S. A synthetic glycan array containing Cryptococcus neoformans glucuronoxylomannan capsular polysaccharide fragments allows the mapping of protective epitopes. *Chemical Science* **2020**, *11* (34), 9209–9217. https://doi.org/10.1039/D0SC01249A.

48. Boutet, J.; Blasco, P.; Guerreiro, C.; Thouron, F.; Dartevelle , S.; Nato , F.; Cañada, F. J.; Ardá, A.; Phalipon, A.; Jiménez-Barbero, J.; Mulard, L. A. Detailed Investigation of the Immunodominant Role of O-Antigen Stoichiometric O-Acetylation as Revealed by Chemical Synthesis, Immunochemistry, Solution Conformation and STD-NMR Spectroscopy for *Shigella flexneri* 3a. *Chem. Eur. J.* **2016**, *22* (31), 10892–10911. https://doi.org/10.1002/chem.201600567.

49. Zhou, H.; Liao, X.; Cook, J. M. Regiospecific, Enantiospecific Total Synthesis of the 12-Alkoxy-Substituted Indole Alkaloids, (+)-12-Methoxy-Na-methylvellosimine, (+)-12-Methoxyaffinisine, and (−)-Fuchsiaefoline. *Org. Lett.* **2004**, *6* (2), 249–252. https://doi.org/10.1021/ol0362212.

50. Nicolaou, K. C.; Claiborne, C. F.; Nantermet, P. G.; Couladouros, E. A.; Sorensen, E. J. Synthesis of Novel Taxoids. *J. Am. Chem. Soc.* **1994**, *116* (4), 1591–1592. https://doi.org/10.1021/ja00083a063.

51. Kozioł, A.; Lendzion-Paluch, A.; Manikowski, A. A Fast and Effective Hydrogenation Process of Protected Pentasaccharide: A Key Step in the Synthesis of Fondaparinux Sodium. *Org. Process Res. Dev.* **2013**, *17* (5), 869–875. https://doi.org/10.1021/op300367c.

52. NG, P. Y.; Jewett, I.; Lucas, M. C.; Padilla, F.; Enyedy, I. J. 6-substituted-9*H*-purine derivatives and related uses. WO2022178256A1, Aug 25, 2022.

53. Tang, L.; Wu, W.; Zhang, C.; Shi, Z.; Chen, D.; Zhai, X.; Jiang, Y. Discovery of the PARP (poly ADP-ribose polymerase) inhibitor 2-(1-(4,4-difluorocyclohexyl)piperidin-4-yl)-1H-benzo[d]imidazole-4-carboxamide for the treatment of cancer. *Bioorg. Chem.* **2021**, *114*, 105026. https://doi.org/10.1016/j.bioorg.2021.105026.

54. Li, Y.; Manickam, G.; Ghoshal, A.; Subramaniam, P. More Efficient Palladium Catalyst for Hydrogenolysis of Benzyl Groups. *Synth. Commun.* **2006**, *36* (7), 925–928. https://doi.org/10.1080/00397910500466199.

55. Faust, M. R.; Höfner, G.; Pabel, J.; Wanner, K. T. Azetidine derivatives as novel γ-aminobutyric acid uptake inhibitors: Synthesis, biological evaluation, and structure–activity relationship. *Eur. J. Med. Chem.* **2010**, *45* (6), 2453–2466. https://doi.org/10.1016/j.ejmech.2010.02.029.

56. Védrine, J. C. Metal Oxides in Heterogeneous Oxidation Catalysis: State of the Art and Challenges for a More Sustainable World. *ChemSusChem* **2019**, *12* (3), 577–588. https://doi.org/10.1002/cssc.201802248.

57. Grice, P.; Ley, S. V.; Pietruszka, J.; Osborn, H. M. I.; Priepke, H. W. M.; Warriner, S. L. A New Strategy for Oligosaccharide Assembly Exploiting Cyclohexane-1,2-diacetal Methodology: An Efficient Synthesis of a High Mannose Type Nonasaccharide. *Chem. Eur. J.* **1997**, *3* (3), 431–440. https://doi.org/10.1002/chem.19970030315.

58. Crawford, C.; Oscarson, S. Optimized Conditions for the Palladium-Catalyzed Hydrogenolysis of Benzyl and Naphthylmethyl Ethers: Preventing Saturation of Aromatic Protecting Groups. *Eur. J. Org. Chem.* **2020**, *2020* (22), 3332–3337. https://doi.org/10.1002/ejoc.202000401.

59. Shao, J.; Zhu, K.; Du, D.; Zhang, Y.; Tao, H.; Chen, Z.; Jiang, H.; Chen, K.; Luo, C.; Duan, W. Discovery of 2-substituted-N-(3-(3,4-dihydroisoquinolin-2(1H)-yl)-2-hydroxypropyl)-1,2,3,4-tetrahydroisoquinoline-6-carboxamide as potent and selective protein arginine methyltransferases 5 inhibitors: Design, synthesis and biological evaluation. *Eur. J. Med. Chem.* **2019**, *164*, 317–333. https://doi.org/10.1016/j.ejmech.2018.12.065.

60. Schudok, M.; Matter, H.; Hofmeister, A. Tetrahydrofurane derivatives for use as inhibitors of matrix metalloproteinases. WO2006077013A1, Jul 27, 2006.

61. Armour, D. R.; Chung, K. M. L.; Congreve, M.; Evans, B.; Guntrip, S.; Hubbard, T.; Kay, C.; Middlemiss, D.; Mordaunt, J. E.; Pegg, N. A.; Vinader, M. V.; Ward, P.; Watson, S. P. Tetrazole NK1 receptor antagonists: The identification of an exceptionally potent orally active antiemetic compound. *Bioorg. Med. Chem. Lett.* **1996**, *6* (9), 1015–1020. https://doi.org/10.1016/0960-894X(96)00163-1.

62. Wagener, T.; Heusler, A.; Nairoukh, Z.; Bergander, K.; Daniliuc, C. G.; Glorius, F. Accessing (Multi)Fluorinated Piperidines Using Heterogeneous Hydrogenation. *ACS Catalysis* **2020**, *10* (20), 12052–12057. https://doi.org/10.1021/acscatal.0c03278.

63. Zhu, J.; Chen, P.-H.; Lu, G.; Liu, P.; Dong, G. Ruthenium-Catalyzed Reductive Cleavage of Unstrained Aryl–Aryl Bonds: Reaction Development and Mechanistic Study. *J. Am. Chem. Soc.* **2019**, *141* (46), 18630–18640. https://doi.org/10.1021/jacs.9b11605.

64. Kim, S.; Loose, F.; Bezdek, M. J.; Wang, X.; Chirik, P. J. Hydrogenation of N-Heteroarenes Using Rhodium Precatalysts: Reductive Elimination Leads to Formation of Multimetallic Clusters. *J. Am. Chem. Soc.* **2019**, *141* (44), 17900–17908. https://doi.org/10.1021/jacs.9b09540.

65. Yu, T.; Wang, J.; Li, X.; Cao, X.; Gu, H. An Improved Method for the Complete Hydrogenation of Aromatic Compounds under 1 Bar H2 with Platinum Nanowires. *ChemCatChem* **2013**, *5* (10), 2852–2855. https://doi.org/10.1002/cctc.201300394.

66. McPhillie, M. J.; Zhou, Y.; Hickman, M. R.; Gordon, J. A.; Weber, C. R.; Li, Q.; Lee, P. J.; Amporndanai, K.; Johnson, R. M.; Darby, H.; Woods, S.; Li, Z.-H.; Priestley, R. S.; Ristroph, K. D.; Biering, S. B.; El Bissati, K.; Hwang, S.; Hakim, F. E.; Dovgin, S. M.; Lykins, J. D.; Roberts, L.; Hargrave, K.; Cong, H.; Sinai, A. P.; Muench, S. P.; Dubey, J. P.; Prud'homme, R. K.; Lorenzi, H. A.; Biagini, G. A.; Moreno, S. N.; Roberts, C. W.; Antonyuk, S. V.; Fishwick, C. W. G.; McLeod, R. Potent Tetrahydroquinolone Eliminates Apicomplexan Parasites. *Frontiers in Cellular and Infection Microbiology* **2020**, *10*. https://doi.org/10.3389/fcimb.2020.00203.

67. Höglund, I. P. J.; Silver, S.; Engström, M. T.; Salo, H.; Tauber, A.; Kyyrönen, H.-K.; Saarenketo, P.; Hoffrén, A.-M.; Kokko, K.; Pohjanoksa, K.; Sallinen, J.; Savola, J.-M.; Wurster, S.; Kallatsa, O. A. Structure–Activity Relationship of Quinoline Derivatives as Potent and Selective α2C-Adrenoceptor Antagonists. *J. Med. Chem.* **2006**, *49* (21), 6351–6363. https://doi.org/10.1021/jm060262x.

68. Matsubara, S.; Yokota, Y.; Oshima, K. Palladium-Catalyzed Decarboxylation and Decarbonylation under Hydrothermal Conditions: Decarboxylative Deuteration. *Org. Lett.* **2004**, *6* (12), 2071–2073. https://doi.org/10.1021/ol0492602.

69. Modak, A.; Maiti, D. Metal catalyzed defunctionalization reactions. *Org. Biomol. Chem.* **2016**, *14* (1), 21–35. https://doi.org/10.1039/C5OB01949D.

70. Hanessian, S.; Sharma, R. The Synthesis of Bicyclic Piperazine-2-carboxylic Acids from L-Proline. *Heterocycles* **2000**, *52* (3), 1231–1239. https://doi.org/10.3987/COM-99-S136.

71. Uozumi, Y.; Shen, G. Pd/C-Catalyzed Reductive N-Methylation of Quinolines. *Synfacts* **2019**, *15* (07), 0790. https://doi.org/10.1055/s-0039-1689752.

72. Goyal, V.; Gahtori, J.; Narani, A.; Gupta, P.; Bordoloi, A.; Natte, K. Commercial Pd/C-Catalyzed N-Methylation of Nitroarenes and Amines Using Methanol as Both C1 and H2 Source. *J. Org. Chem.* **2019**, *84* (23), 15389–15398. https://doi.org/10.1021/acs.joc.9b02141.

73. Matsushima, T.; Takahashi, K.; Funasaka, S.; Obaishi, H.; Shirotori, S. Pyridine derivatives and pyrimidine derivatives. US8288538B2, Oct 16, 2012.

74. Veitch, G. E.; Beckmann, E.; Burke, B. J.; Boyer, A.; Maslen, S. L.; Ley, S. V. Synthesis of Azadirachtin: A Long but Successful Journey. *Angew. Chem. Int. Ed.* **2007**, *46* (40), 7629–7632. https://doi.org/10.1002/anie.200703027.

75. Huang, J.-L.; Dai, X.-J.; Li, C.-J. Iridium-Catalyzed Direct Dehydroxylation of Alcohols. *Eur. J. Org. Chem.* **2013,** *2013* (29), 6496 – 6500. https://doi.org/10.1002/ejoc.201301293.

76. Chan, L. Y.; Lim, J. S. K.; Kim, S. Iron-Catalyzed Reductive Dehydroxylation of Benzylic Alcohols Using Polymethylhydrosiloxane (PMHS). *Synlett* **2011,** *2011* (19), 2862 – 2866. https://doi.org/10.1055/s-0031-1289857.

Information about the authors:
Volodymyr V. Burianov, Postgraduate Student of the Organic Chemistry Department, Taras Shevchenko National University of Kyiv; Head of the High-pressure Synthesis Laboratory, Enamine Ltd.

Dmitry A. Lega, Ph.D. in Pharmacy, Assistant of General Chemistry Department, National University of Pharmacy of the Ministry of Health of Ukraine; Researcher, Enamine Ltd.; https://orcid.org/0000-0002-4505-3646.

Valeriya G. Makhankova, Dr.Sci. in Chemistry, Professor of the Supramolecular Chemistry Department, Institute of High Technologies, Taras Shevchenko National University of Kyiv; Researcher, Enamine Ltd.; https://orcid.org/0000-0002-0012-5108.

Yulian M. Volovenko, Dr.Sci. in Chemistry, Professor of the Organic Chemistry Department, Dean of the Faculty of Chemistry, Taras Shevchenko National University of Kyiv; https://orcid.org/0000-0003-4321-1484.

Sergey V. Kolotilov, Dr.Sci. in Chemistry, Professor, Head of the Department of Porous Compounds and Materials, Deputy Director on Scientific Affairs, L. V. Pisarzhevskii Institute of Physical Chemistry of the National Academy of Sciences of Ukraine; https://orcid.org/0000-0002-4780-4378.

Dmitriy M. Volochnyuk, Dr.Sci. in Chemistry, Professor of the Supramolecular Chemistry Department, Institute of High Technologies, Taras Shevchenko National University of Kyiv; Head of the Biologically Active Compounds Department, Institute of Organic Chemistry of the National Academy of Sciences of Ukraine; Senior Scientific Advisor, Enamine Ltd.; https://orcid.org/0000-0001-6519-1467.

Sergey V. Ryabukhin (*corresponding author*), Dr.Sci. in Chemistry, Professor, Head of the Supramolecular Chemistry Department, Institute of High Technologies, Taras Shevchenko National University of Kyiv; Senior Scientific Advisor, Enamine Ltd.; Senior Researcher of the Department of Physicochemical Investigations, Institute of Organic Chemistry of the National Academy of Sciences of Ukraine; https://orcid.org/0000-0003-4281-8268.

A. O. Shpychak, O. P. Khvorost

National University of Pharmacy of the Ministry of Health of Ukraine,
53, Pushkinska str., Kharkiv, 61002, Ukraine

The Study of the Carbohydrate Composition of *Cetraria islandica* (L.) Ach. Thalli Harvested in Ukraine

Abstract

Aim. To study the component composition of free and total monosaccharides in the raw material of *Cetraria islandica* (L.) Ach. harvested in Ukraine.

Materials and methods. The component composition of free and total monosaccharides in the raw material was determined by gas chromatography with mass-spectrometric detection (GC-MS).

Results and discussion. Among the free monosaccharides, the presence of *D*-perseitol, (6.99 mg g^{-1}) and *D*-mannitol (1.12 mg g^{-1}) was determined. Among the total monosaccharides, the content of *D*-glucose (203.64 mg g^{-1}) prevailed. *D*-mannose (53.74 mg g^{-1}), *D*-galactose (51.71 mg g^{-1}), *D*-xylose (0.83 mg g^{-1}) and *L*-rhamnose (0.53 mg g^{-1}) were found in lower quantities, as well as polyatomic alcohols – *D*-dulcitol (8.46 mg g^{-1}) and *D*-mannitol (3.10 mg g^{-1}).

Conclusions. For the first time, the component composition of free and total monosaccharides in the raw material of *C. islandica* harvested in Ukraine has been determined. The results obtained will be used as a component of the comprehensive systematic study of the raw material of *C. islandica* harvested in Ukraine.

Keywords: *Cetraria islandica*; thalli; component composition; free and total monosaccharides; GC-MS

А. О. Шпичак, О. П. Хворост

Національний фармацевтичний університет Міністерства охорони здоров'я України,
вул. Пушкінська, 53, м. Харків, 61002, Україна

Вивчення вуглеводного складу слані *Cetraria islandica* (L.) Ach., заготовленої в Україні

Анотація

Мета. Визначити компонентний склад вільних та загальних моносахаридів у сировині *Cetraria islandica* (L.) Ach., заготовленої в Україні.

Матеріали та методи. Визначення компонентного складу вільних та загальних моносахаридів у сировині проводили методом газової хроматографії з мас-спектрометричним детектуванням (ГХ-МС).

Результати і обговорення. Серед вільних моносахаридів виявлено наявність *D*-персеїтолу (6,99 мг г$^{-1}$) та *D*-манітолу (1,12 мг г$^{-1}$). Серед загальних моносахаридів переважав вміст *D*-глюкози (203,64 мг г$^{-1}$). У менших кількостях виявлено *D*-манозу (53,74 мг г$^{-1}$), *D*-галактозу (51,71 мг г$^{-1}$), *D*-ксилозу (0,83 мг г$^{-1}$) і *L*-рамнозу (0,53 мг г$^{-1}$), а також багатоатомні спирти *D*-дульцитол (8,46 мг г$^{-1}$) і *D*-манітол (3,10 мг г$^{-1}$).

Висновки. Уперше визначено компонентний склад вільних та загальних моносахаридів у сировині *C. islandica*, заготовленої в Україні. Отримані результати буде використано як складову частину комплексного всебічного вивчення сировини *C. islandica*, заготовленої в Україні.

Ключові слова: *Cetraria islandica*; слань; компонентний склад; вільні та загальні моносахариди; ГХ-МС

■ Introduction

The study of the carbohydrate composition of plant species that are already used in pharmacy as the medicinal plant raw material does not lose its relevance nowadays [1–3]. In recent years, studies of the pharmacological activity of polysaccharides extracted not only from land plants, but also algae, fungi, and lichens have been conducted [4, 5]. In particular, it has been demonstrated that polysaccharides extracted from green algae exhibit antioxidant, antidiabetic and antiobesity effects [6]. There are also data on the ability of polysaccharides obtained from various types of fungi to exhibit the antitumor activity [7].

Polysaccharides are one of the main groups of biologically active substances (BAS) of lichens, which attract attention to study various types of the pharmacological activity [8, 9]. The polysaccharide composition was determined only for a small number of lichens, mainly members of the families *Parmeliaceae*, *Cladoniaceae* and *Teloschistaceae* [10]. It has been stated that lichen polysaccharides are not characterized by significant variability of monosaccharides that are part of their structure. *D*-glucose, *D*-galactose and *D*-mannose commonly prevail in different ratios; *L*-rhamnose, *L*-arabinose and *D*-xylose are less common structural units [8, 10]. The main structural forms found in lichens are *β*- and *α*-glucans and *α*-mannans [9].

β-*D*-1,3/1,4-glucan lichenin and α-*D*-1,3/1,4-glucan isolichenin are specific polysaccharides for *Cetraria islandica* (L.) Ach. [11, 12]. According to the data the quantitative content of lichenin can reach up to 27% of the amount of polymeric carbohydrates in a dry substance [13].

The presence of lichenin and isolichenin in the raw material of *C. islandica* is associated with a strong anti-inflammatory and expectorant effect in diseases of the upper respiratory tract, as well as a stimulating effect on various parts of the immune defense system [11, 14, 15]. The recent research was devoted to the study of mechanisms of wound healing and the antitumor action of lichenin, and showed the absence of such activity for lichenin-derived oligosaccharides [16].

Since the extraction of lichenin and isolichenin from the raw material requires special conditions, in particular temperature and pH of an extractant [16, 17], there are studies devoted to the optimization of the method to obtain these and other polysaccharides from *C. islandica* [18–20].

Studies of the carbohydrate composition of *C. islandica* were actively conducted in the late 1990s–early 2000s [9, 13, 20, 21]. The works were related to the isolation, analysis of the structure and the component composition of polysaccharides, in particular, the determination of the monosaccharide ratios [20, 21], as well as the nutritional value of lichen as fodder for reindeer [13]. The presence of *D*-glucose, *D*-galactose, *D*-mannose, *L*-rhamnose, *L*-arabinose, *D*-xylose and *L*-fucose was determined in the raw material of *C. islandica* collected in Norway [13]. In the literature sources available to us, we found a few data on the carbohydrate composition of the raw material of *C. islandica* harvested in Ukraine – polysaccharides in the raw material harvested in the Ivano-Frankivsk region were studied [22].

Therefore, the study of the component composition of monosaccharides in the thalli of *C. islandica* harvested in Ukraine is a relevant issue as a part of the comprehensive systematic study of the component composition of BAS of the raw material and its further processing and use in pharmacy.

Hence, the aim of the work was to study the component composition of free and total monosaccharides in the raw material of *C. islandica* (L.) Ach. harvested in Ukraine.

■ Materials and methods

Plant raw material

Thalli of *C. islandica* collected in the fall of 2019 in the Rakhiv district of the Zakarpattia region were used for the study. The raw material was dried to an air-dried condition in the open air under a cover and stored in paper bags in a dry place.

Sample preparation. The plant raw material was ground by a laboratory mill LGM-1 (Olis, Ukraine), then 335 mg of the sample was placed in a round-bottom flask and 10 mL of 80% ethyl alcohol; *D*-sorbitol as an internal standard (Sigma-Aldrich, USA) was added (500 μg per sample). Extraction of the free monosaccharides was carried out on a boiling water bath with a reflux condenser for 2 h. After that, 2 mL of the extract was separated, evaporated to remove the solvents in a rotary evaporator and resuspended by adding an aqueous solution of the internal standard (250 μg in 2 mL of water per sample).

To determine the total monosaccharides, 90 mg of the ground raw material was placed in a round-bottomed flask, and 5 mL of 2 M trifluoroacetic

acid was added. Hydrolysis was carried out on a boiling water bath with a reflux condenser for 6 h. Then 2 mL of the hydrolyzate was separated, evaporated until the solvents were removed, in the process water was added several times, with further removal of the hydrolyzate to complete elimination of trifluoroacetic acid. Re-suspending was carried out by adding an aqueous solution of the internal standard (250 µg in 2 mL of water per sample) [3, 23].

Derivatization. To obtain aldononitrile derivatives of monosaccharides, the pre-treated samples of the extract were taken, and 0.3 mL of the derivatizing reagent (32 mg mL^{-1} of hydroxylamine hydrochloride in a mixture of pyridine/methanol (4:1 *v/v*)) was added to each one. The mixture obtained was incubated in an oven at 75°C for 25 min. For acetylation of aldononitrile derivatives of the monosaccharides obtained, 1 mL of acetic anhydride was added, and the mixture was kept in an oven at 75°C for 15 min. Then, 2 mL of dichloroethane was added to the reaction mixture, the excess of derivatization reagents was removed by consecutive processing of the mixture with 1 N hydrochloric acid and water. The dichloroethane layer was dried in a rotary evaporator and dissolved in 300 µL of the mixture of heptane/ethyl acetate (1:1 *v/v*) [23].

Conditions of chromatographic separation. The component composition of free and total monosaccharides in the raw material was determined by gas chromatography with mass-spectrometric detection (GC-MS). For the analysis of free and total monosaccharides, aldononitrile acetates were obtained after the appropriate sample preparation [23].

The chromatographic separation was performed on an Agilent 6890N gas chromatograph with a 5973 inert mass detector (Agilent technologies, USA) and a HP-5ms capillary column (30 m × 0.25 mm × 0.25 µm, Agilent technologies, USA). The temperature of the evaporator was 250°C, the temperature of the interface was 280°C. The separation was carried out in the following temperature programming mode: the initial temperature of 160°C was held for 8 min, then raised to 240°C at the rate of 5°C min^{-1} and maintained at this point for 6 min. 1 µL of the sample was injected in the split mode 1:50. Detection was performed in the SCAN mode in the width range of 38–400 m/z. Helium was used as a carrier gas with a flow rate of 1.2 mL min^{-1} [24].

Identification and quantification. Identification of monosaccharides of the mixture studied was based on their retention times compared to standards of monosaccharides (Sigma-Aldrich, USA) and using the mass spectral library NIST 02.

The quantitative content of monosaccharides (mg g^{-1}) was calculated according to the formula:

$$X = \frac{S_x \times M_{inst} \times V_{sol} \times 1000}{S_{inst} \times m \times V_{extr}},$$

where: S_x is the peak area of the compound; S_{inst} is the peak area of the internal standard; M_{inst} is the mass of the internal standard per sample, mg; m is the mass of the sample, mg; V_{sol} is the volume of the solvent for extraction, mL; V_{extr} is the volume of the extract for derivatization, mL [23].

■ Results and discussion

The chromatogram of the free monosaccharides is shown in Figure 1. The results of the determination of the component composition and the quantitative content of the free monosaccharides in the raw material of *C. islandica*, as well as their chromatographic parameters are shown in Table. 1. The peak with RT 9.77 on the chromatogram corresponds to triacetin that do not belong to the class of BAS studied, and, therefore, is not discussed further.

According to the data in Table 1, sugar alcohols – *D*-perseitol with the content of 6.99 mg g^{-1}, and *D*-mannitol with the content of 1.12 mg g^{-1} were identified.

The chromatogram of the total monosaccharides is shown in Figure 2. The results of determining the component composition and the quantitative content of the total monosaccharides, as well as their chromatographic parameters, are shown in Table 2. The rest of the peaks on the chromatogram correspond to the identified compounds that do not belong to the class BAS studied or have not been identified.

According to the data in Table 2, seven compounds were identified; among them 5 belonged to monosaccharides and 2 – to sugar alcohols. Among monosaccharides, *D*-glucose dominated – 203.64 mg g^{-1}. A high content of *D*-mannose (53.74 mg g^{-1}) and *D*-galactose (51.71 mg g^{-1}) was also determined. Much lower content was observed for *D*-xylose (0.83 mg g^{-1}) and *L*-rhamnose (0.53 mg g^{-1}). The quantitative content of sugar alcohol – *D*-dulcitol (*D*-galactitol) was 8.46 mg g^{-1}, *D*-mannitol – 3.10 mg g^{-1}. The data regarding *D*-dulcitol in the raw material of *C. islandica* was presumably reported for the first time.

Figure 1. The GC-MS chromatogram of the free monosaccharides in the raw material of *C. islandica*

Table 1. The component composition of the free monosaccharides in the raw material of *C. islandica*

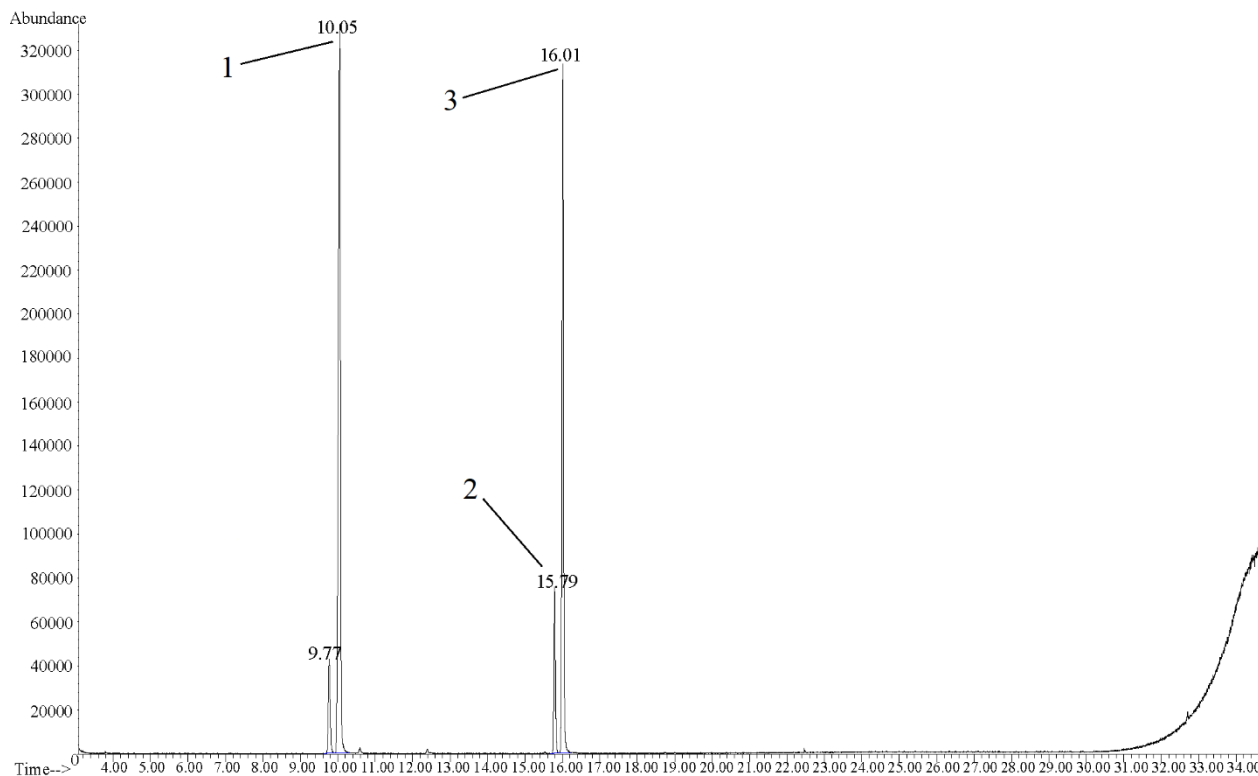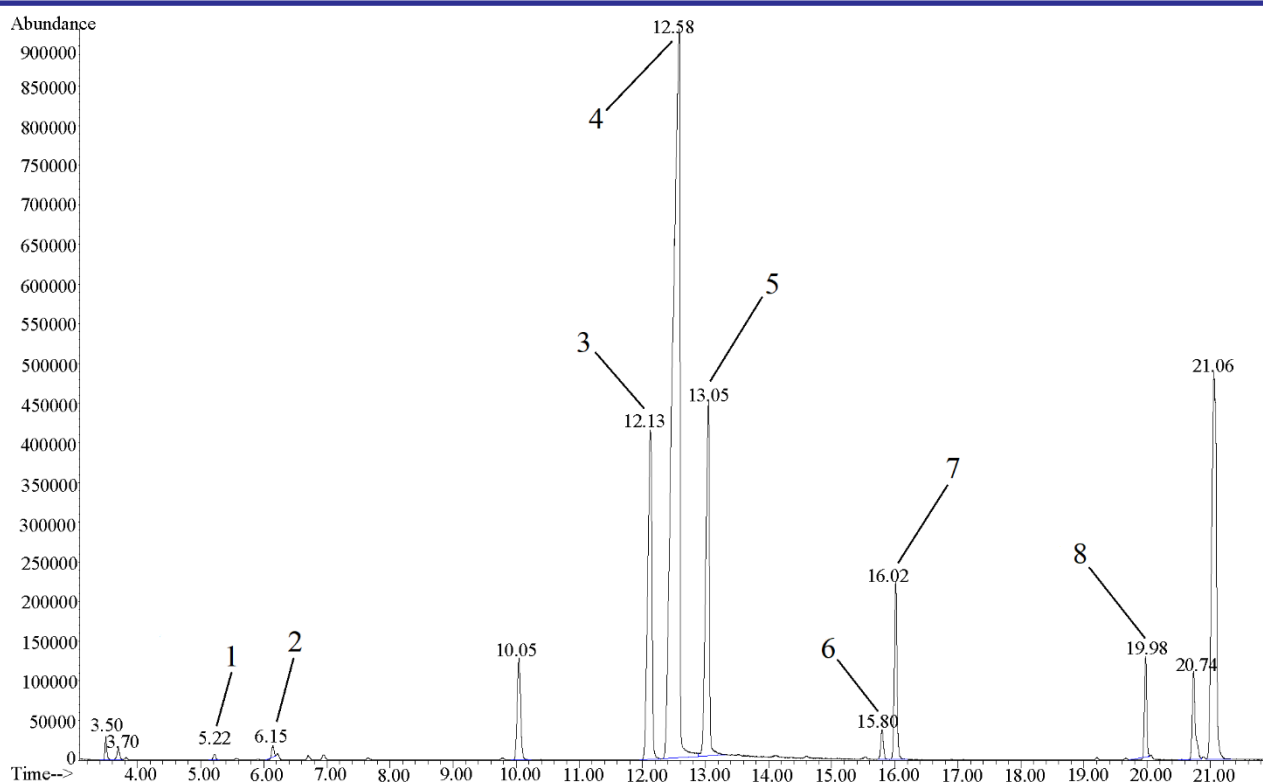| Peak number	Retention time, min	Peak area	Compound	Content, mg g^{-1}
1	10.0503	50.3532	*D*-perseitol	6.99
2	15.792	8.0327	*D*-manitol	1.12
3	16.013	35.8272	*D*-sorbitol	Internal standard

Figure 2. The GC-MS chromatogram of the total monosaccharides in the raw material of *C. islandica*

Table 2. The component composition of the total monosaccharides in the raw material of *C. islandica*

Peak number	Retention time, min	Peak area	Compound	Content, mg g^{-1}
1	5.2224	0.1217	*L*-rhamnose	0.53
2	6.1447	0.1887	*D*-xylose	0.83
3	12.1286	12.244	D-mannose	53.74
4	12.5834	46.3979	*D*-glucose	203.64
5	13.0466	11.7829	*D*-galactose	51.71
6	15.8006	0.7074	*D*-manitol	3.10
7	16.0173	4.2194	*D*-sorbitol	Internal standard
8	19.9783	1.9287	*D*-Dulcitol	8.46

■ Conclusions

1. For the first time, the component composition of free and total monosaccharides in the raw material of *C. islandica* harvested in Ukraine has been determined.

2. Among the free monosaccharides, the presence of D-mannitol has been determined; its quantitative content is 1.12 mg g^{-1}. Among the total monosaccharides, the content of D-glucose (203.64 mg g^{-1}), D-mannose (53.74 mg g^{-1}) and D-galactose (51.71 mg g^{-1}) prevails.

3. The results obtained will be used as a component of the comprehensive systematic study of the raw material of *C. islandica* harvested in Ukraine; they will be taken into account for further research.

■ References

1. Kim, M.; Kim, S.-R.; Park, J.; Mun, S.-H.; Kwak, M.; Ko, H.-J.; Baek, S.-H. Structure and antiviral activity of a pectic polysaccharide from the root of Sanguisorba officinalis against enterovirus 71 in vitro/vivo. *Carbohydr. Polym.* **2022,** *281*, 119057. https://doi.org/10.1016/j.carbpol.2021.119057.

2. Tan, J.; Cui, P.; Ge, S.; Cai, X.; Li, Q.; Xue, H. Ultrasound assisted aqueous two-phase extraction of polysaccharides from Cornus officinalis fruit: Modeling, optimization, purification, and characterization. *Ultrason. Sonochem.* **2022,** *84*, 105966. https://doi.org/10.1016/j.ultsonch.2022.105966.

3. Slobodianiuk, L.; Budniak, L.; Marchyshyn, S.; Kostyshyn, L.; Zakharchuk, O. Analysis of carbohydrates in Saponaria officinalis L. using GC/MS method. *Pharmacia* **2021,** *68* (2), 339 – 345. https://doi.org/10.3897/pharmacia.68.e62691.

4. Qu, J.; Huang, P.; Zhang, L.; Qiu, Y.; Qi, H.; Leng, A.; Shang, D. Hepatoprotective effect of plant polysaccharides from natural resources: A review of the mechanisms and structure-activity relationship. *Int. J. Biol. Macromol.* **2020,** *161*, 24 – 34. https://doi.org/10.1016/j.ijbiomac.2020.05.196.

5. Yin, M.; Zhang, Y.; Li, H. Advances in Research on Immunoregulation of Macrophages by Plant Polysaccharides. *Frontiers in Immunology* **2019,** *10*. https://doi.org/10.3389/fimmu.2019.00145.

6. Park, H.-B.; Hwang, J.; Zhang, W.; Go, S.; Kim, J.; Choi, I.; You, S.; Jin, J.-O. Polysaccharide from *Codium fragile* Induces Anti-Cancer Immunity by Activating Natural Killer Cells. *Mar. Drugs* **2020**, *18*, 626. https://doi.org/10.3390/md18120626.

7. Barbosa, J. R.; Carvalho Junior, R. N. d. Occurrence and possible roles of polysaccharides in fungi and their influence on the development of new technologies. *Carbohydr. Polym.* **2020,** *246*, 116613. https://doi.org/10.1016/j.carbpol.2020.116613.

8. Shrestha, G.; St. Clair, L. L.; O'Neill, K. L. The Immunostimulating Role of Lichen Polysaccharides: A Review. *Phytotherapy Research* **2015,** *29* (3), 317 – 322. https://doi.org/10.1002/ptr.5251.

9. Olafsdottir, E. S.; Ingólfsdottir, K. Polysaccharides from Lichens: Structural Characteristics and Biological Activity. *Planta Med.* **2001,** *67* (03), 199 – 208. https://doi.org/10.1055/s-2001-12012.

10. Spribille, T.; Tagirdzhanova, G.; Goyette, S.; Tuovinen, V.; Case, R.; Zandberg, W. F. 3D biofilms: in search of the polysaccharides holding together lichen symbioses. *FEMS Microbiol. Lett.* **2020,** *367* (5). https://doi.org/10.1093/femsle/fnaa023.

11. Ingólfsdóttir, K.; Jurcic, K.; Wagner, H. Immunomodulating polysaccharides from aqueous extracts of Cetraria islandica (Iceland moss). *Phytomedicine* **1998,** *5* (5), 333 – 339. https://doi.org/10.1016/S0944-7113(98)80014-7.

12. Surayot, U.; Yelithao, K.; Tabarsa, M.; Lee, D.-H.; Palanisamy, S.; Marimuthu Prabhu, N.; Lee, J.; You, S. Structural characterization of a polysaccharide from Certaria islandica and assessment of immunostimulatory activity. *Process Biochem.* **2019,** *83*, 214 – 221. https://doi.org/10.1016/j.procbio.2019.05.022.

13. Svihus, B.; Holand, Ø. Lichen Polysaccharides and Their Relation to Reindeer/Caribou Nutrition. *Journal of Range Management* **2000,** *53* (6), 642 – 648. https://doi.org/10.2307/4003160.

14. Salama, M. E.-D.; Amani, W. N. *Cetraria Islandica* as a Pulmonary Cytoprotective and Supportive Herbal Remedy for Lung Complications Related to COVID-19. *Scholars International Journal of Traditional and Complementary Medicine* **2021**, *4* (10), 168 – 173.

15. Ingolfsdottir, K. Bioactive compounds from Iceland moss. In *Bioactive Carbohydrate Polymers*; Paulsen B. S., Ed.; Kluwer Academic Publishers, 2000; pp 25 – 36.

16. Zacharski, D. M.; Esch, S.; König, S.; Mormann, M.; Brandt, S.; Ulrich-Merzenich, G.; Hensel, A. β-1,3/1,4-Glucan Lichenan from Cetraria islandica (L.) ACH. induces cellular differentiation of human keratinocytes. *Fitoterapia* **2018,** *129*, 226 – 236. https://doi.org/10.1016/j.fitote.2018.07.010.

17. Sánchez, M.; Ureña-Vacas, I.; González-Burgos, E.; Divakar, P.K.; Gómez-Serranillos, M.P. The Genus *Cetraria* s. str.—A Review of Its Botany, Phytochemistry, Traditional Uses and Pharmacology. *Molecules* **2022**, *27*, 4990. https://doi.org/10.3390/molecules27154990.

18. Krämer, P.; Wincierz, U.; Grübler, G.; Tschakert, J.; Voelter, W.; Mayer, H. Rational approach to fractionation, isolation, and characterization of polysaccharides from the lichen *Cetraria islandica*. *Arzneimittel-Forschung* **1995,** *45* (6), 726 – 731.

19. Freysdottir, J.; Omarsdottir, S.; Ingólfsdóttir, K.; Vikingsson, A.; Olafsdottir, E. S. *In vitro* and *in vivo* immunomodulating effects of traditionally prepared extract and purified compounds from *Cetraria islandica*. *International Immunopharmacology* **2008,** *8* (3), 423−430. https://doi.org/10.1016/j.intimp.2007.11.007.

20. Olafsdottir, E. S.; Ingolfsdottir, K.; Barsett, H.; Smestad Paulsen, B.; Jurcic, K.; Wagner, H. Immunologically active (1→3)-(1→4)-α-*D*-Glucan from *Cetraria islandica*. *Phytomedicine* **1999,** *6* (1), 33−39. https://doi.org/10.1016/S0944-7113(99)80032-4.

21. Ingolfsdottir, K.; Jurcic, K.; Fischer, B.; Wagner, H. Immunologically Active Polysaccharide from Cetraria islandica. *Planta Med.* **1994,** *60* (06), 527−531. https://doi.org/10.1055/s-2006-959564.

22. Kobernik, A. O.; Kravchenko, I. A.; Chervonenko, O. F.; Myhaylova, T. V.; Nabych, M. Identifikatsiya biologicheski aktivnykh veshchestv v sloyevishche *Cetraria islandica* [The identification of active compound content in the thallus *Cetraria islandica*, *in Russian*]. *Aktualni problemy transportnoi medytsyny* **2015**, *2* (40), 144–148.

23. Guan, J.; Yang, F.-Q.; Li, S.-P. Evaluation of Carbohydrates in Natural and Cultured *Cordyceps* by Pressurized Liquid Extraction and Gas Chromatography Coupled with Mass Spectrometry. *Molecules* **2010**, *15*, 4227−4241. https://doi.org/10.3390/molecules15064227.

24. Chen, Y.; Xie, M.-Y.; Wang, Y.-X.; Nie, S.-P.; Li, C. Analysis of the monosaccharide composition of purified polysaccharides in Ganoderma atrum by capillary gas chromatography. *Phytochem. Anal.* **2009,** *20* (6), 503−510. https://doi.org/10.1002/pca.1153.

Information about the authors:
Alina O. Shpychak (*corresponding author*), Postgraduate Student of the Department of Chemistry of Natural Compounds and Nutritiology, National University of Pharmacy of the Ministry of Health of Ukraine; https://orcid.org/0000-0001-6847-7655; e-mail for correspondence: shpichakalina@gmail.com; tel. +380 99 4910210.
Olga P. Khvorost, Dr.Sci. in Pharmacy, Professor of the Department of Chemistry of Natural Compounds and Nutritiology, National University of Pharmacy of the Ministry of Health of Ukraine; https://orcid.org/0000-0002-9534-1507.

V. M. Polishchuk, M. P. Shandura

Institute of Organic Chemistry of the National Academy of Sciences of Ukraine,
5, Akademika Kukharya str., Kyiv, 02094, Ukraine

Polymethine Dyes Based on 2,2-Difluoro-1,3,2-dioxaborine: A Minireview

Abstract

Aim. To summarize and analyze literature data on the polymethine dyes containing the 2,2-difluoro-1,3,2-dioxaborine ring.

Results and discussion. Boron difluoride complex of *β*-diketone (2,2-difluoro-1,3,2-dioxaborine, F_2DB) is a unique structural motif endowing organic compounds with prominent physicochemical properties, such as a strong fluorescence and high molar attenuation coefficients. Incorporation of the F_2DB core into a polymethine chromophore either as an end-group or as an integral part of the polymethine chain allows obtaining dyes with exceptional characteristics, highly appealing for design of up-to-date functional materials. This review focuses on the synthesis and spectral properties of the F_2DB-containing polymethines along with the latest advancement in the synthesis of highly fluorescent polyanionic polymethines. A brief discussion of the effects of the structural modification of the π-conjugated system on the photophysical properties of dyes is included.

Conclusions. The literature on the F_2DB-containing polymethines demonstrates a high potential of the F_2DB core for the development of strongly fluorescent and intensely absorbing dyes.

Keywords: dioxaborine; polymethine; merocyanine; anionic dye; absorption; fluorescence

В. М. Поліщук, М. П. Шандура
Інститут органічної хімії Національної академії наук України,
вул. Академіка Кухаря, 5, м. Київ, 02660, Україна

Поліметинові барвники на основі 2,2-дифлуоро-1,3,2-діоксаборину: міні-огляд

Анотація

Мета. Узагальнити та проаналізувати літературні дані про поліметинові барвники на основі 2,2-дифлуоро-1,3,2-діоксаборину.

Результати та їх обговорення. Бородифлуоридний комплекс *β*-дикетону (2,2-дифлуоро-1,3,2-діоксаборин, F_2DB) є унікальним структурним елементом, який надає органічним сполукам особливі фізико-хімічні властивості, такі, як сильна флуоресценція та високі коефіцієнти молярної екстинкції. Уведення ядра F_2DB до поліметинового хромофора як кінцевої групи чи як складової частини поліметинового ланцюга дає змогу отримувати барвники з винятковими характеристиками, привабливі для розробки сучасних функціональних матеріалів. У цьому огляді висвітлено питання синтезу та спектральних властивостей поліметинів, що містять ядро F_2DB, а також останні досягнення в синтезі високофлуоресцентних поліаніонних поліметинів. Додано коротке обговорення впливу структурних модифікацій π-спряженої системи на фотофізичні властивості барвників.

Висновки. Аналіз літератури про поліметини, що містять ядро F_2DB, свідчить про високий потенціал діоксаборинового комплексу для розробки барвників з яскравою флуоресценцією та інтенсивним світлопоглинанням.

Ключові слова: діоксаборин; поліметин; мероціанін; аніонний барвник; абсорбція; флуоресценція

■ Introduction

Polymethines are arguably the most versatile class of organic dyes due to a broad viable range of structural fine-tuning that allows obtaining dyes with predetermined characteristics [1]. Numerous polymethine dyes of varying structure are reported to date, of which those bearing the 2,2-difluoro-1,3,2-dioxaborine ring have only recently gained a particular attention. The interest in dioxaborine-containing polymethines is mostly driven by their unique physicochemical properties, in particular, high molar attenuation coefficients (ε), a strong fluorescence in both visible and near-infrared (NIR) spectral regions, high stability in solutions and in the solid state. Accordingly, they became promising objects for applications in NLO materials [2–7], as fluorogenic probes for labeling of DNA [8], lipids [9, 10], and proteins [11, 12], as molecular rotors [13, 14], and as photosensitizers for a long-wavelength cationic photopolymerization [15].

This Perspective summarizes the advancements in research of the F$_2$DB-containing polymethines, as well as the fundamentals of their structure/property relationships. Dioxaborines bearing other than fluorine substituents at the boron atom, such as CN$_2$DB- or Ph$_2$DB-containing compounds [16, 17], are not included. The content is organized in regard to the position of the dioxaborine ring within the polymethine chromophore (as an end-group or as an integral part of the π-chain) and the electronic composition of the π-conjugated system (dipolar/quadrupolar merocyanines or anionic dyes). Although a short note regarding the applications of the F$_2$DB-containing polymethines is included, for more sophisticated discussion of the dioxaborine applications readers are encouraged to consult recent reviews [18–20].

■ Results and discussion

1. 2,2-Difluoro-1,3,2-dioxaborine

According to the IUPAC recommendations, the dioxaborine core, specifically, its betainic valence formulae, should be named as follows: 2,2-difluoro-1,3,2-oxaoxoniaborinine (Figure 1, compound **1**: R^1 = R^2 = R^3 = H). Nevertheless, the name "2,2-difluoro-1,3,2-dioxaborine" for the F$_2$DB complex, first introduced in 1969 [21] has got a wide acceptance. For simplicity, throughout this Perspective dubbings "dioxaborine" and "F$_2$DB" are consistently used, though no acronym for the

2,2-difluoro-1,3,2-dioxaborine core, (as "BODIPY" for compounds with the borondipyromethene core) has been established yet.

1.1. General synthetic methods

The ability of *β*-diketones to form coordination complexes with metalloids (boron, silicon, germanium, etc.) was demonstrated more than a century ago when the synthesis of the first boron *β*-diketonate complexes – bis(acetylacetone) boronium salts [(C$_5$H$_7$O$_2$)$_2$B]AuCl$_4$ and [(C$_5$H$_7$O$_2$)$_2$B]PtCl$_6$ – was reported [22]. These complexes were obtained by the reaction of acetylacetone with boron trichloride followed by the treatment of the intermediate (C$_5$H$_7$O$_2$)$_2$BCl with tetrachloroaurate or hexachloroplatinate salts. However, boronium salts were not formed when boron trifluoride was used instead of BCl$_3$. The treatment of acetylacetone with boron trifluoride results in a substitution of only one fluorine atom, yielding the difluoroboron complex of acetylacetone (BF$_2$-acetylacetone) [23]. The report on obtaining BF$_2$-acetylacetone is the first account of the dioxaborine synthesis employing enolizable *β*-diketones and boron trifluoride. This method has since become the most common synthetic approach to dioxaborines (Scheme 1) [3, 23]. As for the synthesis of enolizable *β*-diketones, the synthetic methods varied broadly, from Claisen condensation to modern practices of using strong bases and a wide variety of both acylating agents and alkyl(aryl)substituted ketones [24, 25].

β-Diketones can also be synthesized through the Lewis base promoted acylation of aromatic compounds. Boron trifluoride as a Lewis base allows obtaining dioxaborines from aromatic compounds in one stage (Scheme 2) [26–42]. This method is particularly convenient for the synthesis of arylsubstituted and benzannelated dioxaborines.

4,5-Disubstituted dioxaborines can be obtained directly from epoxy(aryl)ketones though the ring-opening → rearrangement → BF$_2$-complexation sequence initiated by BF$_3$ (Scheme 3) [43–45]. Electron-donating substituents as R^1 and R^2 tend to accelerate the rearrangement, while electron-withdrawing ones slow it down.
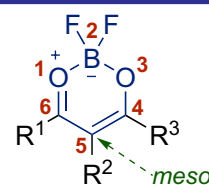
2,2-difluoro-1,3,2-dioxaborine

Figure 1. The structure of the F$_2$DB core
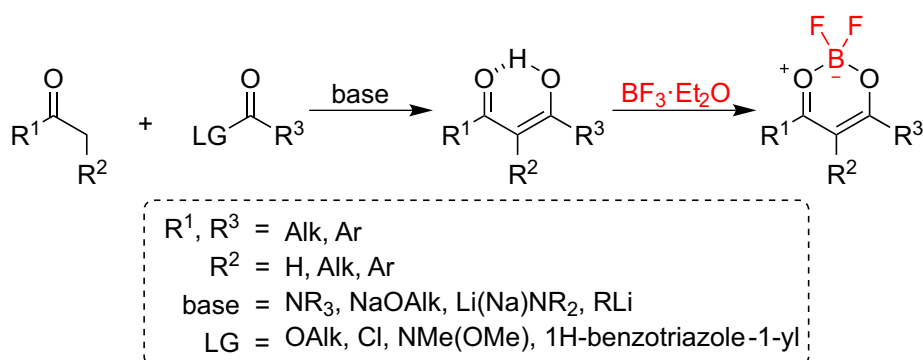
Scheme 1. The general approach to the dioxaborine synthesis
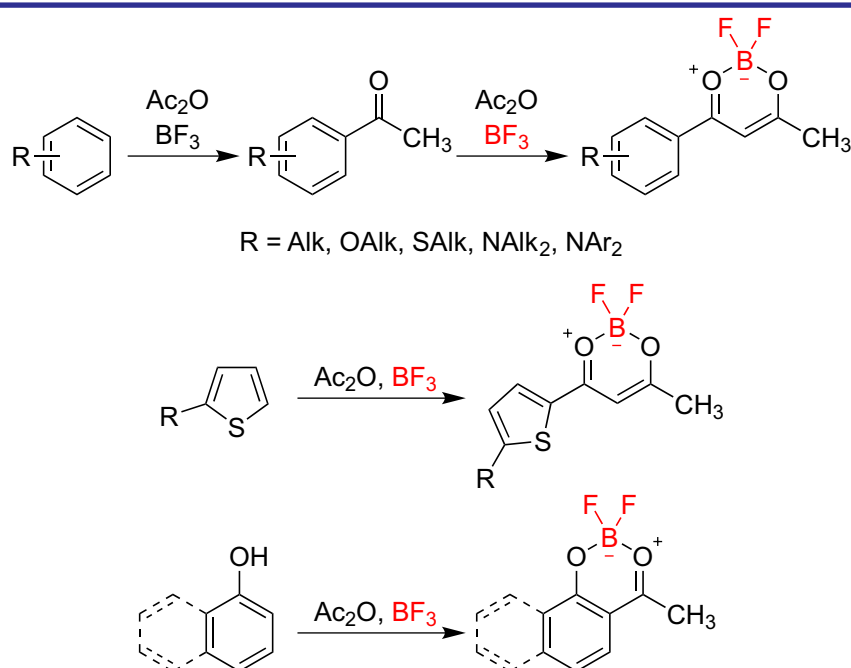
Scheme 2. Examples of the dioxaborine synthesis *via* the BF$_3$-promoted acylation of aromatics
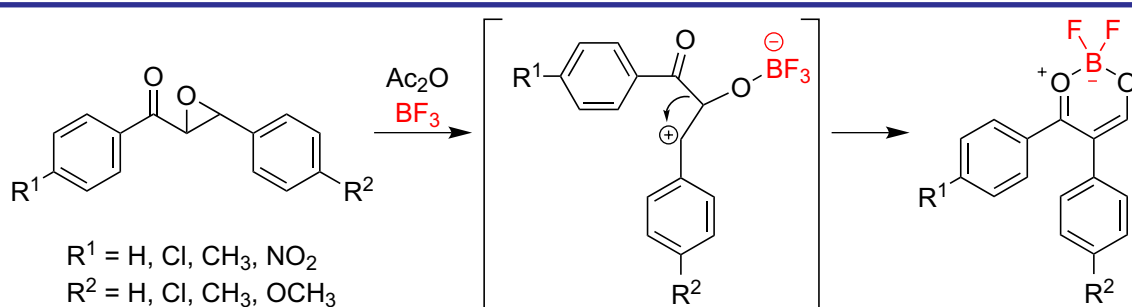
Scheme 3. The synthesis of dioxaborines through the rearrangement of epoxy(aryl)ketones

1.2. Fundamental properties

The 2,2-difluoro-1,3,2-dioxaborine complex is a donor-acceptor system constituting the β-diketonate ligand as an electron donor and boron difluoride as an electron acceptor (Figure 2, **a**). A dipolar character of the F$_2$DB core implies the high dipole moment, amounting to, for example, 7.6($\pm$0.3) D and 6.7($\pm$0.3) D in 1,4-dioxane for the BF$_2$-complexes of benzoylacetone and dibenzoylmethane, respectively [46]. Theoretical investigations suggest

that the major contribution to such a strong polarization is the shift of the π-electron cloud of β-diketonate toward the acceptor BF$_2$ group (Figure 2, **b**: structure **C**) [47].

The depiction of the F$_2$DB core in a charge-separated resonance form can be misleading since a boron atom carries no negative charge. Analogously to inorganic borates (e.g., BF$_4$) [48], the negative charge is shifted to more electronegative fluorine atoms (Figure 2, **b**: structures **A** and **B**) [47].
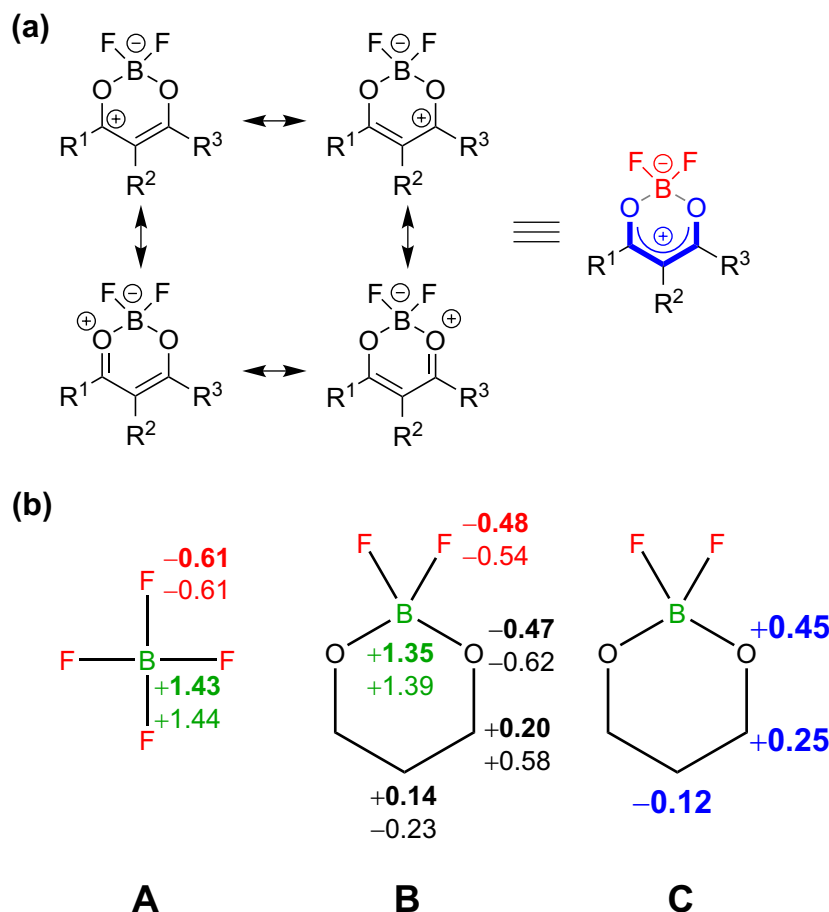
Figure 2. (a) The resonance forms of 2,2-difluoro-1,3,2-dioxaborine; (b) total charges of compound **1** (B) and tetrafluoroborate anion (A) according to the Mulliken population analysis (bold) and the natural population analysis (italics; DFT B3-LYP); charges of the π-system of **1** (C; Pariser–Parr–Pople approach)

Aromatic delocalization is not realized in the dioxaborine ring – the Nucleus-Independent Chemical Shift for **1** (Table 1) amounts to +2.3 ppm [47]. The calculated NICS implies negligible contribution of the BF_2 group into the cyclic delocalization (for the aromatic system, the NICS should be lesser than –3 ppm [49]). In addition, the quantum-chemical calculations have shown the Bp_π–Op_π bonding is more than 4 times weaker than both Op_π–$C_\alpha p_\pi$ and $C_\alpha p_\pi$–$C_\beta p_\pi$ bonding, thus indicating the absence of the ring current. The results of the detailed investigation of the electronic structure of the dioxaborine core, including the energies and spatial distribution of the molecular orbitals, as well as the X-ray and spectral data of the simplest dioxaborines, are reported elsewhere [46, 47, 50–53].

The chelation of the β-diketonate structure by boron difluoride results in a substantial alteration of its properties. Closing of β-diketonate by the BF_2 group is usually accompanied by a bathochromic shift of the absorption maximum (λ^a_{max}) and an increase of the molar attenuation coefficient (ε). The magnitude of these effects is largely dependent on the structure of the parent

Table 1. Electron affinities of substituted dioxaborines calculated by DFT-B3LYP
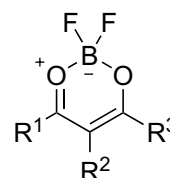
Compound	R^1	R^2	R^3	EA, eV[a]
1	H	H	H	0.97
2	CH₃	H	CH₃	0.63
3	CH₃	H	Ph	2.31
4	Ph	H	Ph	2.11
5	H	CN	H	1.81
6	CN	H	H	2.17
7	H	NO₂	H	1.8
8	NO₂	H	H	2.51
9	CF₃	H	CF₃	2.34
10	p-NO₂Ph	H	p-NO₂Ph	2.98
11	CN	H	CN	3.37
12	NO₂	H	NO₂	3.52

Note: [a] The EA value measures the ability of a neutral molecule (X) to gain an electron:

$$X + e^- \rightarrow X^- + EA$$
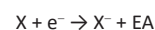
where EA is the energy released upon addition of an electron.

compound. For example, the absorption band of the BF$_2$-complex of acetylacetone lies 11 nm bathochromically and is twice as intense as that of acetylacetone (Figure 3), while for BF$_2$-curcumin the redshift vs. curcumin is much larger (see Figure 9). The downfield shift of the ^{1}H NMR signal of methyl groups of BF$_2$-acetylacetone complies with the electron-withdrawing effect of the BF$_2$ group on the β-diketonate scaffold [46].

The ^{19}F NMR spectra of dioxaborines do not conform with the theoretical model based on the properties of the ^{19}F, ^{10}B, ^{11}B nuclei. Considering the number of B nuclei (n) in *2nI+1* is one and nuclear spins (*I*) of ^{10}B and ^{11}B are equal to 3 and 3/2, respectively, the ^{11}B–^{19}F coupling should lead to an appearance of a quartet (1:1:1:1 intensity ratio), while the ^{10}B–^{19}F coupling should result in a heptet (1:1:1:1:1:1:1). Instead, the ^{19}F NMR spectra of compounds containing the F$_2$DB unit usually comprise a doublet with the intensity ratio of 1:4, reflecting the natural abundances of ^{10}B (19.09%) and ^{11}B (80.1%) isotopes [54]. Interestingly, such a coupling-deprived pattern with different resonance frequencies of ^{19}F atom bonded to ^{10}B and ^{11}B is also observed for AgBF$_4$ in 80% aqueous acetonitrile [55]. The absence of ^{11}B–^{19}F and ^{10}B–^{19}F coupling has not been conclusively explained so far; a suggestion of the rapid quadrupolar relaxation of the boron nuclear-spin states, which effectively decouples the boron from the fluorine nuclei, is debunked experimentally by examining their ^{11}B resonance [46]. In contrast to dioxaborines, BODIPYs are characterized by the appearance of a quartet in their ^{19}F NMR spectra reflecting the ^{11}B–^{19}F coupling (the ^{10}B–^{19}F coupling pattern is rarely visible due to a low abundance of the ^{10}B isotope and its small magnetogyric ratio, though for compounds with inequivalent fluorine atoms such a pattern can be spotted [56]).

As was described above, the electron-accepting nature of the dioxaborine core results from the withdrawal of the π-electron cloud from β-diketonate towards BF$_2$, thus making the OCCCO scaffold electron deficient. Modulation of the accepting strength can be achieved through the introduction of various substituents at positions 4, 5, and 6 of the dioxaborine scaffold. As a quantitative measure of the accepting strength, a molecular electron affinity (EA) can be used (Table 1) [47, 57]. Thus, considering the calculated values of EA, unsubstituted dioxaborine complex **1** is an acceptor of a moderate strength (EA = 0.97 eV)

comparable to nitrobenzene (EA = 1.00 eV [58]). The insertion of one strong electron-withdrawing substituent into a β-diketonate backbone, such as CN or NO$_2$, doubles the magnitude of EA (compounds **5**–**8**), while the *bis*-substitution into positions 4 and 6 makes the F$_2$DB core a strong acceptor (compounds **9**–**12**) comparable to tetracyanoethylene (EA = 3.17 eV [59]).

1.3. Simple dioxaborine-containing π-conjugated systems

Although BF$_2$-acetylacetone absorbs in the near UV region (Figure 3), its absorption maximum can be red-shifted via the substitution of methyl groups with other alkyl or aryl groups. For example, the replacement of both CH$_3$ by *tert*-butyls results in a 10 nm bathochromic shift and a slight increase of the molar absorptivity due to hyperconjugation (Table 2) [46]. Extending the effective length of the conjugated π-system by the introduction of unsubstituted phenyl rings results in larger bathochromic shifts ($\Delta\lambda^a_{max}$ = 47 nm when **2** → **3** and 35 nm when **3** → **4**).

The absorption bands of the arylsubstituted dioxaborines have several maxima attributed to different electronic transitions. The DFT calculations ascribed the long-wavelength band (328–365 nm) of compounds **3**, **4**, **15**–**17** to the ^{1}π–π* excitation delocalized within the whole molecule, while the short-wavelength peak (265–270 nm) was linked to the redistribution of the electron density from aromatic substituents to the F$_2$DB core (light-induced intermolecular charge transfer) [51, 52].

The introduction of electron-donating substituents (methoxy or dialkylamino) into the *para*-position of the phenyl ring of compound **3** leads to a substantial redshift of the absorption maximum and large increase of the fluorescence intensity (Table 3) [60]. The reasoning behind such spectral changes is not only due to an enhancement of the intermolecular charge transfer, but
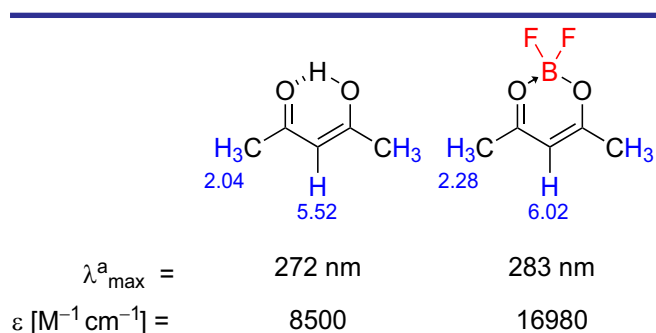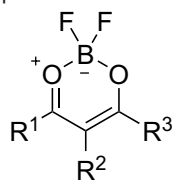

Figure 3. The impact of the BF$_2$-chelation of acetylacetone on the spectral properties (NMR data in CDCl$_3$; λ^a_{max} and ε in CHCl$_3$ as the solvent)

Table 2. Characteristics of the UV absorption spectra of simple dioxaborines in $CHCl_3$

Compound	R^1	R^2	R^3	λ^a_{max} [nm]	$\log(\varepsilon)$
2	CH_3	H	CH_3	283	4.23
3	CH_3	H	Ph	265, 328, 342	3.69, 4.47, 4.29
4	Ph	H	Ph	270, 365, 378	3.69, 4.62, 4.57
13	CH_3	H	*t*-Bu	289	4.26
14	*t*Bu	H	*t*-Bu	293	4.35
15	*n*Pr	H	Ph	265, 330, 346	3.69, 4.51, 4.35
16	*i*Pr	H	Ph	265, 333, 346	3.69, 4.50, 4.32
17	*t*Bu	H	Ph	265, 332, 346	3.69, 4.49, 4.33
18	2-pyridyl	H	Ph	368, 385	4.54, 4.49
19	2-thienyl	H	CF_3	325, 365	4.27, 4.37
20	CH_3	CH_3	CH_3	304	4.19
21	CH_3	CH_3	Ph	260, 334	3.65, 4.36
22	Ph	CH_3	Ph	260, 360	3.65, 4.48

Table 3. Spectral properties of compounds **3**, **23**, and **24** in $CHCl_3$ and MeCN

R = H   OMe   NMe$_2$

3   **23**   **24**
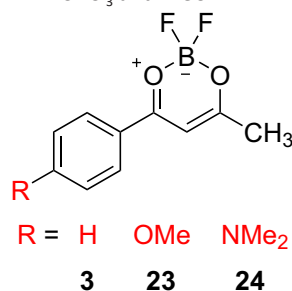
Compound	Solvent	λ^a_{max} [nm]	$\varepsilon \times 10^{-4}$ [M^{-1} cm^{-1}]	λ^f_{max} [nm]	Φ_f	Δv_s [cm^{-1}]
3	$CHCl_3$	328	2.95	382	$9 \cdot 10^{-4}$	4310
	CH_3CN	328	2.69	–	–	–
23	$CHCl_3$	359	4.57	388	0.37	2080
	CH_3CN	356	–	399	0.27	3030
24	$CHCl_3$	422	2.88	463	0.45	2100
	CH_3CN	423	–	485	$1 \cdot 10^{-3}$	3020

also due to the incorporation of an additional electron pair from O- and N-atom to the π-system, thus slightly expanding the effective conjugation length and altering its electronic structure.

The fluorescence intensity of compound **3** can also be increased by hindering free rotation of the phenyl ring around the bond linking it to the F_2DB core. For instance, the insertion of –CH_2–CH_2– and –C(O)–O– bridges via the *ortho*-position of the phenyl ring and position 5 of the F_2DB core leads to a substantial increase of the fluorescence intensity (820-fold for **3 → 25** and 102-fold for **3 → 27**; Table 4) [32, 60]. Further insertion of methoxy or dialkylamino groups into the *para*-position of the phenyl ring greatly increases the molar absorptivity (compounds **26** and **28**).

Benzannelation of the phenyl ring of compound **3** results in a redshift of λ^a_{max}, a significant increase of ε, and a considerable fluorescence enhancement (**3 → 29**; Table 4) [61]. The replacement of the naphthyl substituent with 3-coumarinyl (**29 → 30**) shifts the absorption maximum bathochromically by 37 nm, while the molar absorptivity drops drastically, and the fluorescence is nearly quenched [32]. Expectedly, the introduction of a dialkylamino group into the *para*-position of the phenyl ring (**30 → 32**) induces both a large redshift of λ^a_{max} and an increase of the fluorescence quantum yield. Note that dioxaborine **32** is characterized by an exceptionally high molar attenuation coefficient (ε = 98500 M^{-1} cm^{-1} in DCM) compared to other simple dioxaborines.

Table 4. Optical properties of dyes **25 – 32** in dichloromethane (DCM)

R = H OMe

25 26

R = H NMe$_2$

27 28

29

R = H OH NEt$_2$

30 31 32
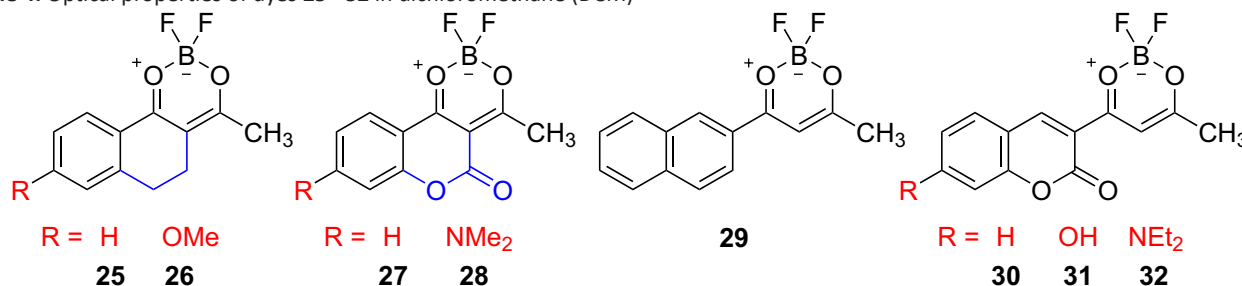
Compound	λ^a_{max} [nm]	$\varepsilon \times 10^{-4}$ [M^{-1} cm^{-1}]	λ^f_{max} [nm]	Φ_f	Δv_s [cm^{-1}]
25	360	2.09	418	0.74	3850
26	383	3.63	414	0.69	1960
27	343	0.87	423	0.092	5510
28	424	5.68	465	0.11	2080
29	344	3.43	–	0.63	–
	380[a]	0.99[a]	459	–	4530
30	381	2.97	489	0.094	5800
31	385	2.70	443	0.23	3400
32	498	9.85	532	0.78	1280

Note: [a] shoulder

## 2. Dioxaborine as an end-group of the polymethine dyes

Polymethine dyes constituting the F$_2$DB core as an end-group (A) can be divided into neutral dipolar compounds of the A–π–D type (also known as merocyanines [62]; D is the electron donor end-group) and anionic symmetric (A–π–A) or non-symmetric (A–π–A') dyes (Figure 4).

The electronic structure of polymethine dyes in the ground state S$_0$ can be rendered as superposition of two boundary states: (*i*) polyene state, which is characterized by low degree of π-delocalization and a considerable alternation of the single and double bonds along the π-chain; and (*ii*) ideal polymethine state (or cyanine-like state [1, 63]) where π-delocalization is of the highest degree with no alternation of the bond orders along the π-chain [64]. The contribution of each of these states to the resulting electronic structure of a dye in the ground state S$_0$ is dependent on the structure of the end-groups and the length of the polymethine chain. The qualitative assessment of their relative contribution can be made on the grounds of spectral properties of a polymethine dye. An approach to the ideal polymethine state is usually accompanied by a narrowing of the absorption and emission bands, an increase of the molar absorptivity, and enhancement of the fluorescence intensity [65–67]. Taking into account these considerations the dioxaborine-containing merocyanines can be divided into two types of scaffolds depending on the electron-donating power of the end-group – type I containing weakly electron-donating *para*-(dialkyl(aryl)amino)phenyl or *para*-alkoxyphenyl end-groups, and type II dyes with stronger electrondonating end-groups (e. g., benzannelated heterocycles). Generally, the electronic structure of type II F$_2$DB-merocyanines is more closely approaching the ideal polymethine state when compared to type I dyes.

2.1. Synthesis of merocyanines and anionic polymethines

Most of the documented F$_2$DB-merocyanines of type I contain end-group *para*-alkoxy- or *para*-dialkylamino-substituted aromatic rings as an electron donor. These compounds can be prepared

Dipolar merocynines

A — π — D

Type I

Type II

Anionic polymethines

A — π — A'
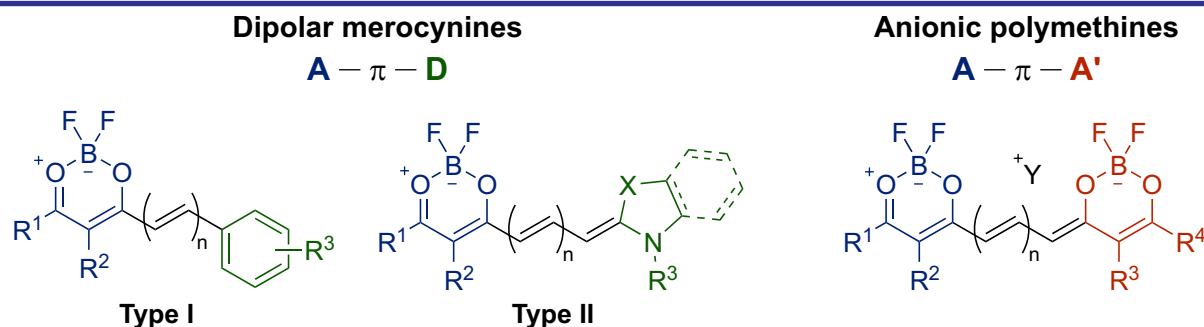
Figure 4. The general structures of merocyanines and anionic dyes containing the F$_2$DB core as an end-group

Path A
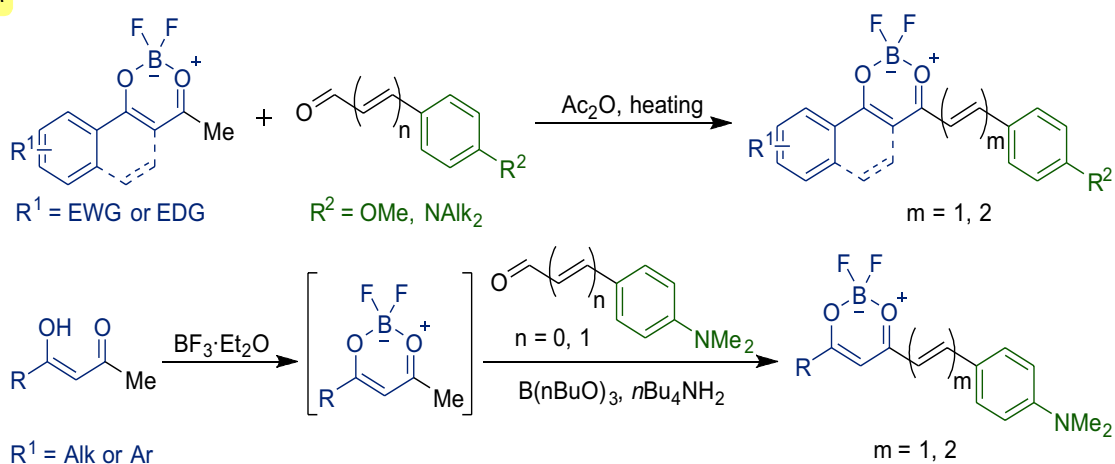
Path B
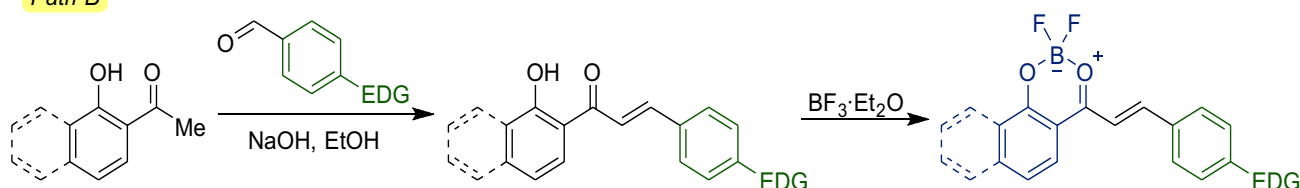
Scheme 4. The synthesis of type I F$_2$DB-containing merocyanines

by (I) condensation of methyl-substituted dioxaborines with benzaldehydes or cinnamic aldehydes when heating in acetic anhydride (Scheme 4, *Path A*) [2, 10, 21, 68, 69], or (II) aldol condensation of *ortho*-hydroxyphenones with benzaldehydes followed by treating with trifluoroborate etherate (Scheme 4, *Path B*) [70, 71]. The modification of the first method includes the initial *in situ* synthesis of the dioxaborine core from β-diketonate and BF$_3$·Et$_2$O and further treatment of the intermediate compound with cinnamaldehyde in the presence of trialkylborate and *n*-butylamine [72].

The electron donor group of type II dipolar polymethines with the F$_2$DB core is represented by benzannelated heterocycles, such as *N*-alkyl-3,3-dimethylindolenine, *N*-alkylquinoline or *N*-alkyl-benzothiazole. Similarly to type I polymethines, these dyes can also be synthesized from methyl-substituted dioxaborines and unsaturated aldehydes when heating in acetic anhydride (Scheme 5, *Path A*) [73–77]. Instead of aldehydes, cationic hemicyanines can be used as an electrophilic substrate (Scheme 5, *Path B*) [74].

Neutral hemicyanines derived from dioxaborines are also suitable electrophilic reagents for the synthesis of dioxaborine-containing merocyanines. The two-step synthetic sequence involves the condensation of methyl substituted dioxaborines with dimethylformamide [73, 77], ethyl isoformanilide [74], dianils of malondialdehyde [9, 11, 74, 77, 78] or glutaconaldehyde [9] followed by the reaction of the obtained hemicyanines with quaternary heterocyclic salts (Scheme 5, *Path C*).

Symmetric anionic dioxaborine-containing polymethines can be synthesized in one stage from methyl-substituted dioxaborine and triethyl orthoformate [73, 79, 80], acrolein diethyl acetal [79], dianils of malondialdehyde [6] or glutaconaldehyde [78, 81], salts of 1,7-*bis*(dimethylamino) hepta-1,3,5-trienes [3, 6] in the presence of a base and acetic anhydride (Scheme 6, *Path A*). Polymethines with functional groups in the polymethine chain can be obtained similarly via the condensation of functionalized iminium salts with dioxaborine nucleophiles [3, 5, 79, 80, 82]. An alternative path to F$_2$DB-containing anionic dyes includes the two-stage sequence starting from the F$_2$DB-containing hemicyanine synthesis and subsequent condensation of the obtained intermediate with the nucleophile (Scheme 6, *Path B*) [78]. By this method non-symmetric dyes can be obtained [83].

2.3. Spectral properties of dioxaborine-containing merocyanines

Dipolar type I F$_2$DB-merocyanines are characterized by absorption in the visible region (400–650 nm). The bathochromic shift upon extending of the polymethine chain by one vinylene group (vinylene shift) amounts to nearly 50 nm (50 nm for **36 → 38** in MeCN or 42 nm for **39 → 40**
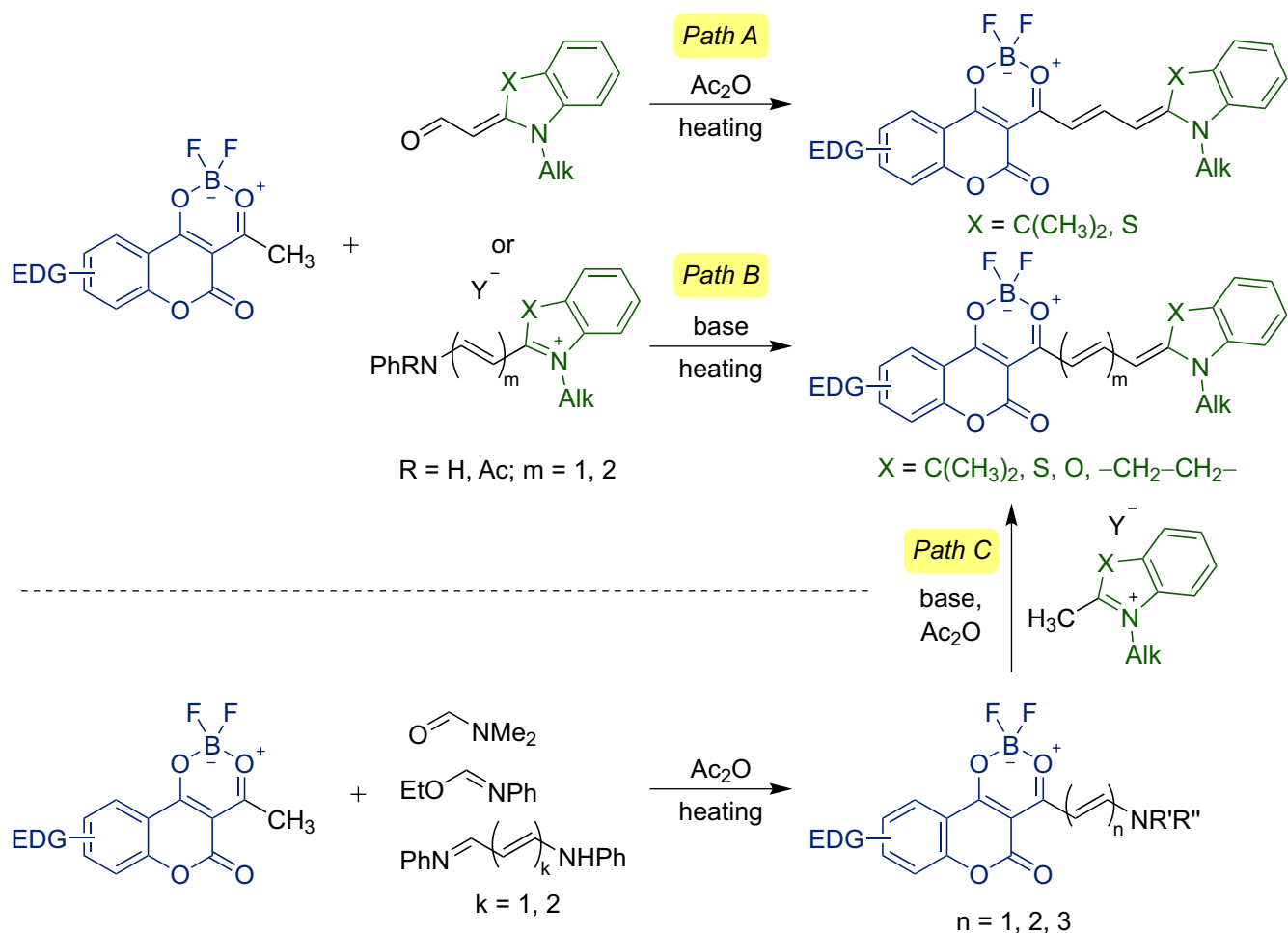
Scheme 5. The synthesis of type II F$_2$DB-containing merocyanines
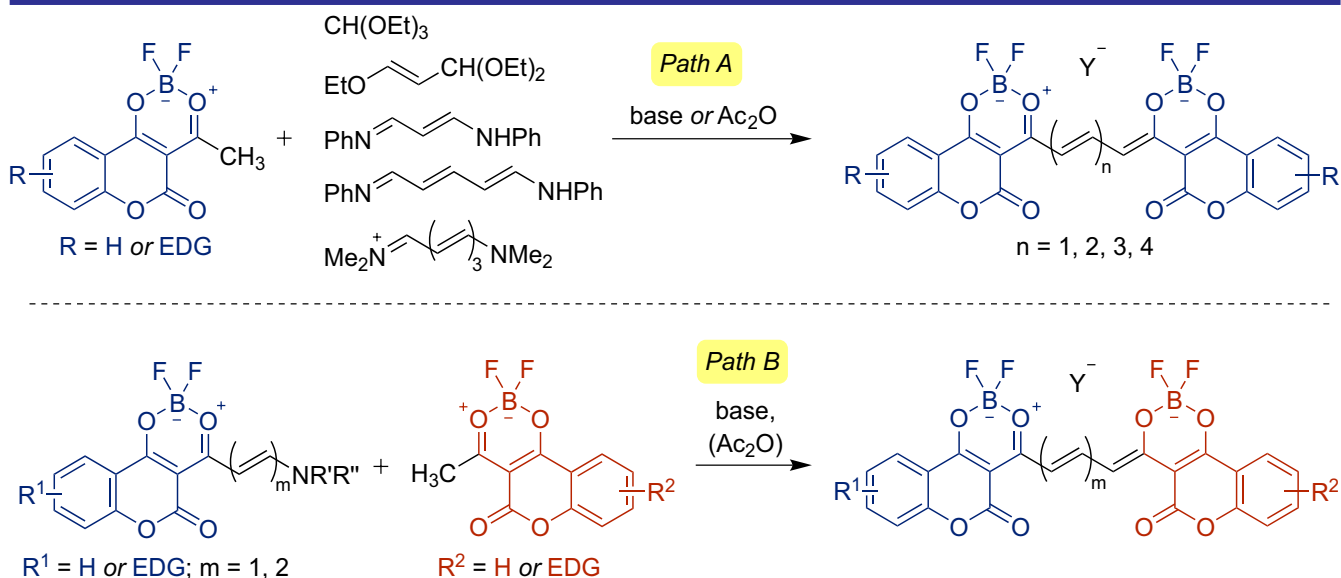
Scheme 6. The synthesis of symmetric and asymmetric F$_2$DB-containing anionic polymethines

in 1,2-dichloroethane; Tables 5 and 6) [21, 69], while for the dye with a diethylamine end-group vinylene shift reaches 84 nm in MeCN (**33 → 34**). Considering that the vinylene shift of symmetric cyanine dyes – polymethines, which approach the ideal polymethine state in the ground state S$_0$, –

reaches 100 nm [63], such a low vinylene shift of type I F$_2$DB-merocyaniens marks their polyenic-like electronic structure.

In addition to the lengthening of the π-chain, the structural modification of the electron donor end-group can also yield a significant bathochromic

Table 5. Spectral properties of type I F$_2$DB-merocyanines in CHCl$_3$
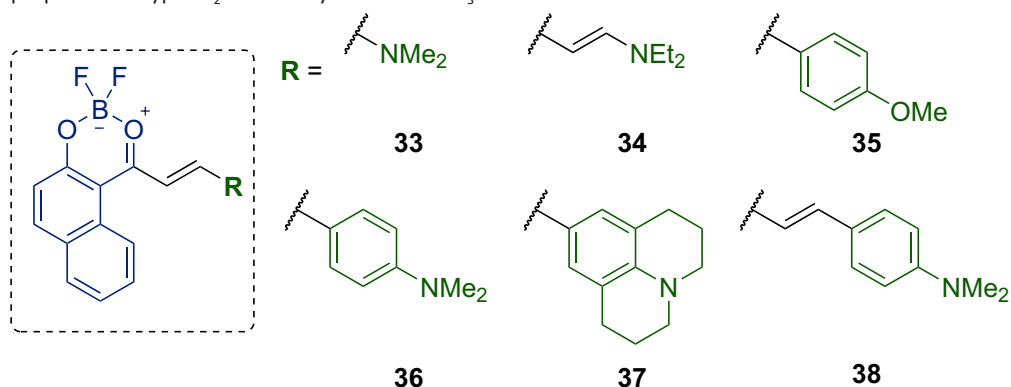
Compound	λ^{a}_{max} [nm] ($\varepsilon \times 10^{-4}$ [M^{-1} cm^{-1}])		
33	245 (*2.38*)	412 (*3.12*)	428 (*2.76*)
34	240 (*1.35*)	484 (*5.47*)	512 (*5.78*)
35	224 (*4.36*)	374 (*1.24*)	470 (*2.10*)
36	252 (*1.08*)	–	570 (*7.2*)
37	–	–	610 (*6.3*)
38	230 (*3.0*)	–	620 (*5.55*)

Table 6. Optical properties of dyes **39** and **40** in various solvents
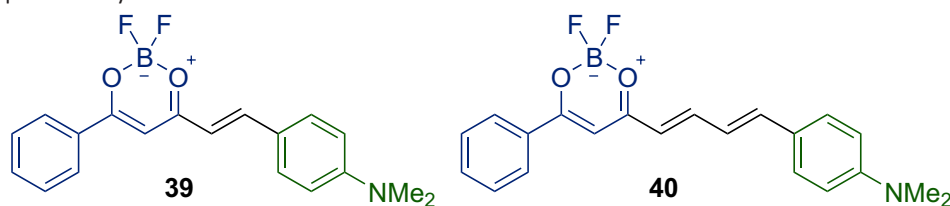
Compound	Solvent	λ^{a}_{max} [nm]	λ^{f}_{max} [nm]	Φ_f
39	toluene	519	571	0.8
	1,2-dichloroethane	536	635	0.025
	DMSO	553	660	0.002
40	toluene	555	640	0.35
	1,2-dichloroethane	578	712	0.071
	DMSO	580	770	0.003

shift. For instance, the replacement of the methoxy by a dialkylamino group leads to a 100 nm redshift of λ^{a}_{max} (**35** → **36** in MeCN) and a three-fold increase of the molar absorptivity. The fluorescence quantum yield of 4-(dialkylamino)phenyl-containing polymethines is also exceptionally high as for polymethine dyes (0.8 in toluene for dye **39**). The fluorescence intensity of the type I F$_2$DB-containing merocyanines significantly decreases with a decrease of the solvent polarity. Such sensitivity to the environment polarity stimulated an extensive research on dimethine- and tetramethine-bridged donor-acceptor systems as fluorescent probes for bioimaging [10, 72, 84–88].

Merocyanines bearing the BF$_2$-complex of 8-(dialkylamino)-3-acetyl-4-hydroxycoumarin have outstanding spectral properties among the type I F$_2$DB-merocyanines, such as a high molar extinction coefficient and a strong fluorescence

(Table 7) [10, 14]. Similar to compounds **39** and **40**, dyes **41** and **42** are characterized by a high sensitivity of the fluorescence intensity to the solvent polarity. Besides, dyes **41** and **42** possess the highest molar absorption coefficients among the type I F$_2$DB-merocyanines.

Non-linear optical properties of several type I F$_2$DB-merocyanines have also been evaluated. The electro-optic coefficient r_{33}, as well as the product of the ground state dipole moment and the first hyperpolarizability $\mu\beta$ can be adjusted in a broad range via the structural modification of the phenyl ring of the dioxaborine end-group. For instance, the introduction of the NO$_2$ group into the *para*-position of the phenyl ring of the dioxaborine core results in a three-fold increase of the $\mu\beta$ magnitude (**45** → **46**; Table 8) [2]. Lengthening of the π-chain by one vinylene group induces a two-fold increase of r_{33} and $\mu\beta$

Table 7. Spectral properties of polymethines **41** and **42**
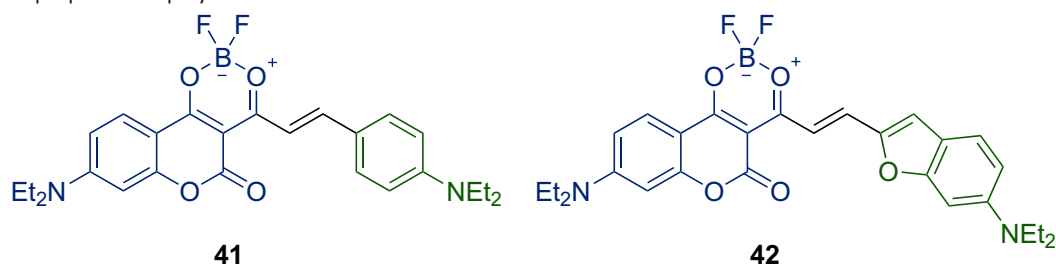
Compound	Solvent	λ^a_{max} [nm]	$\varepsilon \times 10^{-4}$ [M^{-1} cm^{-1}]	λ^f_{max} [nm]	Φ_f
41	cyclohexane	542	–	556	0.46
	toluene	567	–	597	0.93
	ethanol	581	12.0	635	0.044
	DMSO	607	–	659	0.035
42	cyclohexane	602	12.8	622	0.93
	toluene	627	–	687	0.81
	ethanol	645	12.3	748	0.18
	DMSO	678	9.3	778	0.03

Table 8. Non-linear optical properties of type I F$_2$DB-merocyanines

Compound	R^1	R^2	R^3	λ^a_{max} (CHCl$_3$) [nm]	r_{33} [nm V^{-1}]	$\mu\beta \times 10^{-48}$ [esu]
39	H	NMe$_2$	H	530	1.98	364
43	OMe	NEt$_2$	H	538	1.57	284
44	F	NBu$_2$	H	546	2.97	514
45	H	–N–	–(CH$_2$)$_3$–	570	3.26	512
46	NO$_2$	–N–	–(CH$_2$)$_3$–	609	11.4	1400
47	NO$_2$	NMe$_2$	H	614	23.64	3150

values (**46** → **47**), thus rendering dye **47** and its derivatives promising objects for non-linear optical devices.

In contrast to type I dyes, type II F$_2$DB-merocyanines absorb not only in the visible region, but also in the near-infrared (Table 9). While type I dyes have a moderate magnitude of ε, the molar absorbance of type II dyes is typically nearly twice as intense and often exceeds the value of 200000 M^{-1} cm^{-1} in the band maximum [78]. Vinylene shifts are also larger for type II polymethines, reaching 100 nm (e.g., **56** → **50**). These properties along with sharp absorption bands imply a high similarity of the ground S$_0$ and excited S$_1$ states of type II F$_2$DB-merocyanines, thus indicating an effective delocalization of the π-electrons along the chromophore. Interestingly, a decrease of the accepting strength of the dioxaborine core by insertion

of dialkylamino substituents into the aromatic ring (**48** → **51** → **57**) enhances stability of the dyes toward the hydrolytic cleavage of the boron difluoride group [75].

In addition to type II polymethines designed from the BF$_2$-complex of 3-acetylcoumarin, merocyanines derived from the BF$_2$-complex of 5-acetylbarbituric acid (**58–63**) are also characterized by notable spectral properties [9]. For example, the molar absorptivity for dye **60** reaches 363000 M^{-1} cm^{-1} in DMSO, while dye **62** intensely fluoresces in the NIR region (λ^f_{max} = 779 nm and Φ_f = 0.33 in DMSO). Moreover, the fluorescence brightness (ε × Φ_f) of dye **60** amounts to 152000 M^{-1} cm^{-1}, which is one of the highest magnitudes among merocyanines. These dyes also possess prominent non-linear optical properties, making them suitable candidates for application in two-photon excitation microscopy.

Table 9. Spectral properties of type II F_2DB-merocyanines in $CHCl_3$

48, 50-56 **49**, **57**
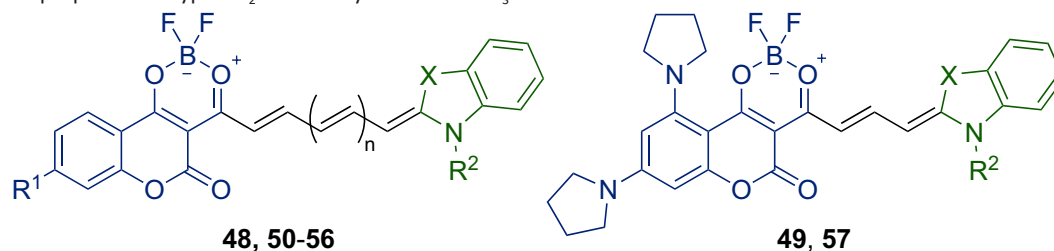
Dye	X	n	R^1	R^2	λ^a_{max} [nm]	$\varepsilon \times 10^{-5}$ [M^{-1} cm^{-1}]	λ^f_{max} [nm]	Φ_f	$t_{0.5}$ [a] [s]	k [b] [s^{-1}]
48	$C(CH_3)_2$	0	H	Me	569	1.49	590	0.03	50	1.40×10^{-2}
49	S	–	–	Me	601	–	620	0.49	–	–
50	CH=CH	1	NEt_2	Bu	721	3.15	729	–	–	–
51	$C(CH_3)_2$	0	NEt_2	Me	582	2.31	601	0.74	300	2.33×10^{-3}
52	$C(CH_3)_2$	1	H	Me	665	2.57	677	0.26	–	–
53	$C(CH_3)_2$	1	NEt_2	Me	668	2.33	686	0.52	42	1.64×10^{-2}
54	S	0	NEt_2	Et	594	–	606	0.40	1050	6.61×10^{-4}
55	S	1	NEt_2	Et	687	–	702	0.67	–	–
56	CH=CH	0	NEt_2	Bu	617	2.48	639	0.02	–	–
57	$C(CH_3)_2$	–	–	Me	585	–	608	0.55	7330	9.46×10^{-5}

Note: [a] half lifetime [75]; [b] hydrolytic rate constant

Table 10. Spectral properties of dyes bearing the BF_2-complex of 5-acetylbarbituric acid as the end-group

Cy = cyclohexyl

58, 60, 62 **59, 61, 63**
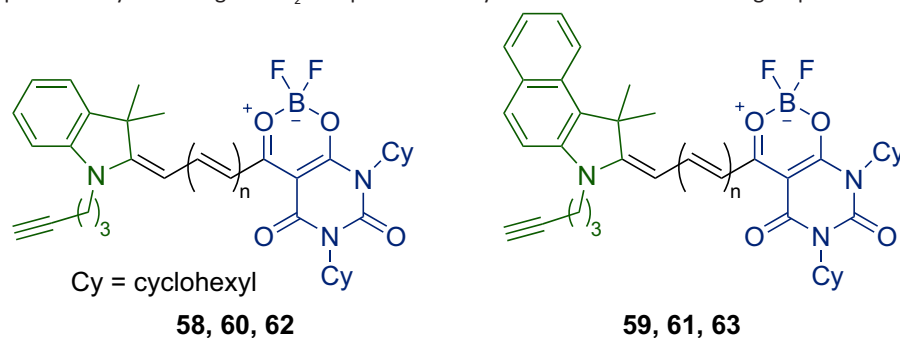
Dye	n	Solvent	λ^a_{max} [nm]	$\varepsilon \times 10^{-5}$ [M^{-1} cm^{-1}]	λ^f_{max} [nm]	Φ_f	$\varepsilon \times \Phi_f \times 10^{-5}$
58	1	toluene	528	0.94	550	0.3	0.28
		DMSO	540	0.77	558	0.37	0.29
59	1	toluene	551	1.24	572	0.68	0.84
		DMSO	563	1.10	583	0.18	0.20
60	2	toluene	615	2.03	642	0.35	0.71
		DMSO	644	3.63	665	0.42	1.52
61	2	toluene	634	1.68	661	0.65	1.09
		DMSO	663	2.41	687	0.26	0.63
62	3	toluene	683	1.09	727	0.21	0.23
		DMSO	748	2.31	779	0.33	0.76
63	3	toluene	705	0.89	746	0.18	0.16
		DMSO	770	1.83	794	0.18	0.33

2.4. Spectral properties of anionic dioxaborine-based polymethines

Spectral properties of anionic F_2DB-containing polymethines can be significantly altered by minor changes in both the structure of the end-groups and the length of the π-chain. For example, the insertion of $-CH_2-$ bridges into the end-groups of dye **64** via the *ortho*-position of the phenyl rings and position 5 of the F_2DB core induces a signifi-

cant increase of the molar absorptivity (Table 11; ε(**65**)/ε(**64**) = 1.30) [83]. Compound **65** also intensely fluoresces at λ^f_{max} = 621 nm (Φ_f = 0.50 in DCM). However, when $-CH_2-CH_2-$ bridges are introduced, molar attenuation coefficients drop (ε(**66**)/ε(**64**) = 0.75), though its fluorescence intensity remains comparable to those of **65**.

Stiffening of the end-groups of dye **64** by $-C(O)-O-$ bridges leads to a considerable increase

Table 11. Optical characteristics of anionic dioxaborine-containing polymethines in DCM

64

65: n = 1
66: n = 2

67: n = 1, m = 0
68: n = 2, m = 1

Compound	λ^a_{max} [nm]	$\varepsilon \times 10^{-5}$ [M^{-1} cm^{-1}]	λ^f_{max} [nm]	Δv_s [cm^{-1}]	Φ_f
64	600	1.38	–	–	–
65	613	1.80	621	210	0.50
66	625	1.04	636	277	0.30
67	638	1.52	648	249	0.21
68	622	1.32	644	549	0.10

Table 12. Optical properties of symmetric anionic polymethines

69, 70, 71-73

74-76

Compound	n	R	Alk	Solvent	λ^a_{max} [nm]	$\varepsilon \times 10^{-5}$ [M^{-1} cm^{-1}]	λ^f_{max} [nm]	Δv_s [cm^{-1}]	Φ_f
69	1	H	Et	CHCl$_3$	581	2.11	588	205	0.19
				MeCN	572	2.15	581	271	0.04
70	1	NEt$_2$	*n*Bu	CHCl$_3$	625	2.36	635	252	0.85
				MeCN	615	2.52	639	611	0.4
71	2	H	Et	CHCl$_3$	678	2.13	687	193	0.16
				MeCN	671	2.29	678	154	0.16
72	2	NEt$_2$	Et	CHCl$_3$	715	3.03	730	287	
				MeCN	712	3.00	732	384	0.76
73	3	NEt$_2$	Et	CHCl$_3$	817	–	–	–	–
				MeCN	810	2.86	–	–	–
74	1	–	Et	CH$_2$Cl$_2$	530	1.69	546	553	0.31
				MeCN	525	2.10	–	–	–
75	2	–	Et	CH$_2$Cl$_2$	630	2.03	651	512	0.82
				MeCN	625	2.22	–	–	–
76	3	–	Et	CH$_2$Cl$_2$	735	1.77	760	448	0.43
				MeCN	725	1.61	–	–	–

of the molar absorptivity (ε(**69**)/ε(**64**) = 1.53; Table 12) though its absorption maximum shifts hypsochromically by 19 nm in chlorinated solvents [78]. The insertion of a dialkylamino group into the *para*-position of the aromatic ring of the F$_2$DB end-group leads to an increase of the fluorescence quantum yield (Φ_f(**70**)/Φ_f(**69**) = 4.47 in CHCl$_3$). Lengthening of the polymethine chain of dye **70** by one vinylene group enhances the fluorescence intensity by almost two-fold in MeCN (**70** → **72**). Considering a high molar absorptivity of dye **72** (300000 M^{-1} cm^{-1} in MeCN), its brightness ($\varepsilon \times \Phi_f$) reaches the magnitude of

228000 M^{-1} cm^{-1}, which is outstandingly high for polymethine dyes, especially those emitting in the NIR region (λ^f_{max} = 732 nm for **72**). Similar to dyes **69**, **70**, and **71**−**73**, anionic polymethines **74**−**76** constructed from the BF$_2$-complex of 5-acetylbarbituric acid are also characterized by an intense absorption and a strong fluorescence [80].

Among the documented symmetric anionic dioxaborine-containing polymethines, the most deep-colored dyes are compounds **77** (λ^a_{max} = 844 nm in DCM) [80] and **78** (λ^a_{max} = 928 nm in DCM) [5]. Although these dyes are virtually non-fluorescent, their non-linear optical properties are
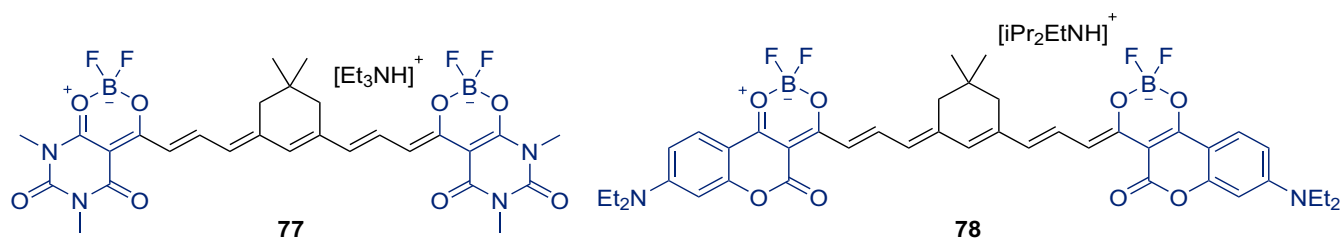
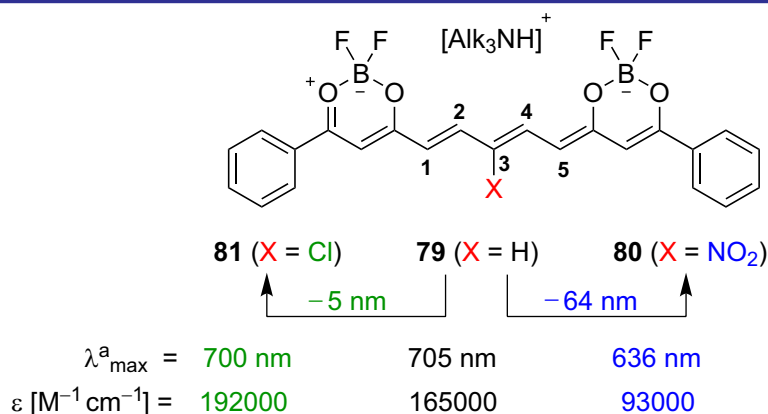**Figure 5.** The long-chained symmetric anionic polymethines

Figure 6. An example of alterations of the optical properties of the anionic dye through structural modifications of the π-chain (in DMSO)

more appealing [3, 6, 7]. For instance, the two-photon cross-section of compound **78** amounts to 17000 GM at 1100 nm in MeCN.

The vinylene shift of anionic polymethines is approximately 100 nm, which is similar to that of symmetric cationic dyes. The nature of a solvent (polar/non-polar, protic/aprotic) has a little effect on the positions of both absorption and emission maxima, while a small blueshift is observed when going from acetonitrile to DCM (or CHCl₃) [74, 78, 80]. Anionic F₂DB-containing polymethines are more resistant to the hydrolytic cleavage of the BF₂ group compared to F₂DB-containing merocyanines. Similar to merocyanines, the stability upon hydrolysis also increases when electron-donating functional groups are introduced into the aromatic ring of the F₂DB core [75].

Spectral properties of anionic polymethines can be significantly altered by the insertion of either electron-donating or electron-withdrawing substituents into the π-chain (Figure 6) [82]. For example, the replacement of H-atom at the *meso*-position of the pentamethine-bridged anionic dye by the NO₂ group (**79 → 80**) leads to a blueshift of the absorption maximum and a significant decrease of the absorption intensity (ε(**80**)/ε(**79**) = 0.56 in DMSO). These spectral changes agree with the Dewar-Knott color rules, according to which the electron-withdrawing substituents at odd-numbered positions of the π-chain

induce a hypsochromic shift of the absorption maximum [89, 90].

The detailed investigation of the electronic structure of the anionic F₂DB-containing polymethines is reported elsewhere [80, 83, 91, 92]. In general, anionic dioxaborine-containing polymethines can be regarded as oxonol dyes, in which the negative charge is delocalized from the terminal O-atom of one end-group along the π-chain to the terminal O-atom of another end-group. A virtual build-up of the dioxaborine complex atop the heptamethine oxonol (**82 → 83**) results in a stabilization of HOMO (ΔE = 1.83 eV) and LUMO (ΔE = 0.85 eV) of the π-conjugated system [80, 93]. The long-wavelength absorption maximum of anionic polymethines is attributed to the S₀ → S₁ electronic transition, while a less-intense higher energy shoulder (Δν = 1200–1400 cm⁻¹) is attributed to the 0 → 1′ vibronic transition [92]. The BF₂-fragment is not involved in low-energy electronic transitions though it stabilizes significantly the anionic π-system.

3. Dyes with the dioxaborine ring in the polymethine chain

Dioxaborine can be regarded as integrated into the π-chain when the polymethine linkage is connected to positions 4 and 6 of the F₂DB core. When in such a framework the end-groups are electron donors, the overall electronic structure of the π-conjugated system attains a quadrupolar
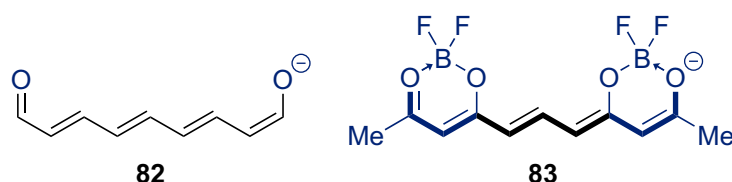
Figure 7. Structures of compounds **82** and **83**

character (the D–п–A–п–D type) [94]. In contrast to mesoionic cyanines built on the squarate or croconate core [95, 96], which also have a quadrupolar structure, the F₂DB-containing polymethines of the D–п–A–п–D type are characterized by the predominance of the neutral resonance form (without a charge separation) in the ground state.

The research on the F₂DB-containing quadrupolar merocyanines laid essentially dormant until 2009 when compounds **84** and **85** were discovered to have a strong fluorescent response upon binding to amyloid-*β* (A*β*) deposits [97] – a hallmark of Alzheimer's disease [98]. From this time on, both the diversity of the F₂DB-containing quadrupolar merocyanines and the range of their applications have been constantly growing.

3.1. Synthesis of BF₂-curcuminoids

Two general methods have been developed for the synthesis of dyes with the dioxaborine ring in the polymethine chain. The first one is the condensation of BF₂-acetylacetone with aromatic or cinnamic aldehydes [99] in the presence of either (i) base only (such as triethylamine [97], tetrahydroisoquinoline [68], or piperidine [100]) or (ii) base (often *n*-butylamine) with trialkyl borate as an additive [8, 101]. Trialkyl borate is shown to significantly increase the product yield though its mechanism of action has not been conclusively understood so far.
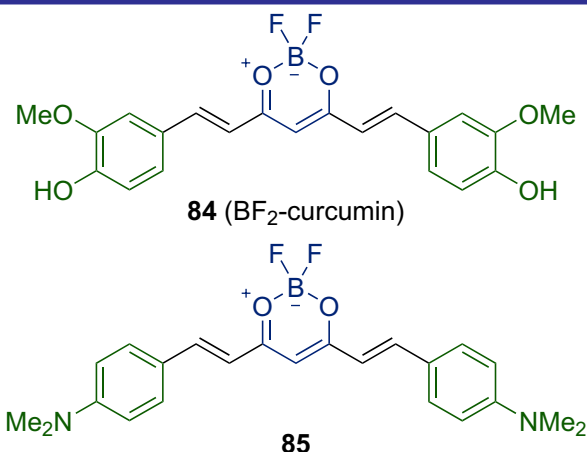
Figure 8. Structures of BF₂-curcumin and its analog **85**

The intermediate half-product can be isolated and put into the reaction with another aldehyde, thus yielding an asymmetric dye (Scheme 8) [68, 94, 99, 101].

The second method is a two-stage sequence with the initial construction of the *β*-diketonate-containing polymethine (curcumin-like scaffold or curcuminoid) followed by its treatment with BF₃ (Scheme 9) [102–105]. Acetylacetone (or its 5-alkyl- or 5-arylsubstituted derivative) reacts with boric anhydride producing the tetracoordinated boronic intermediate, which is further subjected into the reaction with aromatic aldehydes in the
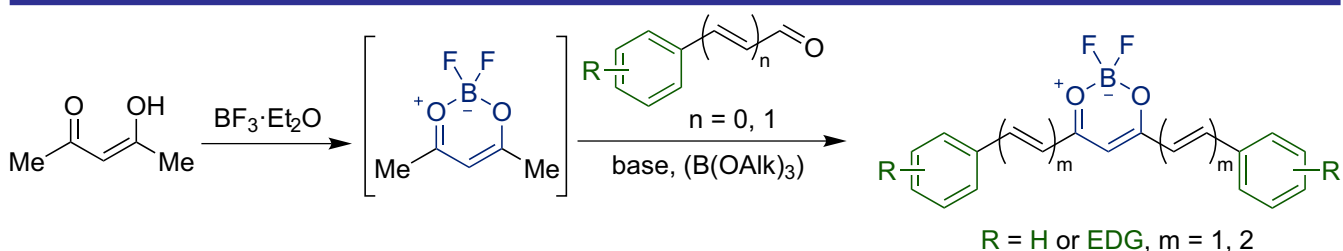
Scheme 7. The synthesis of symmetric BF₂-curcuminoids
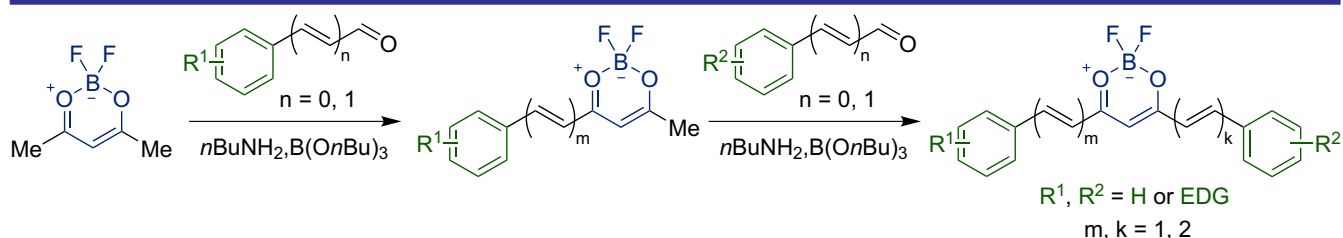
Scheme 8. The synthesis of asymmetric BF₂-curcuminoids
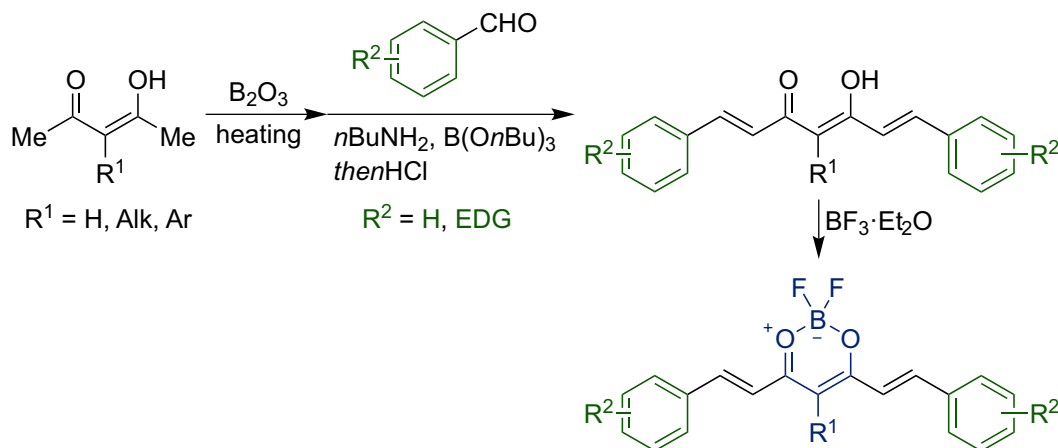
Scheme 9. An alternative route to symmetric BF$_2$-curcuminoids

λ$^a_{max}$ [nm]	λ$^f_{max}$ [nm]	ε [M^{-1}cm^{-1}]	Φ$_f$	λ$^a_{max}$ [nm]	λ$^f_{max}$ [nm]	ε [M^{-1}cm^{-1}]	Φ$_f$
418	495	55000	0.10	**500**	**560**	**77000**	**0.34**
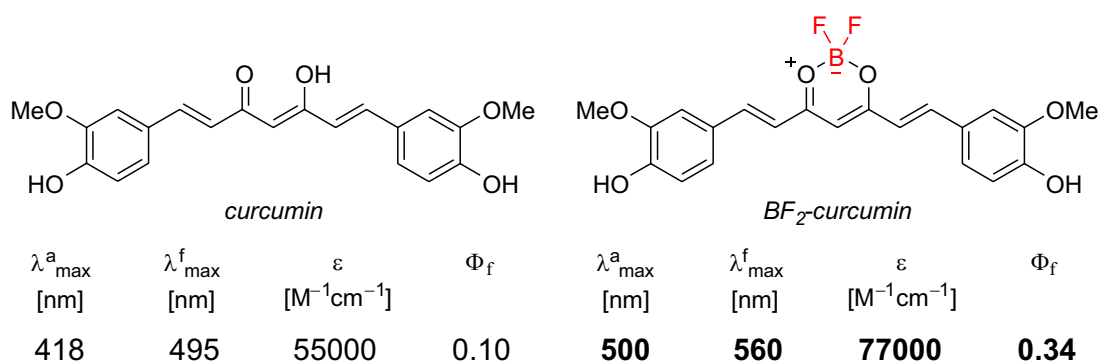
Figure 9. The influence of BF$_2$-chelation on spectral properties of curcumin

presence of *n*-butylamine and trialkyl borate. The product of this reaction is a tetracoordinated bis-curcuminoid, the acid-promoted decomposition of which results in a release of the curcuminoid scaffold. Then its treatment with BF$_3$·Et$_2$O fastens the β-diketonate backbone with the BF$_2$ group, forming the dioxaborine core.

3.2. Spectral characteristics

Basic spectral properties of the BF$_2$-curcuminoids are similar to those of dipolar F$_2$DB-merocyanines of type I: they absorb mostly in the visible range with the molar attenuation coefficients rarely exceeding 100000 M^{-1} cm^{-1}.
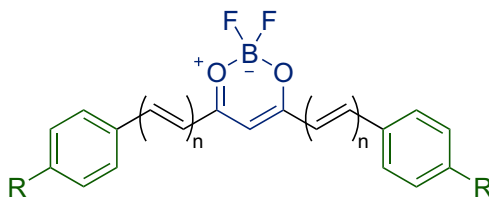
BF$_2$-chelated curcumin absorbs bathochromically by 82 nm (in DCM) and more intensely than the parent compound (Figure 9) [106]. The fluorescence quantum yield is also larger for the BF$_2$-derivative though the reported data on the Φ$_f$ range of BF$_2$-curcumin is not conclusive. For example, paper [106] provides the Φ$_f$ value of 0.34 in DCM, while earlier data from [107] give twice as large figure.

Similar to dipolar type I merocyanines, the position of λ$^a_{max}$ is more sensitive to the structural modification of the end-groups than to the change of the π-chain length. For example, vinylene shifts of quadrupolar BF$_2$-merocyanines amount

to approximately 50 nm depending on the end-groups (52 nm for **87 → 92**; 34 nm for **91 → 93**; Table 13) [100], while the replacement of H-atom by a dimethylamino group in the *para*-position of phenyl rings shifts the absorption maximum bathochromically by 150 nm (**87 → 85**). Note that the fluorescence intensity of **85** is nearly twice as large as that of **87**. The introduction of an electron-withdrawing cyano group at position 4 of phenyl rings shifts the long-wavelength λ$^a_{max}$ hypsochromically by 26 nm with a little change of the fluorescence intensity [105].

BF$_2$-curcuminoids are positively solvatochromic, though the absorption maximum shift with an increase of the solvent polarity is not as large as for type I F$_2$DB-merocyanines [102]. However, in contrast to both dipolar and anionic dioxaborine-containing polymethines, quadrupolar BF$_2$-merocyanines are characterized by much more noticeable redshift of the emission maximum with the solvent polarity increase (Table 14). Moreover, the fluorochromic effect is larger for dyes bearing stronger electron-donating end-groups (compare Δν$_s$ values of **91** and **94**, Table 14).

The detailed investigation of the impact of both the electron donor strength of the end-groups and the nature of the solvent on spectral properties

Table 13. Spectral properties of BF$_2$-curcuminoids **86−93** in DCM

Dye	n	R	λ^a_{max} [nm]	$\varepsilon \times 10^{-5}$ [M^{-1} cm^{-1}]	λ^f_{max} [nm]	Φ_f	Δv_s [cm^{-1}]
86	1	CN	421	0.59	–	0.19	–
87	1	H	447	0.45	484	0.24	1710
88	1	Me	464	0.56	–	0.15	–
89	1	Br	433	0.41	–	0.08	–
90	1	SMe	503	0.86	–	0.55	–
91	1	OMe	489	0.76	546	0.49	2130
85	1	NMe$_2$	597	0.45	681	0.47	2070
92	2	H	499	0.81	556	0.27	2050
93	2	OMe	523	0.83	625	0.24	3120

Table 14. Spectral properties of dyes **91** and **94** in solvents of different polarity

Solvent	91				94			
	λ^a_{max} [nm]	λ^f_{max} [nm]	Φ_f	Δv_s [cm^{-1}]	λ^a_{max} [nm]	λ^f_{max} [nm]	Φ_f	Δv_s [cm^{-1}]
CCl$_4$	477	492	0.20	640	523	561	0.23	1300
Et$_2$O	475	497	0.24	930	516	587	0.29	2340
AcOEt	480	515	0.35	1420	524	590	0.31	2140
DCM	488	538	0.44	1910	536	616	0.39	2420
acetone	483	534	0.45	1980	532	622	0.21	2720
MeCN	483	549	0.51	2490	530	651	0.12	3510

of BF$_2$-curcuminoids is reported elsewhere [94, 102, 108–111]. Generally, positive fluorochromism can be explained by higher energy requirement for the polar solvent to rearrange the solvate shell around the quadrupolar molecule during the relaxation from the Frank-Condon excited state S$_1$^{FC} to the relaxed state S$_1$ [102]. Since the excited state S$_1$ is more polar than the ground state S$_0$ and is characterized by the intramolecular charge transfer, enhancement of the electron donor power of the end-groups has an additional effect on the energy profile of relaxation S$_1$$^{FC} \rightarrow$ S$_1$, which resulted in higher magnitudes of the Stokes shift [94, 102, 109].

3.3. Applications

The range of applications of BF$_2$-curcuminoids is varied broadly and predominantly relates to biochemical research. For example, besides dyes **84** and **85**, several other similar probes were developed for targeting amyloid-*β* aggregates.

These include dye **95**, which was specifically designed to target soluble forms of A*β* [68], allowing detection of the early stages of the disease, when symptoms had not yet become apparent. Bifunctional probe **96** is proved effective for both targeting the A*β* deposits and inhibition of the metal-catalyzed cross-coupling of A*β* [112]. The latter ability greatly diminishes the speed of formation of insoluble forms of A*β* plaques, thus slowing down the disease progression. Probe **97** capable of detecting both soluble and insoluble A*β* species by applying the near-infrared fluorescence (NIRF) molecular imaging [113]. It was the first time when the NIRF technique was demonstrated to be effectively used for the therapy of Alzheimer's disease.

The mechanism of action of compounds **95–97** is based on non-covalent interaction between the probe and a biomolecule. The BF$_2$-curcuminoid scaffold is also suitable for designing probes for
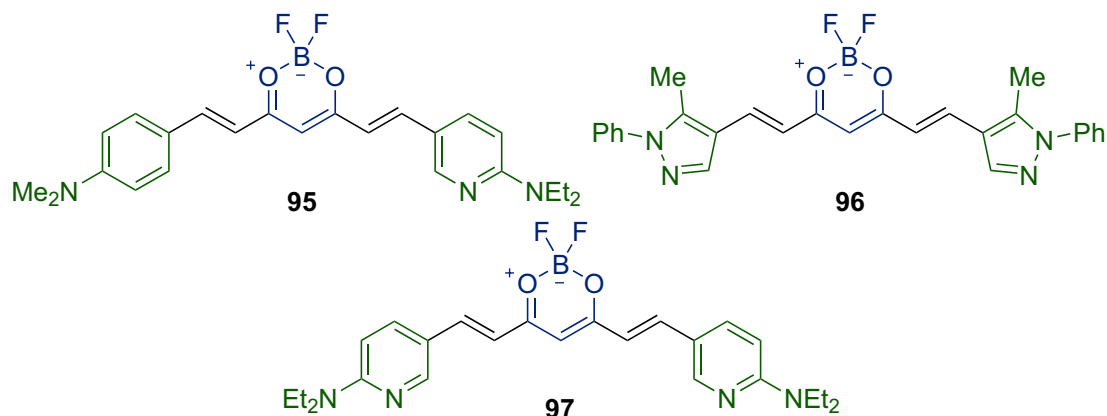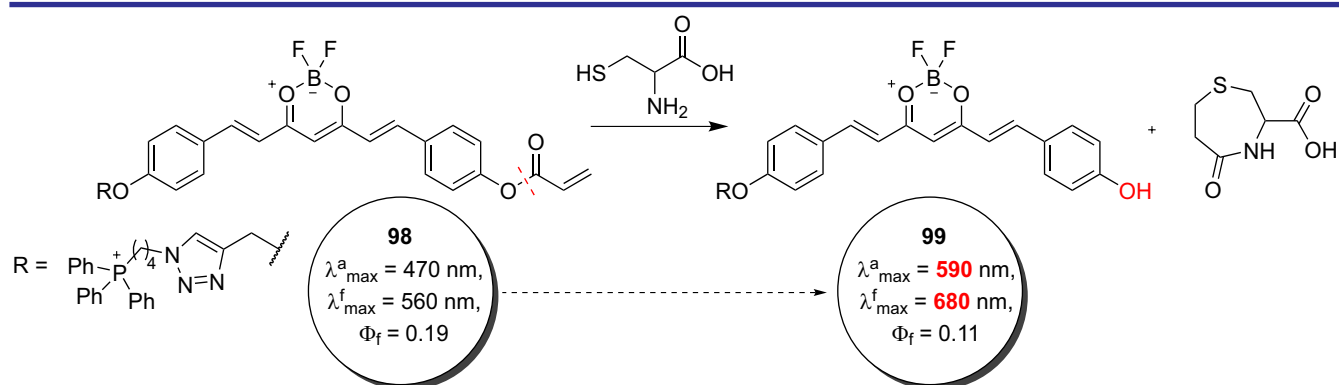
**Figure 10.** Fluorogenic probes for the therapy of Alzheimer's disease

Scheme 10. Ratiometric detection of cysteine using probe **98**

specific covalent targeting where functionalized electron donor end-groups serve as active sites. The illustrative example is compound **98**, which was developed for detecting mitochondrial cysteine (Cys) [114]. The acrylic ester active site of probe **98** cleaves upon the presence of cysteine, thus ratiometrically detecting the biothiol.

Besides cysteine, homocysteine (Hcy) and glutathione (GSH) can be targeted using fluorogenic probe **100** [115]. Upon the interaction with biothiols the 2.4-(dinitrobenzene)sulfonate active groups are cleaved releasing BF$_2$-curcumin. The process is accompanied by an increase of the fluorescence intensity at 610 nm.

For targeting of γ-glutamyl transpeptidase (GGT) – a biomarker, the accumulation of which is connected with progression of several types of cancer – the fluorogenic probe **101** was designed [116]. The cleavage of the glutamyl substituent of compound **101** in the presence of GGT is accompanied by a strong fluorescence response in the far-visible region.

In addition to biomedical research, BF$_2$-curcuminoids were also examined for applications in photovoltaics. For example, compounds **103**–**105** were utilized as donor materials in solution-processed bulk-heterojunction organic solar cells (BHJ OSCs) by blending with acceptor [6,6]-phenyl-C$_{61}$-butyric acid methyl ester [117]. The result-
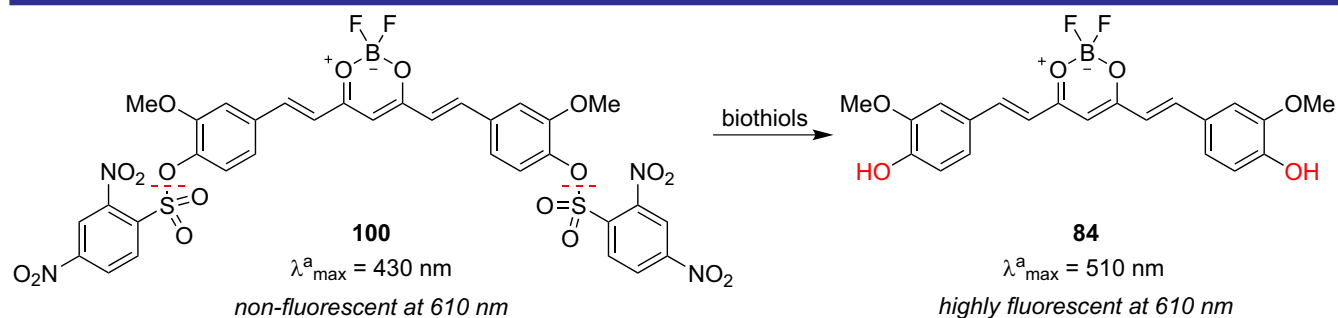
Scheme 11. Application of probe **100** for detection of biothiols
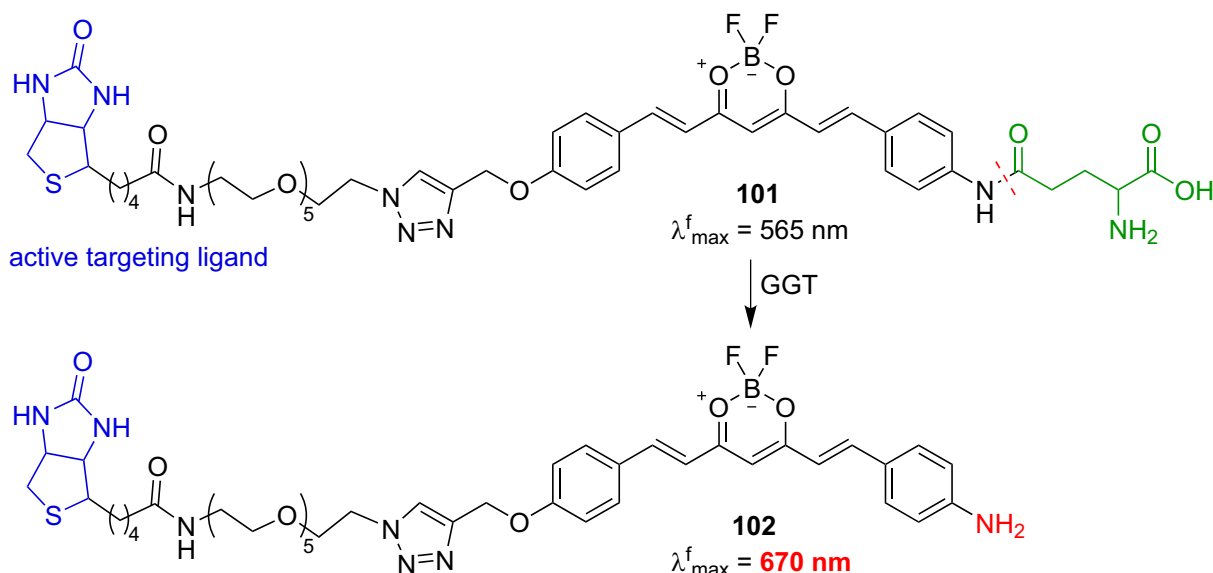
Scheme 12. Targeting of GGT using a selective fluorogenic probe **101**

Scheme 13. Detection of a bisulfite ion with curcumin

Figure 11. BF$_2$-curcuminoids used in photovoltaics
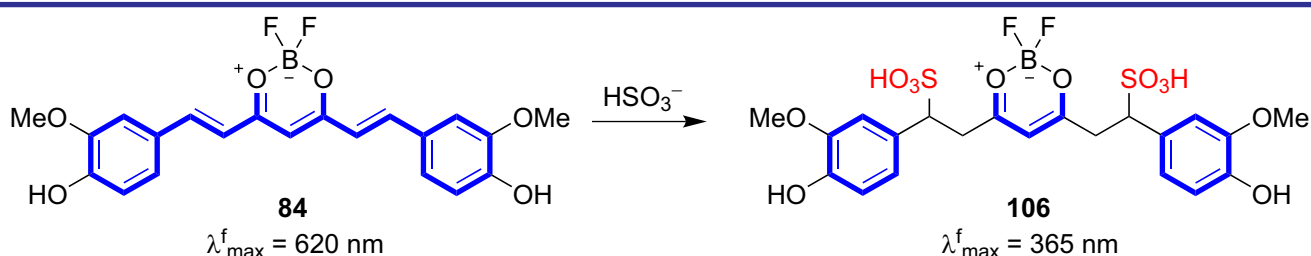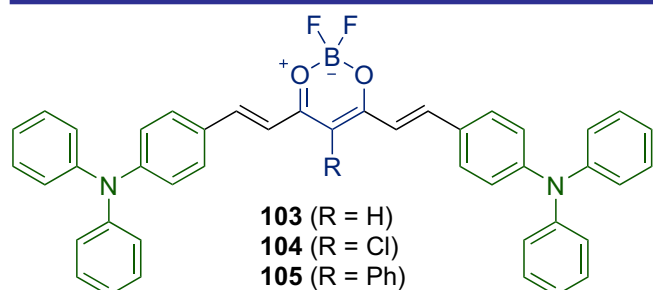
ing photoelements displayed the power conversion efficiency up to 4.14%, thus showing potential of quadrupolar BF$_2$-merocyanines for fabrication of BHJ OSCs.

The very BF$_2$-curcumin was shown to be highly sensitive to the presence of a cyanide ion [107, 118]. The interaction of CN$^-$ with BF$_2$-curcumin leads to a considerable redshift of the absorption maximum (from 507 nm to 649 nm) with concomitant quenching of the fluorescence emission. These spectral effects are caused by deprotonation of hydroxy substituents of the end-groups yielding the dianion (in non-aqueous media), which have no detectable emission due to the photoinduced charge transfer from the negatively charged end-groups to the dioxaborine core.

Besides cyanide, bisulfite ion can be also detected by BF$_2$-curcumin [119] though in this case the sensory mechanism is different. HSO$_3^-$ acts as a Michael donor attacking the double bonds of the π-chain and forming adduct **106** (Scheme 13). As a result, the π-conjugated system of the dye becomes fragmented and the peak at 620 nm disappears.

4. *Meso*-cyano-substituted dioxaborine – a new building block for the brightest polymethines

Despite a broad range of applications, quadrupolar dioxaborine-containing merocyanines were only represented by BF$_2$-curcuminoids not so long ago. While there is a vast diversity of dipolar F$_2$DB-merocynines with weak (type I) and strong (type II) electron-donor end-groups until recently there was only one quadrupolar F$_2$DB-merocyanine constituting strong electron-donor end-groups [120]. With the advent of the BF$_2$-complex of *meso*-cyano acetylacetone the diversity of such compounds has become greatly enriched (Figure 12). Moreover, the exploration of chemical properties of **107** yielded new types of polymethine dyes, such as mero-anionic and polyanionic polymethines possessing outstanding spectral properties.
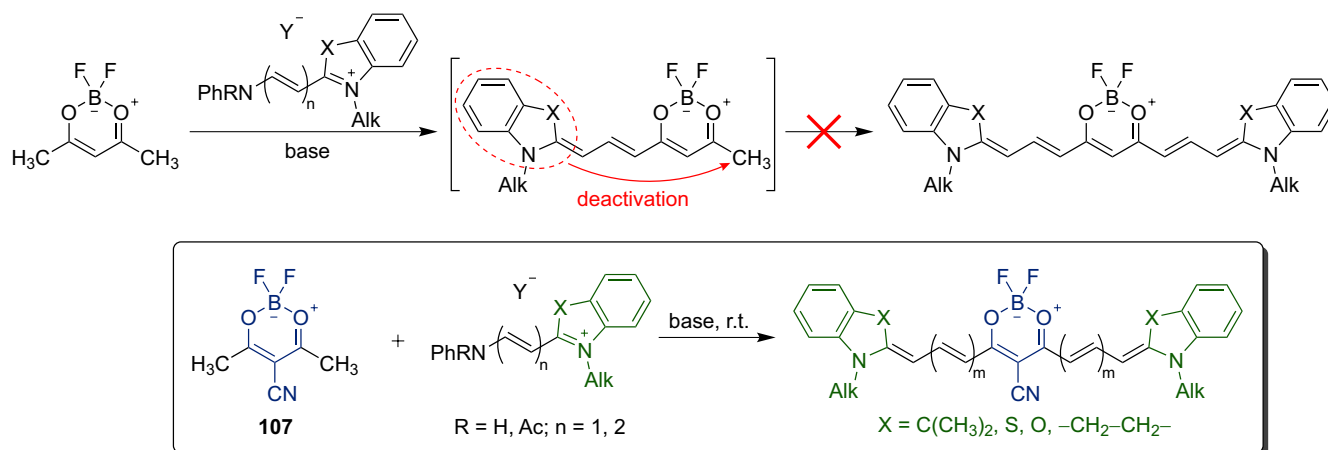
Scheme 14. The synthesis of quadrupolar merocyanines from *meso*-cyano-substituted dioxaborine
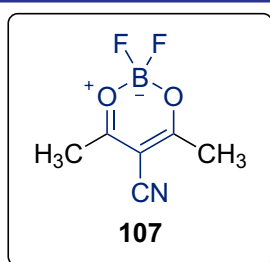
Figure 12. The BF$_2$-complex of *meso*-cyano acetylacetone

4.1. Quadrupolar merocyanines and mero-anionic dyes

The key feature of the cyano-substituted BF$_2$-acetylacetone is higher acidity of its methyl groups compared to the parent compound **2**, thus making substrate **107** more active towards electrophiles. Thus, while the reaction of BF$_2$-acetylacteone with cationic hemicyanines often results in mono-condensation, since the activity of the second methyl group gets too low for the reaction to proceed further, bis-condensation products are easily obtained by the reaction of **107** with hemicyanines even at room temperature (Scheme 14) [121].

A high activity of the methyl group of the half-product (i. e., the product of the mono-condensation of **107** with hemicyanines) allows carrying out chemical transformations with other electrophiles. For example, the reaction of such half-products with ethoxymethylene or 2-anilinovinyl derivatives of CH-acids in the presence of a base, such as triethylamine or diisopropylethylamine, and acetic anhydride results in the formation of polymethines of the unusual D–π–A–π–A′ type (Scheme 15). Since these compounds comprise the dipolar merocyanine (D–π–A) and non-symmetric anionic (A–π–A′) parts in their scaffold, the dubbing "mero-anionic" dyes was introduced for distinguishing them from other types of polymethines [122].

The tendencies in alterations of spectral properties upon the transition from BF$_2$-curcuminoids to quadrupolar merocyanines with heterocyclic
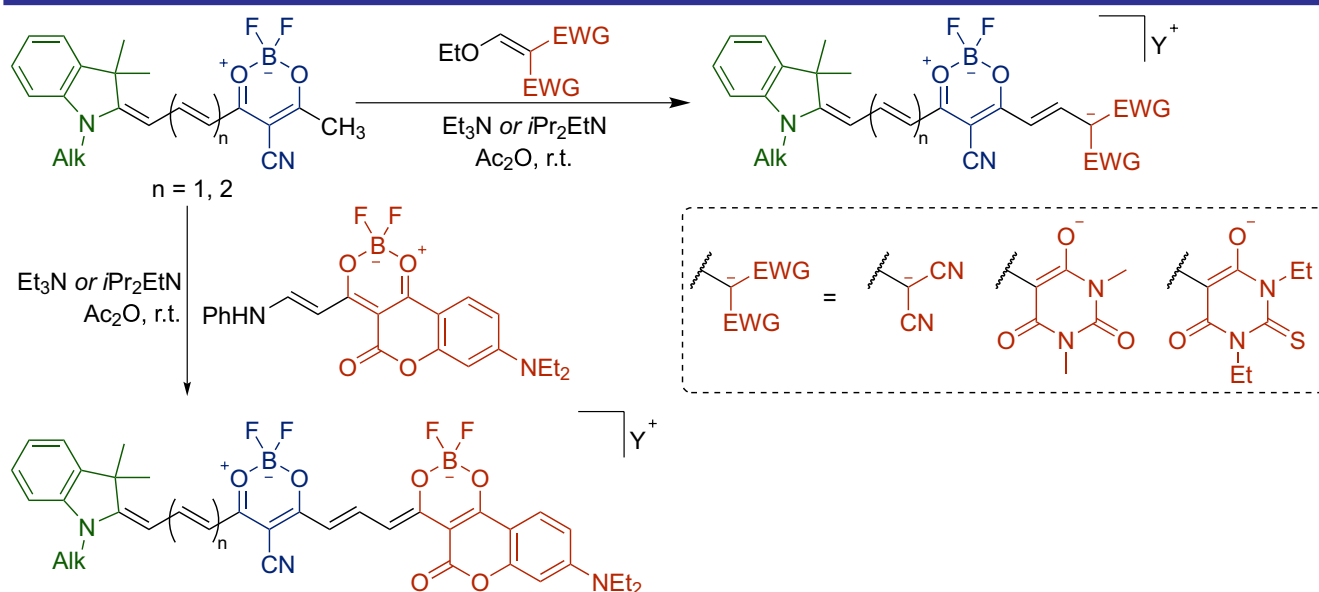
Scheme 15. The synthesis of mero-anionic polymethines

Table 15. Spectral properties of quadrupolar cyanodioxaborine-containing polymethines in DCM
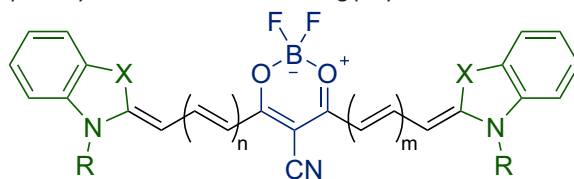
Dye	X	R	n	m	λ^a_{max} [nm]	$\varepsilon \times 10^{-4}$ [M^{-1} cm^{-1}]	λ^f_{max} [nm]	Φ_f
108	C(CH$_3$)$_2$	CH$_3$	1	1	667	2.75	702	0.72
109	S	C$_{10}$H$_{21}$	1	1	702	2.89	730	0.68
110	C(CH$_3$)$_2$	CH$_3$	1	2	740	2.42	792	0.45
111	C(CH$_3$)$_2$	CH$_3$	2	2	808	2.59	880	0.07

Table 16. UV-Vis spectral characteristics of mero-anionic dyes

112, 116   **113, 117**   **114, 118**   **115, 119**

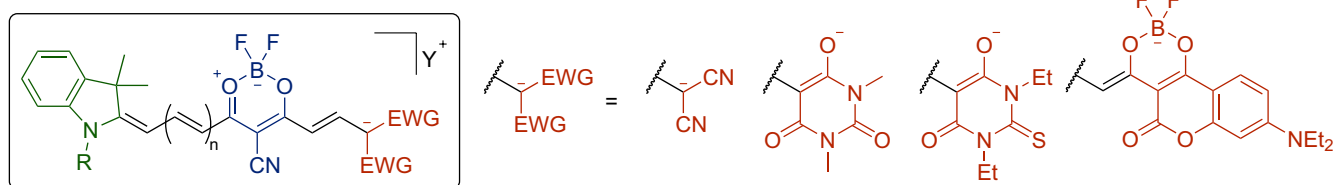| Dye	R	n	Y$^+$	Solvent	λ_a [nm]	$\varepsilon \times 10^{-5}$ [M^{-1} cm^{-1}]	λ_f [nm]	Φ_f	$\varepsilon \times \Phi_f \times 10^{-5}$ [M^{-1} cm^{-1}]
112	CH$_3$	1	[Et$_4$N]$^+$	DCM	598	0.86	629	0.20	0.17
				DMF	605	1.59	634	0.61	0.97
113	CH$_3$	1	[Et$_3$NH]$^+$	DCM	621	2.18	652	0.84	1.83
				DMF	623	2.09	651	0.64	1.34
114	CH$_3$	1	[Et$_3$NH]$^+$	DCM	634	2.33	664	0.83	1.92
				DMF	638	2.52	663	0.80	2.02
115	CH$_3$	1	[Et$_3$NH]$^+$	DCM	706	2.86	729	0.50	1.42
				DMF	706	3.37	733	0.52	1.30
116	*n*Pr	2	[Et$_3$NH]$^+$	DCM	670	1.19	724	0.19	0.22
				DMF	675	1.20	729	0.37	0.44
117	*n*Bu	2	[*i*Pr$_2$EtNH]$^+$	DCM	697	1.59	743	0.32	0.51
				DMF	694	1.47	743	0.32	0.46
118	*n*Bu	2	[*i*Pr$_2$EtNH]$^+$	DCM	710	1.79	757	0.41	0.74
				DMF	716	2.08	759	0.49	1.02
119	*n*Pr	2	[Et$_3$NH]$^+$	DCM	776	2.61	813	0.20	0.53
				DMF	777	3.03	823	0.060	0.18

end-groups is similar to those of the transition from type I to type II dipolar F$_2$DB-merocyanines (see Sect 3.3.). For example, the quadrupolar merocyanines absorb and emit mostly in the NIR spectral range (Table 15) [121]. While molar absorptivities of BF$_2$-curcuminoids are usually below 100000 M^{-1} cm^{-1}, the D–π–A–π–D type F$_2$DB-containing polymethines have the attenuation coefficients of 250000 M^{-1} cm^{-1} and above. Their fluorescence quantum yields also tend to be higher, reaching, for example, 0.72 and 0.68 in DCM for polymethines with indolenine and benzothiazole end-groups (**108** and **109**), respectively. Vinylene shifts are also higher than in BF$_2$-curcuminoids, equaling 73 nm for **108** → **110** and 68 nm for **110** → **111**.

Mero-anionic dyes are also characterized by an intense absorption and a strong fluorescence in far-visible and NIR regions (Table 16) [122]. The distinctive feature of mero-anionic dyes is a broad range of modulation of optical properties by tuning the structure of the accepting end-group. For example, dyes with the malononitrile end-group (**112** and **116**) are characterized by relatively low molar attenuation coefficients, while the molar absorptivity of dyes **115** and **119** bearing the coumarinodioxaborine end-group reaches 300000 M^{-1} cm^{-1}. The vinylene shift is in a range of 60–80 nm depending on the structure of the end-groups.

4.2. Polyanionic polymethines

Synthetic possibilities of *meso*-cyano-substituted dioxaborine **107** go beyond synthesis of
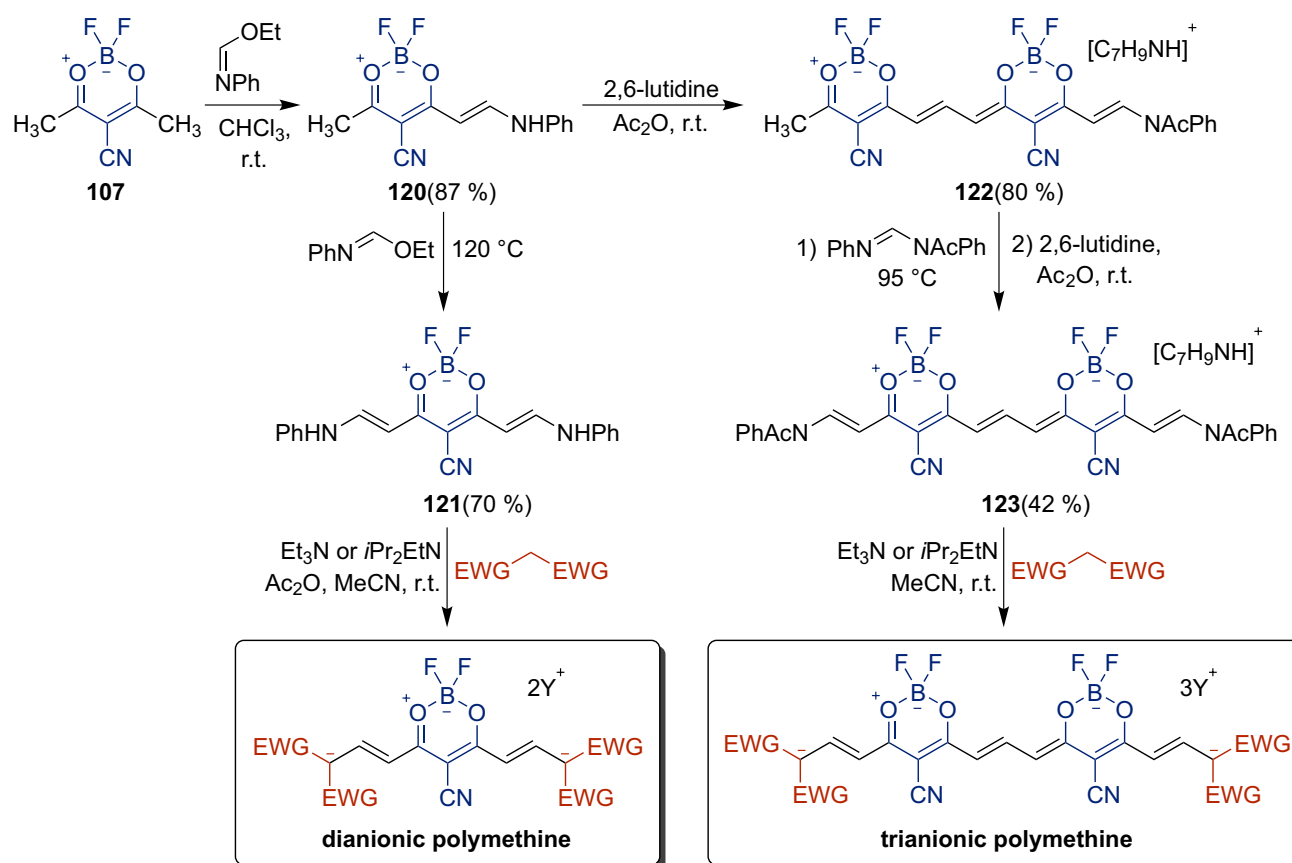
Scheme 16. The synthesis of dianionic and trianionic dyes

Table 17. Spectral properties of polyanionic dyes in DMF

Dye	End-group	Y^+	λ^a_{max} [nm]	$\varepsilon \times 10^{-5}$ [M^{-1} cm^{-1}]	λ^f_{max} [nm]	Φ_f	$\varepsilon \times \Phi_f \times 10^{-5}$ [M^{-1} cm^{-1}]
Dianionic polymethines							
124	malononitrile	$[Et_4N]^+$	538	2.38	553	0.90	2.14
125	1,3-dimethylbarbituric acid	$[Et_3NH]^+$	570	2.53	586	0.92	2.33
126	1,3-diethylthiobarbituric acid	$[Et_3NH]^+$	597	2.93	614	0.87	2.55
127	1,3-indandione	$[iPr_2EtNH]^+$	624	3.26	640	0.61	1.99
Trianionic polymethines							
128	malononitrile	$[nBu_4N]^+$	687	4.29	705	0.73	3.13
129	1,3-dimethylbarbituric acid	$[nBu_4N]^+$	705	4.21	725	0.64	2.69
130	1,3-diethylthiobarbituric acid	$[nBu_4N]^+$	722	4.32	741	0.49	2.12
131	1,3-indandione	$[nBu_4N]^+$	751	4.95	770	0.50	2.48

quadrupolar merocyanines and mero-anionic dyes. Recently, the first representatives of dianionic [123] and trianionic [124] polymethines were synthesized (Scheme 16). For the synthesis of dianionic polymethines, the intermediate bis-hemicyanine **121** was obtained, while bis-hemicyanine **123**, a precursor to trianionic dyes, was obtained in several steps from compound **120**. Subjecting compounds **121** and **123** into reactions with CH-

acids (malononitrile, 1,3-indandione, barbituric and thiobarbituric acids) yields the corresponding dianionic and trianionic polymethines.

Dianionic and trianionic dioxaborine-containing polymethines are strongly emissive, with the fluorescence quantum yield reaching 0.90 for dianionic and 0.73 for trianionic dyes in DMF (Table 17). While dianionic dyes fluoresce in the far-visible region, trianionic dyes emit in the NIR

region, thus becoming the brightest reported NIR-emitters among the polymethine dyes. Moreover, trianionic dyes are characterized by a remarkably high molar attenuation coefficients, reaching, for example, 495000 M^{-1} cm^{-1} for dye **131** in DMF. The fluorescence brightness of polyanionic dioxaborine dyes is also unmatched among polymethines, reaching or exceeding the value of 250000 M^{-1} cm^{-1} in DMF.

◼ Conclusions

Modern organic chemistry is driven by a rising demand for high-performance materials for applications in both existing and emerging technologies. Dioxaborine-containing π-conjugated systems are a good example of versatile functional compounds that combine high synthetic potential and flexibility in molecular modelling. As was outlined in the present Perspective, these features allow creating highly effective solutions based on the F_2DB-containing dyes for various kinds of photoenergy-transformation domains, ranging from biomedical research to non-linear optics. With scores of new publications each year, the contribution of dioxaborine-containing compounds to the development of a new generation of materials possessing specific physicochemical properties has been constantly growing. An illustrative example is the recently reported synthesis of highly fluorescent polyanionic dyes, which exposed vast potential of the F_2DB core for obtaining bright NIR fluorophores. Further research may revolve around the synthesis of water-soluble dioxaborine-containing polymethines, which makes them highly attractive probes for medicinal application. Overcoming the intrinsic instability in relation to acidic and basic solvolysis is another promising path for further investigations. We believe that this review will serve as a useful guide in navigating a vast body of research dedicated to diverse types of dioxaborine-containing polymethines, kindling thus an additional interest for future studies.

◼ References

1. Mishra, A.; Behera, R. K.; Behera, P. K.; Mishra, B. K.; Behera, G. B. Cyanines during the 1990s: A Review. *Chem. Rev.* **2000**, *100* (6), 1973–2012. https://doi.org/10.1021/cr990402t.

2. Kammler, R.; Bourhill, G.; Jin, Y.; Bräuchle, C.; Görlitz, G.; Hartmann, H. Second-Order Optical Non-Linearity of New 1,3,2(2H)-Dioxaborine Dyes. *J. Chem. Soc., Faraday Trans.* **1996**, *92* (6), 945–947. https://doi.org/10.1039/FT9969200945.

3. Hales, J. M.; Zheng, S.; Barlow, S.; Marder, S. R.; Perry, J. W. Bisdioxaborine Polymethines with Large Third-Order Nonlinearities for All-Optical Signal Processing. *J. Am. Chem. Soc.* **2006**, *128* (35), 11362–11363. https://doi.org/10.1021/ja063535m.

4. Padilha, L. A.; Webster, S.; Przhonska, O. V.; Hu, H.; Peceli, D.; Rosch, J. L.; Bondar, M. V.; Gerasov, A. O.; Kovtun, Y. P.; Shandura, M. P.; Kachkovski, A. D.; Hagan, D. J.; Van Stryland, E. W. Nonlinear Absorption in a Series of Donor–π–Acceptor Cyanines with Different Conjugation Lengths. *J. Mater. Chem.* **2009**, *19* (40), 7503. https://doi.org/10.1039/b907344b.

5. Padilha, L. A.; Webster, S.; Przhonska, O. V.; Hu, H.; Peceli, D.; Ensley, T. R.; Bondar, M. V.; Gerasov, A. O.; Kovtun, Y. P.; Shandura, M. P.; Kachkovski, A. D.; Hagan, D. J.; Stryland, E. W. Van. Efficient Two-Photon Absorbing Acceptor-π-Acceptor Polymethine Dyes. *J. Phys. Chem. A* **2010**, *114* (23), 6493–6501. https://doi.org/10.1021/jp100963e.

6. Matichak, J. D.; Hales, J. M.; Ohira, S.; Barlow, S.; Jang, S.-H.; Jen, A. K.-Y.; Brédas, J.-L.; Perry, J. W.; Marder, S. R. Using End Groups to Tune the Linear and Nonlinear Optical Properties of Bis(Dioxaborine)-Terminated Polymethine Dyes. *ChemPhysChem* **2010**, *11* (1), 130–138. https://doi.org/10.1002/cphc.200900635.

7. Lin, H.-C.; Kim, H.; Barlow, S.; Hales, J. M.; Perry, J. W.; Marder, S. R. Synthesis and Linear and Nonlinear Optical Properties of Metal-Terminated Bis(Dioxaborine) Polymethines. *Chem. Commun.* **2011**, *47* (2), 782–784. https://doi.org/10.1039/C0CC02003F.

8. Pitter, D. R. G.; Brown, A. S.; Baker, J. D.; Wilson, J. N. One Probe, Two-Channel Imaging of Nuclear and Cytosolic Compartments with Orange and Red Emissive Dyes. *Org. Biomol. Chem.* **2015**, *13* (36), 9477–9484. https://doi.org/10.1039/C5OB01428J.

9. Collot, M.; Fam, T. K.; Ashokkumar, P.; Faklaris, O.; Galli, T.; Danglot, L.; Klymchenko, A. S. Ultrabright and Fluorogenic Probes for Multicolor Imaging and Tracking of Lipid Droplets in Cells and Tissues. *J. Am. Chem. Soc.* **2018**, *140* (16), 5401–5411. https://doi.org/10.1021/jacs.7b12817.

10. Ashoka, A. H.; Ashokkumar, P.; Kovtun, Y. P.; Klymchenko, A. S. Solvatochromic Near-Infrared Probe for Polarity Mapping of Biomembranes and Lipid Droplets in Cells under Stress. *J. Phys. Chem. Lett.* **2019**, *10* (10), 2414–2421. https://doi.org/10.1021/acs.jpclett.9b00668.

11. Gerasov, A.; Shandura, M.; Kovtun, Y.; Losytskyy, M.; Negrutska, V.; Dubey, I. Fluorescent Labeling of Proteins with Amine-Specific 1,3,2-(2H)-Dioxaborine Polymethine Dye. *Anal. Biochem.* **2012**, *420* (2), 115–120. https://doi.org/10.1016/j.ab.2011.09.018.

12. Sun, Q.; Wang, W.; Chen, Z.; Yao, Y.; Zhang, W.; Duan, L.; Qian, J. A Fluorescence Turn-on Probe for Human (Bovine) Serum Albumin Based on the Hydrolysis of a Dioxaborine Group Promoted by Proteins. *Chem. Commun.* **2017**, *53* (48), 6432–6435. https://doi.org/10.1039/C7CC03587J.

13. Li, Z.; Wang, Y.; Li, M.; Chen, H.; Xie, Y.; Li, P.; Guo, H.; Ya, H. Solvent-Dependent and Visible Light-Activated NIR Photochromic Dithienylethene Modified by Difluoroboron β-Diketonates as Fluorescent Turn-on pH Sensor. *Dyes Pigm.* **2019**, *162*, 339–347. https://doi.org/10.1016/j.dyepig.2018.10.049.

14. Karpenko, I. A.; Niko, Y.; Yakubovskyi, V. P.; Gerasov, A. O.; Bonnet, D.; Kovtun, Y. P.; Klymchenko, A. S. Push–Pull Dioxaborine as Fluorescent Molecular Rotor: Far-Red Fluorogenic Probe for Ligand–Receptor Interactions. *J. Mater. Chem. C* **2016**, *4* (14), 3002–3009. https://doi.org/10.1039/C5TC03411F.

15. Han, W.; You, J.; Li, H.; Zhao, D.; Nie, J.; Wang, T. Curcuminoid-Based Difluoroboron Dyes as High-Performance Photosensitizers in Long-Wavelength (Yellow and Red) Cationic Photopolymerization. *Macromol. Rapid Commun.* **2019**, *40* (20), 1900291. https://doi.org/10.1002/marc.201900291.

16. Zhou, Y.; Chen, Y.-Z.; Cao, J.-H.; Yang, Q.-Z.; Wu, L.-Z.; Tung, C.-H.; Wu, D.-Y. Dicyanoboron Diketonate Dyes: Synthesis, Photophysical Properties and Bioimaging. *Dyes Pigm.* **2015**, *112*, 162–169. https://doi.org/10.1016/j.dyepig.2014.07.001.

17. Cheng, X.; Li, D.; Zhang, Z.; Zhang, H.; Wang, Y. Organoboron Compounds with Morphology-Dependent NIR Emissions and Dual-Channel Fluorescent ON/OFF Switching. *Org. Lett.* **2014**, *16* (3), 880–883. https://doi.org/10.1021/ol403639n.

18. Chen, P.-Z.; Niu, L.-Y.; Chen, Y.-Z.; Yang, Q.-Z. Difluoroboron β-Diketonate Dyes: Spectroscopic Properties and Applications. *Coord. Chem. Rev.* **2017**, *350*, 196–216. https://doi.org/10.1016/j.ccr.2017.06.026.

19. Collot, M. Recent Advances in Dioxaborine-Bxased Fluorescent Materials for Bioimaging Applications. *Mater. Horiz.* **2021**, *8* (2), 501–514. https://doi.org/10.1039/D0MH01186J.

20. Delgado, D.; Abonia, R. Synthetic Approaches for BF2-Containing Adducts of Outstanding Biological Potential. A Review. *Arabian J. Chem.* **2022**, *15* (1), 103528. https://doi.org/10.1016/j.arabjc.2021.103528.

21. Vanallan, J. A.; Reynolds, G. A. The Reactions of 2,2-Difluoro-4-Methylnaphtho[l,2-e]-1,3,2-Dioxaborin and Its [2,1-e] Isomer with Carbonyl Compounds and with Aniline. *J. Heterocycl. Chem.* **1969**, *6* (1), 29–35. https://doi.org/10.1002/jhet.5570060106.

22. Dilthey, W.; Eduardoff, F.; Schumacher, F. J. Ueber Siliconium-, Boronium- Und Titanoniumsalze. Zum Theil Gemeinschaftlich Mit. *Justus Liebigs Ann. Chem.* **1906**, *344* (3), 300–313. https://doi.org/10.1002/jlac.19063440305.

23. Morgan, G. T.; Tunstall, R. B. CCLIII.—Researches on Residual Affinity and Coordination. Part XXI. Boron β-Diketone Difluorides. *J. Chem. Soc., Trans.* **1924**, *125*, 1963–1967. https://doi.org/10.1039/CT9242501963.

24. Shokova, E. A.; Kim, J. K.; Kovalev, V. V. evich. 1,3-Diketones. Synthesis and Properties. *Russ. J. Org. Chem.* **2015**, *51* (6), 755–830. https://doi.org/10.1134/S1070428015060019.

25. Kel'in, A. Recent Advances in the Synthesis of 1,3-Diketones. *Curr. Org. Chem.* **2003**, *7* (16), 1691–1711. https://doi.org/10.2174/1385272033486233.

26. Young, F. G.; Frostick, F. C.; Sanderson, J. J.; Hauser, C. R. Conversion of Ketone Enol Esters to β-Diketones by Intramolecular Thermal Rearrangement and by Intermolecular Acylations Using Boron Fluoride. *J. Am. Chem. Soc.* **1950**, *72* (8), 3635–3642. https://doi.org/10.1021/ja01164a088.

27. Meerwein, H.; Vossen, D. Synthesen von Ketonen Und β-Diketonen Mit Hilfe von Borfluorid. *Journal für Praktische Chemie* **1934**, *141* (5–8), 149–166. https://doi.org/10.1002/PRAC.19341410503.

28. Hauser, C. R.; Frostick, F. C.; Man, E. H. Mechanism of Acetylation of Ketone Enol Acetates with Acetic Anhydride by Boron Trifluoride to Form β-Diketones. *J. Am. Chem. Soc.* **1952**, *74* (13), 3231–3233. https://doi.org/10.1021/ja01133a008.

29. Youssefyeh, R. D. Acylations of Ketals and Enol Ethers. *J. Am. Chem. Soc.* **1963**, *85* (23), 3901–3902. https://doi.org/10.1021/ja00906a047.

30. Durden, J. A.; Crosby, D. G. The Boron Trifluoride Catalyzed Reaction of Acetophenone with Acetic Anhydride. *J. Org. Chem.* **1965**, *30* (5), 1684–1687. https://doi.org/10.1021/jo01016a527.

31. Schiemenz, G. P.; Schmidt, U. Trimethoxyphenylverbindungen, IX. Borheterocyclen in Der Präparativen Naturstoffchemie: Eine Einfache Synthese Des Aurentiacins. *Liebigs Annalen der Chemie* **1982**, *1982* (8), 1509–1513. https://doi.org/10.1002/JLAC.198219820810.

32. Czerney, P.; Igney, C.; Haucke, G.; Hartmann, H. Zur Synthese Und Spektralen Charakterisierung von Verbrückten 2, 2-Difluoro-1,3,2-Dioxaborinen. *Zeitschrift für Chemie* **1988**, *28* (1), 23–24. https://doi.org/10.1002/ZFCH.19880280105.

33. Görlitz, G.; Hartmann, H. On the Formation and Solvolysis of 4-Aryl-2,2-Difluoro-6-Methyl-1,3,2-(2H)-Dioxaborines. *Heteroat. Chem.* **1997**, *8* (2), 147–155. https://doi.org/10.1002/(SICI)1098-1071(1997)8:2<147::AID-HC7>3.0.CO;2-B.

34. Görlitz, G.; Hartmann, H.; Nuber, B.; Wolff, J. J. A Simple Route to 4-Aryl and 4-Hetaryl Substituted 6-Methyl-2,2-Difluoro-1,3,2-(2H)-Dioxaborines. *Journal für praktische Chemie* **1999**, *341* (2), 167–172. https://doi.org/10.1002/(SICI)1521-3897(199902)341:2<167::AID-PRAC167>3.0.CO;2-A.

35. Hauser, C. R.; Eby, C. J. The Conversion of β-Ketonitriles to β-Ketoamides by Boron Fluoride in Aqueous Acetic Acid and by Polyphosphoric Acid 1. *J. Am. Chem. Soc.* **1957**, *79* (3), 725–727. https://doi.org/10.1021/ja01560a061.

36. Hartmann H.; Hunze A.; Kanitz A.; Rogler W.; Rohde D. Amorphous organic 1,3,2-dioxaborine luminophores method for the production and use thereof. U. S. Patent US20040065867A1, April 8, 2004.

37. Kamisky D. Process for the preparation of substituted pyrano(3,2-c)(1,2)benzo-thiazine 6,6-dioxides. U. S. Patent US3898218A, August 5, 1975.

38. Kamisky D.; Klutchko S. Polycyclic gamma-pyrone-3-carboxaldehyde deriva-tives U. S. Patent US3959480A, May 25, 1976.

39. Kamisky D. Polycyclic dioxaborin complexes. U. S. Patent US3936488A, February 3, 1976.

40. Kamisky D. Hydroxymethylene-substituted chromone-3-carboxaldehydes, process for their preparation and intermediates produced thereby. U. S. Patent US3936563A, February 3, 1976.

41. Kamisky D. Process for the preparation of gamma-pyrone-3-carboxaldehydes. U. S. Patent US3862144A, January 21, 1975.

42. Kamisky D.; Klutchko S. Polycyclic gamma-pyrone-3-carboxaldehyde deriva-tives. U. S. Patent US3887585A, June 3, 1975.

43. House, H. O.; Reif, D. J. The Rearrangement of α,β-Epoxy Ketones. II. Migratory Aptitudes 1. *J. Am. Chem. Soc.* **1955**, *77* (24), 6525–6532. https://doi.org/10.1021/ja01629a035.

44. House, H. O.; Reif, D. J. The Rearrangement of α,β-Epoxy Ketones. VII. The α-Ethylbenzalacetophenone Oxide System. *J. Am. Chem. Soc.* **1957**, *79* (24), 6491–6495. https://doi.org/10.1021/ja01581a035.

45. House, H. O.; Ryerson, G. D. The Rearrangement of α,β-Epoxy Ketones. VIII. Effect of Substituents on the Rate of Rearrangement. *J. Am. Chem. Soc.* **1961**, *83* (4), 979–983. https://doi.org/10.1021/ja01465a052.

46. Brown, N. M. D.; Bladon, P. Spectroscopy and Structure of (1,3-Diketonato)Boron Difluorides and Related Compounds. *J. Chem. Soc. A* **1969**, 526. https://doi.org/10.1039/j19690000526.

47. Fabian, J.; Hartmann, H. 1,3,2-Dioxaborines as Potential Components in Advanced Materials-a Theoretical Study on Electron Affinity. *J. Phys. Org. Chem.* **2004**, *17* (5), 359–369. https://doi.org/10.1002/poc.736.

48. Giron, R. G. P.; Ferguson, G. S. Tetrafluoroborate and Hexafluorophosphate Ions Are Not Interchangeable: A Density Functional Theory Comparison of Hydrogen Bonding. *ChemistrySelect* **2017**, *2* (33), 10895–10901. https://doi.org/10.1002/SLCT.201702176.

49. Schleyer, P. von R.; Maerker, C.; Dransfeld, A.; Jiao, H.; van Eikema Hommes, N. J. R. Nucleus-Independent Chemical Shifts: A Simple and Efficient Aromaticity Probe. *J. Am. Chem. Soc.* **1996**, *118* (26), 6317–6318. https://doi.org/10.1021/ja960582d.

50. Borisenko, A. V.; Vovna, V. I.; Gorachakov, V. V.; Korotkikh, O. A. Photoelectron Spectra and Electron Structures of Some Boron b-Diketonates. *J. Struct. Chem.* **1987**, *28* (1), 127–130. https://doi.org/10.1007/BF00749560.

51. Vovna, V. I.; Kazachek, M. V.; L'vov, I. B. Excited States and Absorption Spectra of β-Diketonate Complexes of Boron Difluoride with Aromatic Substituents. *Opt. Spectrosc.* **2012**, *112* (4), 497–505. https://doi.org/10.1134/S0030400X12030228.

52. Vovna, V. I.; Tikhonov, S. A.; Lvov, I. B. Photoelectron Spectra and Electronic Structure of Boron Difluoride β-Diketonates with Aromatic Substituents. *Russ. J. Phys. Chem. A* **2013**, *87* (4), 688–693. https://doi.org/10.1134/S0036024413040304.

53. Tikhonov, S. A.; Vovna, V. I. Boron Chelate Complexes: X-Ray and UV Photoelectron Spectra and Electronic Structure. *Russ. Chem. Bull.* **2018**, *67* (7), 1153–1166. https://doi.org/10.1007/s11172-018-2196-2.

54. Foris, A. On ^{19}F NMR Spectra of BF$_2$ and BF Complexes and Related Compounds, **2016**. https://doi.org/10.13140/RG.2.2.30488.60160.

55. Gillespie, R. J.; Hartman, J. S. Change of Sign of the Boron–Fluorine Spin–Spin Coupling Constant in the Tetrafluoroborate Anion. *J. Chem. Phys.* **1966**, *45* (7), 2712–2713. https://doi.org/10.1063/1.1728005.

56. Tay, A. C. Y.; Frogley, B. J.; Ware, D. C.; Brothers, P. J. Boron Calixphyrin Complexes: Exploring the Coordination Chemistry of a BODIPY/Porphyrin Hybrid. *Dalton Trans.* **2018**, *47* (10), 3388–3399. https://doi.org/10.1039/C7DT04575A.

57. Minkin, V. I. Glossary of Terms Used in Theoretical Organic Chemistry. *Pure Appl. Chem.* **1999**, *71* (10), 1919–1981. https://doi.org/10.1351/pac199971101919.

58. Desfrançois, C.; Périquet, V.; Lyapustina, S. A.; Lippa, T. P.; Robinson, D. W.; Bowen, K. H.; Nonaka, H.; Compton, R. N. Electron Binding to Valence and Multipole States of Molecules: Nitrobenzene, Para- and Meta-Dinitrobenzenes. *J. Chem. Phys.* **1999**, *111* (10), 4569–4576. https://doi.org/10.1063/1.479218.

59. Chowdhury, S.; Kebarle, P. Electron Affinities of Di- and Tetracyanoethylene and Cyanobenzenes Based on Measurements of Gas-Phase Electron-Transfer Equilibria. *J. Am. Chem. Soc.* **1986**, *108* (18), 5453–5459. https://doi.org/10.1021/JA00278A014/ASSET/JA00278A014.FP.PNG_V03.

60. Görlitz, G.; Hartmann, H.; Kossanyi, J.; Valat, P.; Wintgens, V. Spectroscopic Anomalies in the 4-Aryl-2,2-Difluoro-6-Methyl-1,3,2-Dioxaborine Series. *Berichte der Bunsengesellschaft für physikalische chemie* **1998**, *102* (10), 1449–1458. https://doi.org/10.1002/bbpc.199800013.

61. Xu, S.; Evans, R. E.; Liu, T.; Zhang, G.; Demas, J. N.; Trindle, C. O.; Fraser, C. L. Aromatic Difluoroboron β-Diketonate Complexes: Effects of π-Conjugation and Media on Optical Properties. *Inorg. Chem.* **2013**, *52* (7), 3597–3610. https://doi.org/10.1021/IC300077G/SUPPL_FILE/IC300077G_SI_001.PDF.

62. Kulinich, A. V; Ishchenko, A. A. Merocyanine Dyes: Synthesis, Structure, Properties and Applications. *Russ. Chem. Rev.* **2009**, *78* (2), 141–164. https://doi.org/10.1070/RC2009v078n02ABEH003900.

63. Sturmer, D. M. Synthesis and Properties of Cyanine and Related Dyes. In *Chemistry of Heterocyclic Compounds: Special Topics in Heterocyclic Chemistry, Volume 30*; Weissberger, A; Taylor, E. C., Eds.; John Wiley & Sons: New York, 1977; pp. 441–587.

64. Dähne, S. Color and Constitution: One Hundred Years of Research. *Science* **1978**, *199* (4334), 1163–1167. https://doi.org/10.1126/science.199.4334.1163.

65. Bach, G.; Daehne, S. Chapter 15 – Cyanine dyes and related compounds. In *Second Supplements to the 2nd Edition of Rodd's Chemistry of Carbon Compounds, Volume IV*; Sainsbury, M. Ed.; Elsevier: Amsterdam, 1997; pp. 383–481. https://doi.org/10.1016/B978-044453347-0.50165-8.

66. Lawrentz, U.; Grahn, W.; Lukaszuk, K.; Klein, C.; Wortmann, R.; Feldner, A.; Scherer, D. Donor-Acceptor Oligoenes with a Locked All-Trans Conformation: Synthesis and Linear and Nonlinear Optical Properties. *Chem. - Eur. J.* **2002**, *8* (7), 1573–1590. https://doi.org/10.1002/1521-3765(20020402)8:7<1573::AID-CHEM1573>3.0.CO;2-T.

67. Ishchenko, A. A.; Kulinich, A. V.; Bondarev, S. L.; Knyukshto, V. N. Photodynamics of Polyene–Polymethine Transformations and Spectral Fluorescent Properties of Merocyanine Dyes. *J. Phys. Chem. A* **2007**, *111* (51), 13629–13637. https://doi.org/10.1021/jp076016u.

68. Zhang, X.; Tian, Y.; Li, Z.; Tian, X.; Sun, H.; Liu, H.; Moore, A.; Ran, C. Design and Synthesis of Curcumin Analogues for in Vivo Fluorescence Imaging and Inhibiting Copper-Induced Cross-Linking of Amyloid Beta Species in Alzheimer's Disease. *J. Am. Chem. Soc.* **2013**, *135* (44), 16397–16409. https://doi.org/10.1021/ja405239v.

69. Gustav, K.; Bartsch, U.; Günther, W. Spektroskopische Untersuchungen an Organischen Carbonylverbindungen, 10. Mitt.: Vergleichende Absorptions-, Fluoreszenz- Und NMR-Messungen an Ausgewählten β-Diketonen Und Ihren BF$_2$- Und Be-Komplexen. *Monatshefte für Chemie / Chemical Monthly* **1994**, *125* (12), 1321–1325. https://doi.org/10.1007/BF00811081.

70. D'Aléo, A.; Gachet, D.; Heresanu, V.; Giorgi, M.; Fages, F. Efficient NIR-Light Emission from Solid-State Complexes of Boron Difluoride with 2'-Hydroxychalcone Derivatives. *Chem. – Eur. J.* **2012**, *18* (40), 12764–12772. https://doi.org/10.1002/CHEM.201201812.

71. D'Aléo, A.; Felouat, A.; Fages, F. Boron Difluoride Complexes of 2'-Hydroxychalcones and Curcuminoids as Fluorescent Dyes for Photonic Applications. *Adv. Nat. Sci.: Nanosci. Nanotechnol.* **2014**, *6* (1), 015009. https://doi.org/10.1088/2043-6262/6/1/015009.

72. Park, K. S.; Kim, M. K.; Seo, Y.; Ha, T.; Yoo, K.; Hyeon, S. J.; Hwang, Y. J.; Lee, J.; Ryu, H.; Choo, H.; Chong, Y. A Difluoroboron β-Diketonate Probe Shows "Turn-on" Near-Infrared Fluorescence Specific for Tau Fibrils. *ACS Chem. Neurosci.* **2017**, *8* (10), 2124–2131. https://doi.org/10.1021/acschemneuro.7b00224.

73. Traven, V. F.; Chibisova, T. A.; Manaev, A. V. Polymethine Dyes Derived from Boron Complexes of Acetylhydroxycoumarins. *Dyes Pigm.* **2003**, *58* (1), 41–46. https://doi.org/10.1016/S0143-7208(03)00022-6.

74. Gerasov, A. O.; Shandura, M. P.; Kovtun, Y. P. Polymethine Dyes Derived from the Boron Difluoride Complex of 3-Acetyl-5,7-Di(Pyrrolidin-1-yl)-4-Hydroxycoumarin. *Dyes Pigm.* **2008**, *79* (3), 252–258. https://doi.org/10.1016/j.dyepig.2008.03.005.

75. Gerasov, A. O.; Zyabrev, K. V.; Shandura, M. P.; Kovtun, Y. P. The Structural Criteria of Hydrolytic Stability in Series of Dioxaborine Polymethine Dyes. *Dyes Pigm.* **2011**, *89* (1), 76–85. https://doi.org/10.1016/j.dyepig.2010.09.007.

76. Zyabrev, K.; Dekhtyar, M.; Vlasenko, Y.; Chernega, A.; Slominskii, Y.; Tolmachev, A. New 2,2-Difluoro-1,3,2(2H)Oxazaborines and Merocyanines Derived from Them. *Dyes Pigm.* **2012**, *92* (1), 749–757. https://doi.org/10.1016/J.DYEPIG.2011.05.025.

77. Traven, V. F.; Manaev, A. V.; Bochkov, A. Y.; Chibisova, T. A.; Ivanov, I. V. New Reactions, Functional Compounds, and Materials in the Series of Coumarin and Its Analogs. *Russ. Chem. Bull.* **2012**, *61* (7), 1342–1362. https://doi.org/10.1007/s11172-012-0179-2.

78. Gerasov, A. O.; Shandura, M. P.; Kovtun, Y. P. Series of Polymethine Dyes Derived from 2,2-Difluoro-1,3,2-(2H)-Dioxaborine of 3-Acetyl-7-Diethylamino-4-Hydroxycoumarin. *Dyes Pigm.* **2008**, *77* (3), 598–607. https://doi.org/10.1016/j.dyepig.2007.08.013.

79. Halik, M.; Hartmann, H. Synthesis and Characterization of New Long-Wavelength-Absorbing Oxonol Dyes from the 2,2-Difluoro-1,3,2-Dioxaborine Type. *Chem. – Eur. J.* **1999**, *5* (9), 2511–2517. https://doi.org/10.1002/(SICI)1521-3765(19990903)5:9<2511::AID-CHEM2511>3.0.CO;2-6.

80. Zyabrev, K.; Doroshenko, A.; Mikitenko, E.; Slominskii, Y.; Tolmachev, A. Design, Synthesis, and Spectral Luminescent Properties of a Novel Polycarbocyanine Series Based on the 2,2-Difluoro-1,3,2-Dioxaborine Nucleus. *Eur. J. Org. Chem.* **2008**, *2008* (9), 1550–1558. https://doi.org/10.1002/EJOC.200701012.

81. Lin, H. C.; Kim, H.; Barlow, S.; Hales, J. M.; Perry, J. W.; Marder, S. R. Synthesis and Linear and Nonlinear Optical Properties of Metal-Terminated Bis(Dioxaborine) Polymethines. *Chem. Commun.* **2010**, *47* (2), 782–784. https://doi.org/10.1039/C0CC02003F.

82. Matichak, J. D.; Hales, J. M.; Barlow, S.; Perry, J. W.; Marder, S. R. Dioxaborine- and Indole-Terminated Polymethines: Effects of Bridge Substitution on Absorption Spectra and Third-Order Polarizabilities. *J. Phys. Chem. A* **2011**, *115* (11), 2160–2168. https://doi.org/10.1021/jp110425r.

83. Zyabrev, K. V.; Il'chenko, A. Y.; Slominskii, Y. L.; Rimanov, N. N.; Tolmachev, A. I. Polymethine Dyes Derived from 2,2-Difluoro-3,1,2-(2H)-Oxaoxoniaboratines with Polymethylene Bridge Groups in the Chromophore. *Dyes Pigm.* **2006**, *71* (3), 199–206. https://doi.org/10.1016/J.DYEPIG.2005.07.006.

84. Rajeshirke, M.; Tathe, A. B.; Sekar, N. Viscosity Sensitive Fluorescent Coumarin-Carbazole Chalcones and Their BF2 Complexes Containing Carboxylic Acid – Synthesis and Solvatochromism. *J. Mol. Liq.* **2018**, *264*, 358–366. https://doi.org/10.1016/J.MOLLIQ.2018.05.074.

85. Sun, Q.; Wang, W.; Chen, Z.; Yao, Y.; Zhang, W.; Duan, L.; Qian, J. A Fluorescence Turn-on Probe for Human (Bovine) Serum Albumin Based on the Hydrolysis of a Dioxaborine Group Promoted by Proteins. *Chem. Commun.* **2017**, *53* (48), 6432–6435. https://doi.org/10.1039/C7CC03587J.

86. Zhou, J.; Jangili, P.; Son, S.; Ji, M. S.; Won, M.; Kim, J. S. Fluorescent Diagnostic Probes in Neurodegenerative Diseases. *Adv. Mater.* **2020**, *32* (51), 2001945. https://doi.org/10.1002/ADMA.202001945.

87. Yang, J.; Zeng, F.; Li, X.; Ran, C.; Xu, Y.; Li, Y. Highly Specific Detection of Aβ Oligomers in Early Alzheimer's Disease by a near-Infrared Fluorescent Probe with a "V-Shaped" Spatial Conformation. *Chem. Commun.* **2020**, *56* (4), 583–586. https://doi.org/10.1039/C9CC08894F.

88. Zhou, Y.; Chen, Y. Z.; Cao, J. H.; Yang, Q. Z.; Wu, L. Z.; Tung, C. H.; Wu, D. Y. Dicyanoboron Diketonate Dyes: Synthesis, Photophysical Properties and Bioimaging. *Dyes Pigm.* **2015**, *112*, 162–169. https://doi.org/10.1016/J.DYEPIG.2014.07.001.

89. Dewar, M. J. S. 478. Colour and Constitution. Part I. Basic Dyes. *J. Chem. Soc.* **1950**, 2329. https://doi.org/10.1039/jr9500002329.

90. Knott, E. B. 227. The Colour of Organic Compounds. Part I. A General Colour Rule. *J. Chem. Soc.* **1951**, 1024. https://doi.org/10.1039/jr9510001024.

91. Borysyuk, V. I.; Yashchuk, V. M.; Naumenko, A. P.; Stanova, A. V.; Gerasova, V. G.; Gerasov, A. O.; Kovtun, Y. P.; Shandura, M. P.; Kachkovsky, O. D. Influence of Surplus Negative Charge on Absorption and Fluorescence Excitation Spectra of Asymmetric Polymethine Dyes. *Ukr. J. Phys.* **2015**, *60* (7), 593-600-593–600. https://doi.org/10.15407/ujpe60.07.0593.

92. Gerasov, A. O.; Shandura, M. P.; Kovtun, Y. P.; Kachkovsky, A. D. The Nature of Electron Transitions in Anionic Dioxaborines, Derivatives of Aminocoumarin. *J. Phys. Org. Chem.* **2008**, *21* (5), 419–425. https://doi.org/10.1002/POC.1368.

93. Tyutyulkov, N.; Fabian, J.; Mehlhorn, A.; Dietz, F.; Tadjer, A. in *Polymethine Dyes. Structure and Properties*; Peters, A. T., Ed.; St. Kliment Ohridski Univer-sity Pres; Sofia, **1991**; pp. 67–68.

94. Uranga-Barandiaran, O.; Catherin, M.; Zaborova, E.; D'Aléo, A.; Fages, F.; Castet, F.; Casanova, D. Optical Properties of Quadrupolar and Bi-Quadrupolar Dyes: Intra and Inter Chromophoric Interactions. *Phys. Chem. Chem. Phys.* **2018**, *20* (38), 24623–24632. https://doi.org/10.1039/C8CP05048A.

95. Dirk, C. W.; Herndon, W. C.; Cervantes-Lee, F.; Selnau, H.; Martinez, S.; Kalamegham, P.; Tan, A.; Campos, G.; Velez, M. Squarylium Dyes: Structural Factors Pertaining to the Negative Third-Order Nonlinear Optical Response. *J. Am. Chem. Soc.* **1995**, *117* (8), 2214–2225. https://doi.org/10.1021/ja00113a011.

96. Terenziani, F.; Painelli, A.; Katan, C.; Charlot, M.; Blanchard-Desce, M. Charge Instability in Quadrupolar Chromophores: Symmetry Breaking and Solvatochromism. *J. Am. Chem. Soc.* **2006**, *128* (49), 15742–15755. https://doi.org/10.1021/ja064521j.

97. Ran, C.; Xu, X.; Raymond, S. B.; Ferrara, B. J.; Neal, K.; Bacskai, B. J.; Medarova, Z.; Moore, A. Design, Synthesis, and Testing of Difluoroboron-Derivatized Curcumins as Near-Infrared Probes for in Vivo Detection of Amyloid-β Deposits. *J. Am. Chem. Soc.* **2009**, *131* (42), 15257–15261. https://doi.org/10.1021/ja9047043.

98. Selkoe, D. J. Translating Cell Biology into Therapeutic Advances in Alzheimer's Disease. *Nature* **1999**, *399* (6738), A23–A31. https://doi.org/10.1038/399a023.

99. Li, Z.; Song, Y.; Lu, Z.; Li, Z.; Li, R.; Li, Y.; Hou, S.; Zhu, Y.-P.; Guo, H. Novel Difluoroboron Complexes of Curcumin Analogues as "Dual-Dual" Sensing Materials for Volatile Acid and Amine Vapors. *Dyes Pigm.* **2020**, *179*, 108406. https://doi.org/10.1016/j.dyepig.2020.108406.

100. Bai, G.; Yu, C.; Cheng, C.; Hao, E.; Wei, Y.; Mu, X.; Jiao, L. Syntheses and Photophysical Properties of BF$_2$ Complexes of Curcumin Analogues. *Org. Biomol. Chem.* **2014**, *12* (10), 1618–1626. https://doi.org/10.1039/C3OB42201A.

101. Liu, K.; Chen, J.; Chojnacki, J.; Zhang, S. BF$_3$·OEt$_2$-Promoted Concise Synthesis of Difluoroboron-Derivatized Curcumins from Aldehydes and 2,4-Pentanedione. *Tetrahedron Lett.* **2013**, *54* (16), 2070–2073. https://doi.org/10.1016/j.tetlet.2013.02.015.

102. Felouat, A.; D'Aléo, A.; Fages, F. Synthesis and Photophysical Properties of Difluoroboron Complexes of Curcuminoid Derivatives Bearing Different Terminal Aromatic Units and a Meso-Aryl Ring. *J. Org. Chem.* **2013**, *78* (9), 4446–4455. https://doi.org/10.1021/jo400389h.

103. Sherin, D. R.; Thomas, S. G.; Rajasekharan, K. N. Mechanochemical Synthesis of 2,2-Difluoro-4,6-Bis(β-Styryl)-1,3,2-Dioxaborines and Their Use in Cyanide Ion Sensing. *Heterocycl. Commun.* **2015**, *21* (6), 381–385. https://doi.org/10.1515/hc-2015-0096.

104. Rivoal, M.; Zaborova, E.; Canard, G.; D'Aléo, A.; Fages, F. Synthesis, Electrochemical and Photophysical Studies of the Borondifluoride Complex of a Meta-Linked Biscurcuminoid. *New J. Chem.* **2016**, *40* (2), 1297–1305. https://doi.org/10.1039/C5NJ00925A.

105. Canard, G.; Ponce-Vargas, M.; Jacquemin, D.; Le Guennic, B.; Felouat, A.; Rivoal, M.; Zaborova, E.; D'Aléo, A.; Fages, F. Influence of the Electron Donor Groups on the Optical and Electrochemical Properties of Borondifluoride Complexes of Curcuminoid Derivatives: A Joint Theoretical and Experimental Study. *RSC Adv.* **2017**, *7* (17), 10132–10142. https://doi.org/10.1039/C6RA25436E.

106. Kamada, K.; Namikawa, T.; Senatore, S.; Matthews, C.; Lenne, P.-F.; Maury, O.; Andraud, C.; Ponce-Vargas, M.; Le Guennic, B.; Jacquemin, D.; Agbo, P.; An, D. D.; Gauny, S. S.; Liu, X.; Abergel, R. J.; Fages, F.; D'Aléo, A. Boron Difluoride Curcuminoid Fluorophores with Enhanced Two-Photon Excited Fluorescence Emission and Versatile Living-Cell Imaging Properties. *Chem. - Eur. J.* **2016**, *22* (15), 5219–5232. https://doi.org/10.1002/chem.201504903.

107. Chaicham, A.; Kulchat, S.; Tumcharern, G.; Tuntulani, T.; Tomapatanaget, B. Synthesis, Photophysical Properties, and Cyanide Detection in Aqueous Solution of BF2-Curcumin Dyes. *Tetrahedron* **2010**, *66* (32), 6217–6223. https://doi.org/10.1016/j.tet.2010.05.088.

108. Margar, S. N.; Rhyman, L.; Ramasami, P.; Sekar, N. Fluorescent Difluoroboron-Curcumin Analogs: An Investigation of the Electronic Structures and Photophysical Properties. *Spectrochim. Acta, Part A* **2016**, *152*, 241–251. https://doi.org/10.1016/j.saa.2015.07.064.

109. Raikwar, M. M.; Rhyman, L.; Ramasami, P.; Sekar, N. Theoretical Investigation of Difluoroboron Complex of Curcuminoid Derivatives with and without Phenyl Substituent (at Meso Position): Linear and Non-Linear Optical Study. *ChemistrySelect* **2018**, *3* (40), 11339–11349. https://doi.org/10.1002/SLCT.201802231.

110. Insuasty, D.; Cabrera, L.; Ortiz, A.; Insuasty, B.; Quiroga, J.; Abonia, R. Synthesis, Photophysical Properties and Theoretical Studies of New Bis-Quinolin Curcuminoid BF2-Complexes and Their Decomplexed Derivatives. *Spectrochim. Acta, Part A* **2020**, *230*, 118065. https://doi.org/10.1016/J.SAA.2020.118065.

111. Choi, K.-R.; Kim, D. H.; Lee, Y. U.; Placide, V.; Huynh, S.; Yao, D.; Canard, G.; Zaborova, E.; Mathevet, F.; Mager, L.; Heinrich, B.; Ribierre, J.-C.; Wu, J. W.; Fages, F.; D'Aléo, A. Effect of the Electron Donating Group on the Excited-State Electronic Nature and Epsilon-near-Zero Properties of Curcuminoid-Borondifluoride Dyes. *RSC Adv.* **2021**, *11* (60), 38247–38257. https://doi.org/10.1039/D1RA08025C.

112. Zhang, X.; Tian, Y.; Yuan, P.; Li, Y.; Yaseen, M. A.; Grutzendler, J.; Moore, A.; Ran, C. A Bifunctional Curcumin Analogue for Two-Photon Imaging and Inhibiting Crosslinking of Amyloid Beta in Alzheimer's Disease. *Chem. Commun.* **2014**, *50* (78), 11550–11553. https://doi.org/10.1039/C4CC03731F.

113. Zhang, X.; Tian, Y.; Zhang, C.; Tian, X.; Ross, A. W.; Moir, R. D.; Sun, H.; Tanzi, R. E.; Moore, A.; Ran, C. Near-Infrared Fluorescence Molecular Imaging of Amyloid Beta Species and Monitoring Therapy in Animal Models of Alzheimer's Disease. *PNAS* **2015**, *112* (31), 9734–9739. https://doi.org/10.1073/pnas.1505420112.

114. Zhang, P.; Guo, Z. Q.; Yan, C. X.; Zhu, W. H. Near-Infrared Mitochondria-Targeted Fluorescent Probe for Cysteine Based on Difluoroboron Curcuminoid Derivatives. *Chin. Chem. Lett.* **2017**, *28* (10), 1952–1956. https://doi.org/10.1016/J.CCLET.2017.08.038.

115. Chen, D.; Yang, J.; Dai, J.; Lou, X.; Zhong, C.; Yu, X.; Xia, F. A Low Background D–A–D Type Fluorescent Probe for Imaging of Biothiols in Living Cells. *J. Mater. Chem. B* **2018**, *6* (32), 5248–5255. https://doi.org/10.1039/C8TB01340C.

116. Bai, B.; Yan, C.; Zhang, Y.; Guo, Z.; Zhu, W. H. Dual-Channel near-Infrared Fluorescent Probe for Real-Time Tracking of Endogenous γ-Glutamyl Transpeptidase Activity. *Chem. Commun.* **2018**, *54* (87), 12393–12396. https://doi.org/10.1039/C8CC07376G.

117. Archet, F.; Yao, D.; Chambon, S.; Abbas, M.; D'Aléo, A.; Canard, G.; Ponce-Vargas, M.; Zaborova, E.; Le Guennic, B.; Wantz, G.; Fages, F. Synthesis of Bioinspired Curcuminoid Small Molecules for Solution-Processed Organic Solar Cells with High Open-Circuit Voltage. *ACS Energy Lett.* **2017**, *2* (6), 1303–1307. https://doi.org/10.1021/acsenergylett.7b00157.

118. Sherin, D. R.; Manojkumar, T. K.; Rajasekharan, K. N. CRANAD-1 as a Cyanide Sensor in Aqueous Media: A Theoretical Study. *RSC Adv.* **2016**, *6* (101), 99385–99390. https://doi.org/10.1039/C6RA19045F.

119. Zhang, Y.; Tu, L.; Lu, L.; Li, Y.; Song, L.; Qi, Q.; Song, H.; Li, Z.; Huang, W. Screening and Application of Boron Difluoride Complexes of Curcumin as Colorimetric and Ratiometric Fluorescent Probes for Bisulfite. *Anal. Methods* **2020**, *12* (11), 1514–1521. https://doi.org/10.1039/D0AY00173B.

120. Zhao, X.; Yang, Y.; Yu, Y.; Guo, S.; Wang, W.; Zhu, S. A Cyanine-Derivative Photosensitizer with Enhanced Photostability for Mitochondria-Targeted Photodynamic Therapy. *Chem. Commun.* **2019**, *55* (90), 13542–13545. https://doi.org/10.1039/C9CC06157F.

121. Polishchuk, V.; Stanko, M.; Kulinich, A.; Shandura, M. D–π–A–π–D Dyes with a 1,3,2-Dioxaborine Cycle in the Polymethine Chain: Efficient Long-Wavelength Fluorophores. *Eur. J. Org. Chem.* **2018**, *2018* (2), 240–246. https://doi.org/10.1002/ejoc.201701466.

122. Polishchuk, V.; Kulinich, A.; Suikov, S.; Rusanov, E.; Shandura, M. 'Hybrid' Mero-Anionic Polymethines with a 1,3,2-Dioxaborine Core. *New J. Chem.* **2022**, *46* (3), 1273–1285. https://doi.org/10.1039/D1NJ05104K.

123. Polishchuk, V.; Kulinich, A.; Rusanov, E.; Shandura, M. Highly Fluorescent Dianionic Polymethines with a 1,3,2-Dioxaborine Core. *J. Org. Chem.* **2021**, *86* (7), 5227–5233. https://doi.org/10.1021/acs.joc.1c00138.

124. Polishchuk, V.; Filatova, M.; Rusanov, E.; Shandura, M. Trianionic 1,3,2-Dioxaborine-Containing Polymethines: Bright Near-Infrared Fluorophores. *Chem. – Eur. J.* **2022**. https://doi.org/10.1002/chem.202202168.

Information about the authors:

Vladyslav M. Polishchuk (*corresponding author*), Ph.D. in Chemistry, Junior Researcher, Department of Color and Structure of Organic Compounds, Institute of Organic Chemistry of the National Academy of Sciences of Ukraine, https://orcid.org/0000-0003-4396-0119; e-mail for correspondence: vlad3ds@gmail.com.

Mykola P. Shandura, Ph.D. in Chemistry, Senior Researcher, Department of Color and Structure of Organic Compounds, Institute of Organic Chemistry of the National Academy of Sciences of Ukraine; https://orcid.org/0000-0003-0896-4376.

O. A. Kovalenko[1], A. V. Drobitko[1], V. D. Palamarchuk[2], U. P. Bahliuk[1]

[1] Mykolaiv National Agrarian University, 9, Georgiy Gongadze str., Mykolaiv, 54020, Ukraine
[2] Vinnytsia National Agrarian University, 3, Sonyachna str., Vinnytsia, 21008, Ukraine

Corn: Sowing Parameters

Abstract

Aim. To highlight the results of the research conducted in 2020–2021 aiming at studying the effect of multi-depth and multifraction sowing of the hybrid corn seeds of the DMS Sticker mid-early maturity group on the yield when grown in the conditions of the Northern Steppe of Ukraine and determine the economic efficiency of the approaches.

Materials and methods. Winter wheat was a predecessor crop in the study. Tillage methods and related conditions are described in the article. Herbicides were used to protect against weeds. Sowing was carried out in the third decade of April at a soil temperature of +8–10 °C. The experiment considered 2 factors, namely the depth of sowing seeds and the size of the seed fraction. The results obtained were processed using measurement, mathematical and statistical methods of research, as well as calculation and comparison approaches.

Results and discussion. On average, depending on the factors studied, the height of the plants varied significantly, as a rule, the tallest plants were obtained from large seeds, which had the highest mass of 1000 seeds. Thus, in particular, on average over two years of research, the height of the plants was 250.4 cm when the weight of 1000 seeds was 255 g, and the seeds were wrapped by 4–5 cm; when the weight of 1000 seeds was 300 g, the height was 251.1 cm, while with the weight of 350 g it was 258.3 cm; with the wrapping depth of 7–8 cm the height was 252.1 cm, 255.8 and 268.5 cm, and with the wrapping depth of 10–11 cm it was 257.6 cm, 261.8 and 266.1 cm.

Conclusions. The use of the large seed fraction provided an increase in the yield of the DMS Sticker corn hybrid by 1.09–1.79 t ha^{-1} compared to the use of the small seed fraction and was 8.70 t ha^{-1}. When using the large seed fraction and the wrapping depth of 10–11 cm, the cost of production was 56,550 UAH ha^{-1}. The cost price of 1 ton of production was the lowest and amounted to UAH 2,247.1, the conditional net profit was the highest – 37,000 UAH ha^{-1}, and the level of profitability was 189.3 %.

Keywords: corn; hybrid; seeds; weight of 1000 seeds; depth of wrapping; height of plants; productivity; conditional net profit; cost price; level of profitability

О. А. Коваленко[1], А. В. Дробітко[1], В. Д. Паламарчук[2], У. П. Баглюк[1]
[1] Миколаївський національний аграрний університет, вул. Георгія Гонгадзе, 9, Миколаїв, 54020, Україна
[2] Вінницький національний аграрний університет, вул. Сонячна, 3, Вінниця, 21008, Україна

Кукурудза: параметри сівби

Анотація

Мета. Висвітлити результати наукових досліджень 2020–2021 рр., метою яких було виявити вплив на врожайність різноглибинної та різнофракційної сівби насіння гібриду кукурудзи середньоранньої групи стиглості DMS Sticker за вирощування в умовах Північного Степу України та визначити економічну ефективність застосування такої сівби.

Матеріали та методи. Культурою-попередником у дослідженні була озима пшениця. Способи оброблення ґрунту та супутні умови описано в статті. Для захисту від бур'янів використовували гербіциди. Посів здійснювали в третій декаді квітня за температури ґрунту +8–10 °C. Експеримент враховував 2 фактори, а саме: глибину посіву насіння та розмір фракції насіння. Отримані результати обробляли, використовуючи вимірювальні, математичні і статистичні методи дослідження, а також розрахунковий та порівняльний підходи.

Результати та їх обговорення. Залежно від досліджуваних факторів висота рослин істотно змінювалася: як правило, найвищі рослини були отримані з крупного насіння, що мало найбільшу масу 1000 насінин. Так, зокрема, за маси 1000 насінин 255 г у разі загортання насіння на 4–5 см пересічно за два роки досліджень висота рослин становила 250,4 см, за маси 1000 насінин 300 г – 251,1 см, а у випадку маси 1000 насінин 350 г – 258,3 см; за глибини загортання 7–8 см – 252,1 см, 255,8 і 268,5 см, а за глибини загортання 10–11 см – 257,6 см, 261,8 і 266,1 см.

Висновки. Використання великої фракції насіння проти використання дрібної фракції забезпечило збільшення врожайності гібрида кукурудзи DMS Sticker на 1,09 – 1,79 т га⁻¹ і становило 8,70 т га⁻¹. За використання великої фракції насіння та глибини загортання 10 – 11 см собівартість продукції становила 56 550 грн га⁻¹. Собівартість 1 т продукції була найнижчою і становила 2 247,1 грн, умовно чистий прибуток був найвищим – 37 000 грн га⁻¹, а рівень рентабельності – 189,3 %.

Ключові слова: кукурудза; гібрид; насіння; маса 1000 насінин; глибина загортання; висота рослин; урожайність; умовно чистий прибуток; собівартість; рівень рентабельності

◼ Introduction

Corn is one of the most valuable agricultural crops. If all agrotechnical requirements are met, it can form a high yield. For the cultivation of corn, especially with intensive technologies, morphological characteristics of plants, which determine suitability for mechanized cultivation and harvesting, are important [1, 2].

In recent years, corn occupies an increasingly stable position in the world grain market. In this field, the natural and economic conditions of Ukraine allow not only to meet domestic needs, but also to significantly increase its export potential. However, in reality, on the way to creating a stable and favorable environment, including market infrastructure, in the production practice of growing corn, there are still numerous obstacles of an agrotechnological nature [1, 3].

A feature of the current technology for growing high-yielding corn hybrids is the optimization of the fractional composition of the seed material and the determination of the optimal depth of its wrapping. A high-quality seed material is the key to a large harvest. It has been determined [4, 5] that due to high-quality seeds, the increase in the corn grain yield can be 20–80%. At the same time, the use of the large fraction of corn seeds provides a significant increase in the grain yield [6–9].

The depth of seed wrapping is also important since very shallow and deep seed wrapping negatively affect field germination, completeness and uniformity of seedlings, and the intensity of growth of corn plants in the initial growing season. To obtain friendly and full-fledged seedlings, seeds are sown to such a depth that it is provided with a sufficient amount of moisture, air and heat [10]. It is important to correctly choose the parameters of the optimal seeding depth depending on the seed fraction, biological properties of the hybrid, moisture availability of the seeding horizon, mechanical composition of the soil, energy of the starting growth of the hybrid, in order to obtain friendly and leveled seedlings with a high field seed germination [12, 13]. In addition, the deeper the seed is sown, the more the seedlings come into contact with pathogenic microorganisms and pests on their way, so they are more affected by them, especially on soils with a heavy mechanical composition [10, 11].

Both very shallow and deep wrapping of seeds negatively affects field germination, completeness and uniformity of seedlings, the growth intensity of corn plants in the initial growing season. The great depth of seed wrapping contributes to the fact that young seedlings have to spend excessive amounts of plastic substances to overcome the seed layer of the soil, as a result of which they are depleted. In addition, the deeper the seed is sown, the more the seedlings encounter pathogenic microorganisms on their way; therefore, they are more affected by them, especially on soils with a heavy mechanical composition. When the depth of seed wrapping, which has micro- and microtraumas, increases, its germination decreases by 20–21% [11], the temperature conditions for seed germination deteriorate, and therefore, the seedlings may be unfriendly and thinned [12]. At the moment, there is a ridge technology for growing corn, which makes it possible to increase productivity by 15–20% due to early sowing in the ridge. However, this technology did not spread in Ukraine due to insufficient moisture in the upper

soil layer during the entire growing season and its high energy consumption. The depth of corn seed wrapping also depends on the timing of sowing. Thus, in particular, when sowing seeds in early periods, for the purpose of better heat supply, the depth of wrapping is reduced to 3–4 cm [10–12]. In order to protect seeds from mold during early sowing, they should be wrapped shallower (4–6 cm), and later – by 6–8 cm [12]. Sowing corn seeds to a depth of more than 7 cm leads to a decrease in field germination by 5.5%, and grain yield by 3.7–12.8%. The greater the mass of 1,000 grains, the deeper the seed penetration into the soil, especially four-line hybrids [12].

With the optimal depth of sowing, the mold of seeds and seedlings of corn is reduced. An increase in the depth of seed wrapping increases the risk of damage to seedlings by soil pathogens – the causative agents of mold and root rot, as well as powdery mildew diseases and damage by wireworms. Full friendly seedlings can be obtained by sowing seeds at such a depth where they will receive a sufficient amount of moisture, air and heat. When the top layer of the soil dries, the seeds are wrapped deeper so that they lie in the moist soil. With the close occurrence of groundwater, the depth of seed wrapping is reduced to 5–6 cm, and on light soils prone to rapid drying, it can be increased to 10–12 cm [11, 12].

There are data that the best development of corn plants is ensured by a seed wrapping depth of 5 cm. Sowing 1 cm deeper or shallower can reduce the yield by 10–20%. In areas with insufficient moisture, after sowing corn, rolling is recommended; it improves the conditions for seed germination, reduces its moldiness and damage by stem and root rots.

Large seeds give aligned and friendly seedlings since the primary (embryonic) roots and the first leaf are formed, practically, only due to the nutrients of the grain. The strength of the germinal roots and the area of the first leaf in a straight line depend on the size of the grain [2, 5, 12].

The variety of the seed material is associated with the location of the grain in the cob (matricular). The grain on the cobs is formed unevenly, everything starts from the middle of the cob, the size of the grains goes from bottom to top. The highest quality seeds are formed in the middle of the cob, i.e., the size of the seeds goes downward from bottom to top. Grains in the middle part of the corn cob contain more enzymes; these seeds start the germination process faster, especially since the swelling of corn seeds before the germination process requires less water than 40% of the weight of the grain [5, 8, 12].

Fractions of different sizes may receive different degrees of damage during harvesting, depending on the harvesting technology and post-harvest processing. In some cases, large fractions can be damaged to a significant extent, in other cases, small ones can be affected due to which their quality varies in different ways. Mechanical damage and thermal cracking of seeds can reach 75–85% [11, 12].

Coarse and medium fractions of seeds have similar sowing and yield properties, while fine fractions lead to a significant decrease in quality. At the same time, it should be noted that such results are possible when separating seeds according to the "grain width" feature [8]. The highest yield of corn grain is obtained for sowing large and medium fractions, for silage – medium ones, for green fodder – small fractions. These recommendations are given for old 3–4-line hybrids [12].

Usually, in production conditions, the minimum seed weight limit for sowing is rarely lower than 200 grams, and in the case of using seeds of a smaller weight, there is always a dispute about its suitability for forming productive sowing. Seeds of larger fractions are used on more structured soils and lighter in mechanical composition, with poorer moisture-holding capacity and in areas with less moisture availability (the possibility of deeper wrapping and greater need for moisture for germination). When using seeds of siliceous and tooth-shaped forms, it is worth starting sowing with siliceous ones since they need more moisture for swelling and germination.

Summarizing data from literary sources, it should be noted that the insufficient study of the size of the seed fraction and the depth of its wrapping requires further research, which is necessary and relevant.

Corn has enormous potential for record grain yields. But this becomes a reality only if the grain cultivation technology is followed, which corresponds to the biological characteristics of the corn plant. Knowing these requirements, it is possible to reduce or completely remove the negative impact of one or another factor [12].

Our aim was to study the effect of the fraction size and the depth of seed wrapping on the productivity of the DMS Sticker mid-early maize hybrid (FAO 250) during 2020–2021 on ordinary chernozem in the conditions of the northern part of the Pervomaysky district of the Mykolaiv region [13].

■ Materials and methods

The predecessor crop in the experiment was winter wheat. After harvesting the predecessor, the field was disked to a depth of 14–16 cm. Plowing was carried out to a depth of 22–25 cm. In the spring, moisture was closed with heavy harrows (BZTS 1) and pre-sowing cultivation (Europak). Protection against weeds included the application of herbicides Harness – 3.0 L ha⁻¹ before seedlings and Milagro in the phase of 5–7 leaves – 1.25 L ha⁻¹. Sowing was carried out in the optimal time (the third decade of April) at a soil temperature of +8–10 ºC using an updated SUPN-8 seeder with a seeding rate of 50,000 pcs. seeds per hectare.

The scheme of the experiment included two factors. *Factor A* (the depth of sowing seeds): 1. depth – 4–5 cm; 2. depth – 7–8 cm; 3. depth – 10–11 cm. *Factor B* (size of seed fraction): 1. small (weight of 1000 grains) – 255 g; 2. medium (weight of 1000 grains) – 300 g; 3. large (weight of 1000 grains) – 350 g [13].

Repetition for hybrids in experiments was 4 times. Placement of plots was performed using the method of randomized repetitions. To determine the productivity level and morphological characteristics of plants, the measurement method of research was used; to assess the importance and reliability of the research results obtained, mathematical and statistical methods were applied; to obtain the economic assessment of the cultivation of a corn hybrid, we used calculation and comparison approaches [14–17].

■ Results and discussion

The results obtained in the studies confirmed the opinion that the height of plants could change depending on the conditions of the year and the features of the elements of growing technology. The year 2021 was the most favorable for the manifestation of plant height, while in 2020, due to a decrease in the amount of moisture and increased temperatures, the height of plants decreased somewhat, but this applied to the depth of seed wrapping of 4–5 and 7–8 cm. When wrapping seeds to a depth of 10–11 cm, due to the better moisture availability of this soil layer, even in 2020, some improvement in the growth processes of the DMS Sticker corn hybrid was observed.

The height of the plants varied significantly depending on the size of the seeds, as a rule, the tallest plants were obtained from large seeds, which had the highest mass of 1000 seeds. Thus, in particular, on average over two years of research, the height of the plants was 250.4 cm when the weight of 1000 seeds was 255 g, and the seeds were wrapped by 4–5 cm; when the weight of 1000 seeds was 300 g, the height was 251.1 cm, while with the weight of 350 g it was 258.3 cm; with the wrapping depth of 7–8 cm the height was 252.1 cm, 255.8 and 268.5 cm, and with the wrapping depth of 10–11 cm it was 257.6 cm, 261.8 and 266.1 cm.

The influence of the size of the seed fraction and the depth of their wrapping on the height of cob laying in the corn hybrids was studied. Thus, with an increase in the mass of the seed fraction, the height of cob laying in the DMS Sticker hybrid also increased, with the weight of 1000 seeds of 255 g, the height of cob laying was 87.5 cm, with the weight of 1000 seeds of 300 g it was 88.5 cm, and with the seed weight of 350 g – 89.8 cm at the seed wrapping depth of 4–5 cm. At the seed wrapping depth of 7–8 cm, it was 90.1 cm, 93.3 and 9.5 cm, and at the seed wrapping depth of 10–11 cm – 86.5 cm, 91.7 cm and 93.5 cm, respectively, for small, medium and large fractions. There was also an increase in the height of cob laying with an increase in the depth of seed wrapping. This is explained by a better moisture supply of the lower layers of the soil, especially in the event of spring droughts.

Significant reserves of nutrients in the endosperm of a corn kernel and a large embryo allow it to germinate from a depth of 10 cm or more and maintain viability for a long time in dry soil. The results of the research conducted showed the influence of the size and depth of seed wrapping on the number of rows of grains.

The data obtained confirm that the size of the seed fraction does not significantly affect the number of rows of grains on the cob, it is only necessary to note that when sowing with seeds of medium and large fractions of the DMS Sticker corn hybrid, the number of rows was slightly higher compared to sowing with small seeds. The largest number of rows on the cob was noted in the DMS Sticker corn hybrid for sowing with seeds of the large fraction – 14.8 pcs, and for the medium fraction – 14.4–14.7 pcs, while for sowing with seeds of the small fraction it was the lowest 14.1–14.3 pcs. The use of medium and large seed fractions ensures a slight increase in the number of grain rows in all hybrids. Therefore, it can be noted that this feature is more

Table 1. The grain moisture content of the DMS Sticker corn hybrid depending on the factors studied (average for 2020-2021), %

Seed fraction (Factor A)	Seed wrapping depth (Factor B)		
	4-5 cm	7-8 cm	10-11 cm
Small (255 g)	23.86	24.43	24.45
Medium (300 g)	24.64	24.79	24.82
Large (350 g)	25.05	25.19	25.43

Table 2. The grain yield of the DMS Sticker corn hybrid in the net weight depending on the factors studied (average for 2020-2021), t ha^{-1}

Seed fraction (Factor A)	Seed wrapping depth (Factor B)		
	4-5 cm	7-8 cm	10-11 cm
Small (255 g)	6.91	7.39	7.61
Medium (300 g)	7.53	7.98	8.33
Large (350 g)	8.15	8.44	8.70

genetically determined, and less dependent on agricultural cultivation techniques.

When the depth of seed wrapping changed, the number of rows of grains changed ambiguously. We did not determine a significant relationship between the increase in the depth of seed wrapping and the number of rows of grains in the DMS Sticker corn hybrid although it was present to some extent.

The next feature that determines the level of productivity of corn hybrids is the number of grains in a row. Thus, the number of grains in a row was largely determined by the size of the seed fraction. When using seeds of medium (30.0–31.0 pcs) and large (31.1–31.4 pcs) fractions for sowing the number of grains in a row was significantly higher than when sowing seeds of small fractions (29.4–30.2 pcs). Thus, the use of the medium and large fraction of seeds ensures a significant increase in the number of grains in a row of the corn hybrid studied.

The number of grains in a row changed ambiguously due to changes in the depth of seed wrapping. Thus, in particular, the number of grains in a row, on average over two years, at the seed wrapping depth of 4–5 cm was 28.5–30.3 pcs, at the wrapping depth of 7–8 it was 28.9–32.3 pcs, and at the depth of 10–11 cm it was the highest – 29.2–32.4 pcs depending on the years of research.

Based on the data obtained, it can be stated that the option of sowing to the depth of 10–11 cm provided more stable indicators of the number of grains both in dry (2020) and in wetter (2021) years when they were carried out with the largest seeds.

Depending on the number of rows of grains and the number of grains in the row of the beginning of corn, a different number of grains were formed on one crop plant, and therefore, the plants had different productivity. Thus, depending on the options, each beginning formed an average of 414.5 to 464.7 grains over the years of research. Moreover, their maximum sphericity was formed at the beginning of plants sown to a depth of 10–11 cm with the largest seeds.

In addition to the number of grains at the beginning, an important element of the productivity of a corn crop is the actual number of ears per plant. Thus, in our options, this indicator varied from 1.38 to 1.49 pieces per plant.

Based on the data obtained, it can be stated that the maximum number of buds (1.49 pcs per plant) was formed when sowing the largest seeds (350 g per 1000 pcs) and sowing them to a depth of 10–11 cm. The least variable was seed sowing with an average weight. Regarding the sowing depth, it was identical.

Depending on the number of grains at the beginning and the number of beginnings on the plant, their productivity varied from 170.5 to 218.1 g per plant, and the maximum was for sowing to a depth of 10–11 cm with the largest seeds.

Therefore, the seed fraction and the depth of its wrapping can change the values of the elements of the crop structure in the DMS Sticker corn hybrid.

As a result of the research conducted, on average over two years, the moisture content of the grain when using the fine fraction was 23.86% for the wrapping depth of 4–5 cm, 24.43% for the seed wrapping depth of 7–8 cm, and 24.45% for the wrapping depth 10–11 cm; when using the medium fraction of seeds – 24.64%, 24.79 and 24.82%, while using the large fraction of seeds – 25.05%, 25.19% and 25.43%, respectively (Table 1).

Therefore, the increase in the size of the seed fraction provided an increase in the level of pre-harvest moisture, which ultimately caused additional costs for grain drying. For changes in the depth of seed wrapping, this dependence was not detected.

As for the yield of grain, it is necessary to note the lowest level of its value, on average over two years of research, for the use of the small fraction of seeds of the DMS Sticker hybrid: 7.67 t ha^{-1} for wrapping depths of 4–5, 8.25 – for 7–8 cm and 8.50 t ha^{-1} for the seed wrapping depth of 10–11 cm (Table 2).

With the use of the medium seed fraction, the yield increased by 0.36–1.1 t ha^{-1}, compared to the fine fraction, and with the use of the large

seed fraction, the yield was the highest and was 9.16 t ha^{-1} at the wrapping depth of 4–5 cm, 9.50 t ha^{-1} for wrapping depths of 7–8 cm and 9.82 t ha^{-1} for wrapping depths of 10–11 cm.

Due to the excess moisture of the harvested grain and the need for additional drying and bringing it to 14% moisture, the parameters of the grain obtained differed from the threshed grain.

Therefore, the use of the large seed fraction provided an increase in the yield of the DMS Sticker corn hybrid by 1.09–1.79 t ha^{-1} compared to the use of the small seed fraction and was 8.70 t ha^{-1} in the net weight. In addition, it is necessary to note the highest value of productivity (8.15–8.70 t ha^{-1})

of this hybrid when sowing the large fraction of the seed material in all variants of the depth of seed wrapping.

■ Conclusions

Thus, based on the results obtained and their analysis in the conditions of the northern part of the Pervomaysky district of the Mykolaiv region, it has been proposed to use the large fraction of seeds weighing 1000 grains of 350 g for the formation of the grain yield of the DMS Sticker corn hybrid (FAO 250) at the level of 8.70 t ha^{-1} and the depth of its wrapping when sowing is 10–11 cm.

■ References

1. Kovalenko, O. A. Ahroekolohichne obgruntuvannia ta rozrobka elementiv biolohizovanykh tekhnolohii vyroshchuvannia silskohospodarskykh kultur v umovakh Pivdnia Ukrainy [Agroecological substantiation and development of elements of biologized technologies for growing agricultural crops in the conditions of southern Ukraine, *in Ukrainian*]. Diss. for the degree of Doctor of Agricultural Sciences, Kherson, 2021.

2. Palamarchuk, V. D.; Polishchuk, M. I.; Palamarchuk, O. D. Kharakterystyka osnovnykh elementiv tekhnolohii vyroshchuvannia zernovoi kukurudzy [Characteristics of the main elements of grain corn cultivation technology, *in Ukrainian*]. *Silske hospodarstvo ta lisivnytstvo* **2016**, *3*, 57 – 64.

3. Palamarchuk, V. D.; Didur, I. M.; Kolisnyk, O. M.; Alekseev, O. O. *Aspekty suchasnoi tekhnolohii vyroshchuvannia vysokokrokhmalnoi kukurudzy v umovakh Lisostepu Pravoberezhnoho* [Aspects of the modern technology of growing high-starch corn in the conditions of the right-bank forest-steppe, *in Ukrainian*]. Druk: Vinnytsia, 2020.

4. Kirpa, M. Ya. Vyznachennia yakosti nasinnia kukurudzy ta pidhotovka yoho do sivby [Determining the quality of corn seeds and preparing them for sowing, *in Ukrainian*]. *Suchasni ahrotekhnolohii* **2013**, *3*, 18 – 22.

5. Tsehmeistruk, M. G.; Muzafarov, N. M.; Manko, K. M. Aspekty vyroshchuvannia kukurudzy. http://agro-business.com.ua/ahrarni-kultury/item/436-aspekty-vyroshchuvannia-kukurudzy.html (accessed Sep 19, 2022).

6. Fadeev, O. Shcho budemo siiaty? [What will we sow?, *in Ukrainian*]. *Ahromarket* 2016, *2*, 28 – 29.

7. Palamarchuk, V. D.; Guts, V. O. Vplyv rozmiriv ta hlybyny zahortannia nasinnia na proiav morfolohichnykh oznak u hibrydiv kukurudzy [The influence of the size and depth of seed wrapping on the manifestation of morphological traits in corn hybrids, *in Ukrainian*]. *Silske hospodarstvo ta lisivnytstvo* **2016**, *4*, 94 – 101.

8. Palamarchuk, V. D. Kharakterystyka hibrydiv kukurudzy za masoiu 1000 zeren ta produktyvnistiu zalezhno vid elementiv tekhnolohii [Characteristics of corn hybrids by the weight of 1000 grains and productivity depending on the elements of technology, *in Ukrainian*]. *Visnyk Umanskoho natsionalnoho universytetu sadivnytstva* **2018**, *1*, 38 – 42. https://doi.org/10.31395/2310-0478-2018-1-38-42.

9. Palamarchuk, V. D. Vplyv chynnykiv tekhnolohii na formuvannia masy 1000 zernyn i produktyvnosti hibrydiv kukurudzy [The influence of technological factors on the formation of the mass of 1000 grains and the productivity of corn hybrids, *in Ukrainian*]. *Ahronom* **2019**, *4*, 86 – 91.

10. Vykhvatnyuk, S. I.; Godovanyuk, M. Ye.; Gavrilyuk, B. M. Nasinnia kukurudzy: v umovakh fermerskoho hospodarstva [Corn seeds: in the conditions of the farm, *in Ukrainian*]. *Nasinnytstvo* **2012**, *9*, 15 – 16.

11. Palamarchuk, V. D. The number of kernel rows and kernel in a raw in corn hybrids as affected by the elements of technology. *Advanced Agritechnologies* **2017**, *5*. https://doi.org/10.21498/na.5.2017.122229.

12. Palamarchuk, V.; Telekalo, N. The effect of seed size and seeding depth on the components of maize yield structure. *Bulgarian Journal of Agricultural Science* **2018**, *24* (5), 785 – 792.

13. Kovalenko, O.; Palamarchuk, V.; Tishechkina, K.; Ovchar, A. Vplyv rozmiriv fraktsii ta hlybyny zahortannia nasinnia na produktyvnist kukurudzy [Effect of fraction size and depth of seed wrapping on corn productivity, *in Ukrainian*]. *Rozvytok ahrarnoi haluzi ta vprovadzhennia naukovykh rozrobok u vyrobnytstvo Materialy,* 5th International scientific conference, Mykolaiv, October 19 – 21, 2022. MNAU: Mykolaiv, pp. 32 – 37.

14. *Metodychni rekomendatsii po provedenniu polovykh doslidiv z kukurudzoiu* [Methodological guide for conducting field experiments with corn, *in Ukrainian*]. All-Union Scientific and Research Institute: Dnipropetrovsk, 1980.

15. Vovkodav, V. V., Ed. *Metodyka derzhavnoho sortovyprobuvannia silskohospodarskykh kultur (zernovi, krupiani ta zernobobovi)* [Methodology of state variety testing of agricultural crops (cereals, cereals and legumes), *in Ukrainian*]. Kyiv, 2001.

16. Metodychni rekomendatsii po provedenniu polovykh doslidiv v umovakh Ukrainskoi RSR [Methodological guide for conducting field experiments in the conditions of the Ukrainian SSR, *in Ukrainian*]. Dnipropetrovsk, 1985.

17. Ushkarenko, V. O.; Nikishenko, V. L.; Holoborodko, S. P.; Kokovikhin, S. V.; Kokovikhin, S. V. *Dyspersiinyi i koreliatsiinyi analiz u zemlerobstvi ta roslynnytstvi* [Dispersion and correlation analysis in agriculture and crop production, *in Ukrainian*]. Ailant: Kherson, 2008.

Information about the authors:

Oleh A. Kovalenko (*corresponding author*), Dr.Sci. in Agriculture, Associate Professor of the Department of Crop Production and Horticulture, Mykolayiv National Agrarian University; https://orcid.org/0000-0002-2724-3614; e-mail for correspondence: kovalenko@mnau.edu.ua; tel. +380 66 9944690.

Antonina V. Drobitko, Dr.Sci. in Agriculture, Associate Professor of the Department of Viticulture and Fruit and Vegetable Growing, Mykolayiv National Agrarian University; https://orcid.org/0000-0002-6492-4558.

Vitalii D. Palamarchuk, Dr.Sci. in Agriculture, Associate Professor of the Department of Plant Breeding, Breeding and Bioenergy Crops, Vinnytsia National Agrarian University; https://orcid.org/0000-0002-4906-3761.

Uliana P. Bahliuk, second-year student, Mykolayiv National Agrarian University; https://orcid.org/0000-0002-5323-0876.

ЗМІСТ / CONTENTS